8-1-2022

Post-Newtonian dynamics of eccentric, spinning binary black holes and the associated gravitational waveforms

Sashwat Tanay

POST-NEWTONIAN DYNAMICS OF ECCENTRIC, SPINNING BINARY BLACK HOLES AND THE ASSOCIATED GRAVITATIONAL WAVEFORMS

A Dissertation
presented in partial fulfillment of requirements
for the degree of Doctor of Philosophy
in the Department of Physics and Astronomy
The University of Mississippi

by

SASHWAT TANAY

August 2022

ABSTRACT

In 2015, the gravitational wave (GW) era of astronomy began. The binary black hole (BBH) system being the primary source of GWs, are at the center stage of GW astronomy. The matched-filtering method of detection of GWs requires accurate modeling of the BBH system and the associated GWs. With the increasing sensitivity of the GW detectors, we need to push our GW models to even higher accuracy in the future. There is also a need to make these models as fast as possible to implement so as to allow for hundreds of detections in a year. This is where the need to model the BBHs and GWs analytically comes into the picture. In this dissertation, we document our series of efforts to construct analytical solutions to the BBH dynamics (spinning and non-spinning) and the associated GWs. Apart from constructing the analytical solutions, we implement our solutions in the form of publicly available PYTHON and MATHEMATICA packages for the GW community to use and improve upon.

ACKNOWLEDGEMENTS

I thank my Ph.D. advisor Dr. Leo C. Stein for being a *teacher* to me and assigning me the *right* problems to work on. I have also had the good fortune of having teachers and mentors like Drs. Achamveedu Gopakumar, José T. Gálvez Ghersi, Emanuele Berti, Gihyuk Cho, and Antoine Klein. Dr. Shrobana Ghosh's counsel and wise words have always served as a compass during my Ph.D. program. Finally, a warm thanks to Drs. Luca Bombelli, Samuel Lisi and Anuradha Gupta for taking time out of their busy schedules and serving on my dissertation committee.

TABLE OF CONTENTS

LIST OF FIGURES

LIST OF TABLES

CHAPTER 1

INTRODUCTION

The last six decades of progress in electromagnetic (EM) astronomy has been quite breath-taking. Many of the phenomena that were uncovered were not even anticipated at the time of building the instruments of astronomy. A few examples are the cosmic microwave background (CMB), pulsars, accelerated expansion of the universe, etc. These phenomena have shaken not just our understanding of astrophysics and cosmology but also fundamental theoretical physics.

With the detection of the first gravitational wave (GW) event in 2015, we have entered the GW era of astronomy. If history is any guide, we expect to discover some even more radical and ground-breaking phenomena using GWs. GWs offer an alternative and complementary (to EM waves) window to the universe. Unlike EM waves, GWs can pass through shrouds of interstellar dust without scattering and can give us information about the sources which would otherwise be hidden (if one were looking only at the EM spectra of these sources).

The effects of GW data on our understanding of the universe could be profound. We expect GW data to contribute greatly to our understanding of •*astrophysics:* compact object distribution in the cosmos, formation channel of the black holes (BHs) •*cosmology:* resolution of the Hubble constant tension and possible discovery of cosmic gravitational wave background (GW equivalent of the CMB) •*fundamental physics:* nuclear equation of state, speed of gravitons, modifications of Einstein's theory of general relativity, quantizing gravity, etc. The above enumeration is just our anticipation. The EM astronomy experience tells us that we will hopefully make many other ground-breaking discoveries using GWs that we never expected to.

The primary sources of GWs are binary black holes (BBHs), wherein two BHs of comparable masses orbit around a common center. The optimal method to detect GWs is matched filtering. It

requires modeling the signal (to be detected) very accurately for the detection to happen. Modeling this GW signal hinges crucially on *modeling the dynamics* of the BBH, i.e., predicting the positions and velocities of the two BHs of the BBH system at any future time. Modeling the dynamics of the BBH system and the associated GWs form the bulk of this dissertation. We now give a brief overview of the contents of each chapter.

Chapter 2 and 3: We construct the action-angle variables of a spinning, eccentric BBH system at 1.5 PN order. More specifically, we give explicit expressions of the actions and we show how to write the usual positions and momenta in terms of the actions and angles. This is equivalent to constructing the closed-form solution of the system. Because of the complex nature of the problem, the fifth and the last action is constructed in Chapter 3.

Chapter 4: Liouville-Arnold theorem implies that the spinning, eccentric BBH must have five constants of motion with vanishing Poisson brackets (PBs) to be integrable. At 2PN order, three of these constants are trivial (Hamiltonian, total angular momentum and its z-component). In this chapter we construct two new 2PN constants of motion such that all these five 2PN constants of motion have a vanishing PB up to 2PN, thereby proving that the system is 2PN integrable.

Chapter 5: We focus on eccentric, non-spinning BBHs in this chapter. Here we construct the 4PN closed-form solution to the system. We also present a MATHEMATICA package which uses our 4PN conservative solution, 3PN radiative effects (already given in Ref. [1]) and generates a full inspiral-merger-ringdown gravitational waveform. Our package is a derivative of the original package built by Ian Hinder [2] which is accurate up to 3PN (2PN) in conservative (radiative) sector. We also explore some data-analysis oriented "match" estimates to assess the importance of these newly added 4PN contributions.

Chapter 6: Ref. [3], constructed the Fourier-domain gravitational waveform for non-spinning, eccentric BBHs which was Newtonian (2PN) order accurate in the conservative (radiative) sector as power series in two small parameters: the PN parameter x and small initial eccentricity e_0. In this chapter we explore the numerical convergence of this bivariate power series in terms of certain data-analysis oriented quantities like match and Fisher-matrix errors.

Finally in Chapter 7, we conclude.

CHAPTER 2

ACTION-ANGLE VARIABLES OF BINARY BLACK HOLES AT 1.5PN

The contents of this chapter can be found at Refs. [4] and [5].

2.1 Introduction

Laser interferometer detectors have made numerous gravitational wave (GW) detections that have originated from compact binaries made up of black holes (BHs) or neutron stars [6–8]. Among these detections, the predominant sources of GWs are from binary black holes (BBHs), whose initial eccentricity is believed to be mostly radiated away by the time they enter the frequency band of the ground-based detectors such as LIGO, Virgo, and KAGRA. Since the upcoming LISA mission [9, 10] will target compact binaries earlier in their inspiral phase compared to the ground based detectors, incorporating eccentricity becomes more relevant. Since the observation time for LISA sources will be much longer, it is imperative to find accurate closed-form solutions to the binary dynamics.

This brings us to the question of working out the closed-form dynamics of a *generic* BBH system, with arbitrary eccentricity, masses, and with both BHs spinning, without special alignment. Many such attempts have been made in the literature [11–19], but most (if not all) of them give the solution of the conservative sector of the dynamics under some simplifying conditions such as the quasi-circular limit, equal-mass case, only one or none of the BHs spinning, orbit-averaging, etc. Only recently, a method was provided to find the closed-form solution to a BBH system with arbitrary eccentricity, spins, and masses at 1.5 post-Newtonian (PN) order for the first time [20], (with the 1PN part of the Hamiltonian being omitted, as it is not complicated to handle). The natural next question is: how can one construct the solutions at 2PN, or is it even feasible?

This line of questioning led us to probe the integrability (and therefore existence of action-angle variables) of the BBH system at 2PN in Ref. [21] (subject of Chapter 4), wherein we found that a BBH system is indeed 2PN integrable when we applied the PN version of the Liouville-Arnold (LA) theorem (see Footnote 1), due to the existence of two new 2PN constants of motion we discovered. Since integrability precludes chaos (which would obstruct finding closed-form solutions), establishing integrability at 2PN instills hope towards finding a closed-form solutions at this order. A straightforward extension of the methods of Ref. [20] from 1.5PN to 2PN appears too difficult to carry out. Our hope is to use non-degenerate canonical perturbation theory, which when starting with 1.5PN action-angle variables, can yield 2PN action-angle variables. If this line of work is to be pursued, the 1.5PN action-angle variables are imperative (the calculation can not start from a lower PN order because of degeneracy, as we will discuss later).

The history of action-angle variables literature dates back centuries. The Kepler equation presented in 1609 gives the Newtonian angle variable [22], long before Newton proposed his laws of motion and gravitation. Important contributions were made by Delaunay to the action-angle formalism of the Newtonian two-body system [22]. More recently, Damour and Deruelle gave the 1PN extension of the angle variable when they worked out the quasi-Keplerian solution to the non-spinning eccentric BBH system [23]. Damour, Schäfer and Jaranowski worked out action variables at 2PN and 3PN ignoring all the spin effects. Such post-Newtonian calculations make use of the work of Sommerfeld for complex contour integration to evaluate the radial action variable [24]. Finally, Damour gave the requisite number (five) of 1.5PN constants of motion in Ref. [25], which is required for integrability as per the LA theorem.

This is a part of the larger program to eventually build analytical waveform models for the generic spinning, eccentric BBH system. In this chapter, we derive four (out of the five) action variables, with the fourth one being in the form of a PN series. The fifth action is derived in the next chapter, due to its complexity. These action variables are closely related to the Keplerian-like parameterization for the generic system at 1.5PN recently presented in Ref. [26] (that work omitted the 1PN orbital terms from the Hamiltonian for simplicity, but the approach will work with the 1PN

terms included). Next we discuss how to compute all the frequencies of the system. Then we give a clear roadmap on how to compute all angle variables of the system implicitly, by expressing the standard phase space variables of the system $(\vec{R}, \vec{P}, \vec{S}_1, \vec{S}_2)$ as explicit functions of the action-angle variables. We then explain how the action-angle variables can be used to construct solutions to the BBH system at 1.5PN and higher PN orders via canonical perturbation theory.

The layout of this chapter is as follows. In Sec. 2.2 we introduce preliminaries like post-Newtonian power counting, Liouville integrability, the Hamiltonian phase space and Poisson bracket structure for the BBH problem, and the 2PN Hamiltonian. In Sec. 2.3, we compute four out of five action variables up to 1.5 PN by integrating along closed loops on the invariant tori in phase space. Then we finally show how to compute the five frequencies, angle variables, and the action-angle based solution to the system in Sec. 2.4 before summarizing our work and suggesting its future extensions in Sec. 2.5.

2.2 The setup

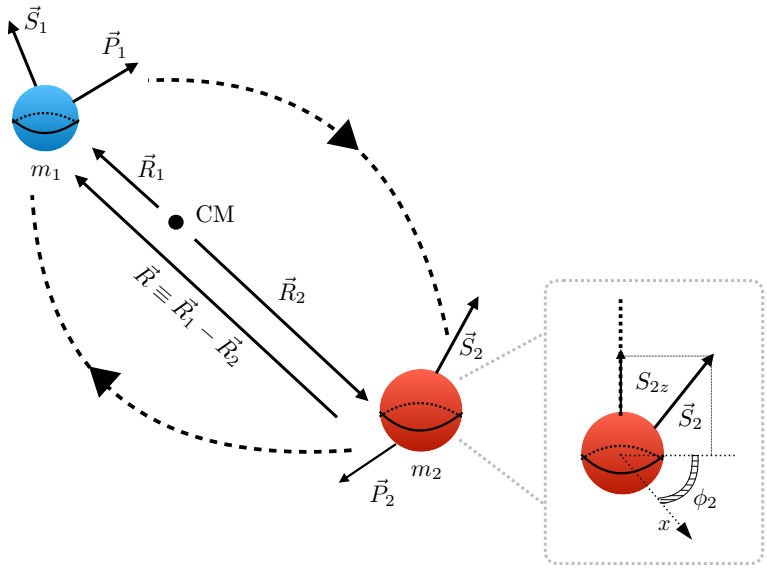

Figure 2.1: Schematic setup of a precessing black hole binary.

We start by describing the canonical variables and the dynamical setup used to study

eccentric binaries of black holes with precessing spins in the PN approximation. The BBH system under consideration is schematically displayed in Fig. 2.1, using its center-of-mass frame [27], to define the separation vector $\vec{R} \equiv \vec{R}_1 - \vec{R}_2$ and the linear momenta $\vec{P} \equiv \vec{P}_1 = -\vec{P}_2$ of a binary of black holes with masses m_1 and m_2. With these quantities, we build the Newtonian orbital angular momentum $\vec{L} \equiv \vec{R} \times \vec{P}$, and the total angular momentum $\vec{J} \equiv \vec{L} + \vec{S}_1 + \vec{S}_2$ which includes the BH spins $\vec{S}_1$ and $\vec{S}_2$. The individual BH masses are m_1 and m_2, and the total mass is $M \equiv m_1 + m_2$. Additionally, the reduced mass is given by $\mu \equiv m_1 m_2/M$ and the symmetric mass ratio $\nu \equiv \mu/M$ is a function of the reduced mass. The constants $\sigma_1 \equiv 1 + 3m_2/4m_1$ and $\sigma_2 \equiv 1 + 3m_1/4m_2$ are used to build the effective spin

$$\vec{S}_{\rm eff} \equiv \sigma_1 \vec{S}_1 + \sigma_2 \vec{S}_2 \,. \tag{2.1}$$

This should not be confused with other common spin parameters used in the literature [28–30], namely the projected effective spin $\chi_{\rm eff} \equiv (m_1\chi_1 + m_2\chi_2)/M$, or the combination $\vec{S}_0 \equiv (1 + m_2/m_1)\vec{S}_1 + (1 + m_1/m_2)\vec{S}_2$. Racine found [29] that $\vec{L} \cdot \vec{S}_0$ is conserved under the Newtonian-orbit-average of the 2PN equations of motion; we will discuss this further in Sec. 4.2.

Even when our approach throughout this chapter is purely Hamiltonian, we may define a velocity $\vec{v} \equiv \vec{P}/\mu$ since the ratio v^2/c^2 is often used as a PN expansion parameter. Latin indices $i = 1, 2, 3$ denote the ith Cartesian component of a vector, and we employ the Einstein summation convention unless stated otherwise.

The spin angular momentum for a Kerr black hole labeled A is

$$\vec{S}_A = \vec{\chi}_A \frac{G m_A^2}{c} \,, \tag{2.2}$$

where $|\vec{\chi}| \leq 1$ so that there are no naked singularities. Notice the factor of $1/c$, which affects the post-Newtonian order of any terms containing spins; this will be detailed in Secs. 2.2.1 and 2.2.4.

2.2.1 Counting post-Newtonian orders

Post-Newtonian counting applies to any function y of phase-space variables, which we expand as an asymptotic series using a certain PN parameter x, i.e., $y = \sum_k y_k x^k$. Depending on context, one of v, an orbital frequency ω, or R is used as the expansion parameter. Specifically, from Newtonian order, we may define x to be any of

$$x \equiv \frac{v^2}{c^2}, \quad \left(\frac{GM\omega}{c^3}\right)^{2/3}, \quad \text{or} \quad \frac{GM}{c^2 R}\,. \tag{2.3}$$

Since we have kept the powers of c explicitly, we can see that any choice is equivalent to counting powers of c^{-2}. This latter observation is important when spins are involved, since spin includes $1/c$ [see Eq. (2.2)] but does not scale with v, ω, or R.

Let a phase-space function y be written in the form

$$y = x^m \sum_{k=0}^{\infty} Y_k x^k\,, \tag{2.4}$$

In Eq. (2.4), $Y_0 \neq 0$ is the first non-vanishing term in the expansion, and we would say that the term Y_k is kPN orders higher than Y_0, or is of "relative kPN order." For example, when including spins in the total angular momentum,

$$\vec{J} = \vec{L} + \vec{S}_1 + \vec{S}_2 = \vec{L}\left[1 + O\left(\frac{v}{c}\right)\right]\,, \tag{2.5}$$

we see that spins are 0.5PN orders higher than orbital angular momentum.

2.2.2 Hamiltonian dynamics on a symplectic manifold

From now on, we will follow the Hamiltonian formulation to study the BBH system; we will review its algebraic structure [31, 32]. Hamiltonian dynamics takes place on an (even-dimensional) symplectic manifold. A smooth manifold equipped with a closed non-degenerate differential 2-form Ω (the symplectic form) is called a symplectic manifold. The algebra of non-vanishing Poisson

brackets (PBs) between the phase-space variables R^i, P_j, S_1^i, and S_2^i is given by

$$\left\{R^i, P_j\right\} = \delta^i_j \quad \text{and} \quad \left\{S_A^i, S_B^j\right\} = \delta_{AB}\epsilon^{ij}{}_k S_A^k \,. \tag{2.6}$$

Notice that all brackets with spins preserve the norms $|\vec{S}_A|$, so although the spin vectors are three-dimensional, each is restricted to evolve on the surface of a 2-sphere. This makes the phase space a ten-dimensional manifold.

Time evolution under a Hamiltonian H of any phase-space quantity $f(\mathcal{Q}^i, \mathcal{P}_i)$ is given by $\dot{f} = \{f, H\}$, where $\mathcal{Q}^i, \mathcal{P}_i$ collectively denote canonical coordinates on phase space. The standard rules of sum, product, anti-commutativity, and chain rule make the PBs in Eq. (2.6) sufficient to evaluate the PB of any quantities built from $\mathcal{Q}^i, \mathcal{P}_i$.[1] The remainder of this section is for readers interested in the symplectic structure, relevant to computing action-angle variables, the subject of Sec. 2.3.

Our symplectic manifold is the product of the 6-dimensional phase space of orbital dynamics, and two 2-dimensional spin phase spaces, each of which is an S^2 (the only S^n that admits a symplectic structure). The symplectic form is correspondingly a sum over the three manifolds. Commonly, symplectic forms are presented in Darboux coordinates,

$$\Omega \equiv \sum_i d\mathcal{P}_i \wedge d\mathcal{Q}^i \,. \tag{2.7}$$

This is possible on the orbital phase space, which is a cotangent space, $T^*\mathbb{R}^3$, and admits the globally-valid canonical form $\Omega^{\text{orb}} = dP_i \wedge dR^i$.

However, there is no globally-valid Darboux coordinate system on the 2-sphere. The symplectic structure on the S^2 is unique up to scaling and is proportional to the standard area element, $\Omega^{\text{spin}}_{ij} \propto \epsilon_{ij}$; the normalization is fixed to agree with Eq. (2.6). Thinking of the S^2 as an

[1] If computing PBs by hand, the following derived identities are also useful: $\left\{L^i, L^j\right\} = \epsilon^{ij}{}_k L^k$; and, for any scalar function f, $\left\{f, \vec{L}\right\} = \vec{P} \times \nabla_P f + \vec{R} \times \nabla_R f$, where the 3-vector $\nabla_P f$ has components $\partial f / \partial P^i$, and similarly for $\nabla_R f$.

embedded submanifold in spin space, the inverse symplectic form can be written as

$$(\Omega^{-1}_{\rm spin})^{ij} = S^k \epsilon_k{}^{ij} \,. \tag{2.8}$$

This representation should make it clear that the symplectic form is SO(3) covariant. An equivalent representation is $\Omega^{\rm spin} = dS_z \wedge d\phi$, where ϕ is the azimuthal angle of the spin about the z axis. The total symplectic form is thus

$$\Omega = dP_i \wedge dR^i + dS_{1z} \wedge d\phi_1 + dS_{2z} \wedge d\phi_2 \,. \tag{2.9}$$

As noted above, it is SO(3) covariant, which will be useful in evaluating some action integrals. Finally let us note that while $\Omega^{\rm orb}$ is c-independent, $\Omega^{-1}_{\rm spin}$ carries one power of spin [seen in Eqs. (2.6) and (2.8)], and spin carries a power of $1/c$. Orbital and spin PBs thus change PN orders in different ways, which will be important in Sec. 4.2.

2.2.3 Integrable systems

A $2n$-dimensional Hamiltonian system is said to be integrable in the Liouville sense if there exist n independent phase-space functions F_i which are all mutually Poisson commuting, $\{F_i, F_j\} = 0$. These functions are said to be "in involution" [31–33].[2] Bound systems that are integrable admit a canonical transformation to a set of phase-space coordinates called action-angle variables. The evolution of such systems is trivial in action-angle variables, so there cannot be any chaos or phase space mixing; all bound orbits are multiply-periodic. Action-angle variables are ideal for studying perturbations of integrable systems. For our purposes, we would like to treat terms of higher PN orders as a perturbation of an integrable system.

A level set of all the constants of motion must be an n-dimensional torus T^n [32]. The actions $\mathcal{J}_i$ can be found via certain coordinate-independent integrals along n closed loops restricted

[2] More precisely, the Liouville-Arnold theorem states that, on a $2n$-dimensional symplectic manifold, if $\partial_t H = 0$ and there are n independent phase-space functions F_i in mutual involution, and if level sets of these functions form a compact and connected manifold, then the system is integrable.

to the tori (holding constant each of the F_i). If global Darboux coordinates are possible, the action integrals are [31–33],

$$\mathcal{J}_k = \frac{1}{2\pi} \oint_{C_k} \sum_i \mathcal{P}_i d\mathcal{Q}^i \,. \tag{2.10}$$

Here C_k is the kth loop on the torus. The set of n loops must be in different homotopy classes (more precisely, the homotopy classes form an integer lattice $\mathbb{Z}^n$, and our n loops' homotopy classes must span the lattice). The 1-form integrand of Eq. (2.10) is a symplectic potential, $\theta = \sum_i \mathcal{P}_i d\mathcal{Q}^i$, whose exterior derivative gives the symplectic 2-form, $\Omega = d\theta$. Since Ω vanishes on the level set of all the constants of motion, it is straightforward to show that the $\mathcal{J}_k$ depend only on homotopy class, and not on choice of loop in that class.

However on some symplectic manifolds, including the 2-sphere, Ω is not an exact form, $\Omega \neq d\theta$. This makes the action integrals Eq. (2.10) ambiguous. One approach is to make a global choice of how to 'cap' the loops to another reference loop, and thus perform integrals of Ω over 2-surfaces. This ambiguity is benign, as it will only shift the action integrals by global constants.[3]

To complete the coordinate system, there will be n angle variables ϕ_i which are conjugate, i.e., $\{\phi_i, \mathcal{J}_j\} = \delta_{ij}$ and all other PBs vanishing. Each angle variable ϕ_i runs from 0 to 2π as one follows the flow $d/d\phi_i = \{-, \mathcal{J}_i\}$ generated by its conjugate action. We will not construct the angle variables in this work.

2.2.4 2PN Hamiltonian with spins included

To write the Hamiltonian at different post-Newtonian orders, we adopt the convention that $H_{n\mathrm{PN}}$ stands for the part of Hamiltonian which is of nPN order relative to the leading Newtonian order term (dubbed H_{N}). The Hamiltonian up to 2PN of the BBH system in the center-of-mass frame is

$$H = H_{\mathrm{N}} + H_{1\mathrm{PN}} + H_{1.5\mathrm{PN}} + H_{2\mathrm{PN}} + O(c^{-5}) \,, \tag{2.11}$$

[3]We thank Samuel Lisi for discussion of the finer points of this ambiguity.

where $O(c^{-5})$ represents corrections of order 2.5PN and higher. To simplify we will use the scaled quantities $\vec{r} \equiv \vec{R}/GM$, $\vec{p} \equiv \vec{P}/\mu$, and the radial component of scaled momentum is $\hat{r} \cdot \vec{p}$, with the implicit understanding that the "hatted" version of any vector in this chapter is the corresponding unit vector. The vector $\vec{p}$ has units of velocity, and $1/r$ has units of velocity squared, enabling the easy reading of PN orders. The individual contributions are [28, 34–37]

$$H_{\rm N} = \mu \left(\frac{p^2}{2} - \frac{1}{r} \right), \tag{2.12}$$

$$H_{\rm 1PN} = \frac{\mu}{c^2} \left\{ \frac{1}{8}(3\nu - 1)p^4 + \frac{1}{2r^2} - \frac{1}{2r} \left[(3+\nu)p^2 + \nu(\hat{r} \cdot \vec{p})^2 \right] \right\}, \tag{2.13}$$

$$H_{\rm 1.5PN} = \frac{2G}{c^2 R^3} \vec{S}_{\rm eff} \cdot \vec{L}, \tag{2.14}$$

$$H_{\rm 2PN} = \frac{\mu}{c^4} \left\{ -\frac{1}{4r^3}(1+3\nu) + \frac{1}{16}\left(1 - 5\nu + 5\nu^2\right) p^6 + \frac{1}{2r^2}\left(3\nu(\hat{r}\cdot\vec{p})^2 + (5+8\nu)p^2\right) + \frac{1}{8r}\left[-3\nu^2(\hat{r}\cdot\vec{p})^4 - 2\nu^2(\hat{r}\cdot\vec{p})^2 p^2 + \left(5 - 20\nu - 3\nu^2\right) p^4 \right] \right\} + H_{\rm SS,2PN}\,. \tag{2.15}$$

The 2PN spin-spin interaction is

$$H_{\rm SS,2PN} = H_{\rm S1S1} + H_{\rm S2S2} + H_{\rm S1S2}, \tag{2.16}$$

$$H_{\rm S1S1} = \frac{G}{c^2}\frac{m_2}{2m_1} S_1^i S_1^j \, \partial_i \partial_j R^{-1}\,, \tag{2.17}$$

$$H_{\rm S2S2} = \frac{G}{c^2}\frac{m_1}{2m_2} S_2^i S_2^j \, \partial_i \partial_j R^{-1}\,, \tag{2.18}$$

$$H_{\rm S1S2} = \frac{G}{c^2} S_1^i S_2^j \, \partial_i \partial_j R^{-1}\,, \tag{2.19}$$

where $\partial_i \partial_j R^{-1} = (3\hat{R}_i \hat{R}_j - \delta_{ij})/R^3$ is symmetric and trace-free.

Notice that since $H_{\rm 1.5PN} \sim O(c^{-2}S)$ and, as previously mentioned, spin goes as $S \sim O(c^{-1})$, so indeed $H_{1.5PN} \sim O(c^{-3})$. Likewise, $H_{\rm SS,2PN} \sim O(c^{-2}S^2) \sim O(c^{-4})$, justifying the claimed PN

orders of these terms.

2.3 Action variables at 1.5PN order

To start, we will focus on integrability at 1.5PN, truncating the Hamiltonian to

$$H = H_{\rm N} + H_{\rm 1PN} + H_{\rm 1.5PN} + O(c^{-4})\,. \tag{2.20}$$

As has been known for many years now [28], truncating at this order gives a 10-dimensional phase space with 5 constants of motion F_i in mutual involution, namely, the set $\{F_i\} = \{H, J^2, J_z, L^2, \vec{S}_{\rm eff}\cdot\vec{L}\}$. At this level, the involution is "exact", for the associated PBs vanish exactly. This involution can be verified by the MATHEMATICA notebook which accompanies this article [38], which makes use of the xACT/xTENSOR suite [39].

This involution implies the existence of action-angle variables. We will construct four out of five action variables in this section. For each action variable $\mathcal{J}_k$, we will consider a different loop C_k tangent to the five-torus given by constancy of the five F_i, and perform the (capped) loop integral of Eq. (2.10).

2.3.1 Loops generated by J^2, J_z, and L^2

We find three of these loops by following the flow of the generators J^2, J_z, and L^2. To demonstrate, let $d/d\lambda_1 = \{-, L^2\}$ be the vector field tangent to the flow generated by L^2. Notice that this flow makes $\vec{R}$ and $\vec{P}$ rigidly rotate about the constant $\hat{L}$, while the two $\vec{S}_A$ are not moved. Thus we have (with $\vec{V}$ representing either $\vec{R}$ or $\vec{P}$)

$$\frac{d\vec{V}}{d\lambda_1} = \left\{\vec{V}, L^2\right\} = 2\vec{L}\times\vec{V}\,, \qquad\qquad \frac{d\vec{S}_A}{d\lambda_1} = 0\,. \tag{2.21}$$

As this is a rigid rotation, the phase-space flow will complete one cycle as the parameter λ_1 increases by $\Delta\lambda_1 = 2\pi/|2\vec{L}|$. Similarly, let $d/d\lambda_2 \equiv \{-, J_z\}$. This time all vectors rotate rigidly about the $\hat{z}$

axis,

$$\frac{d\vec{V}}{d\lambda_2} = \hat{z} \times \vec{V}, \tag{2.22}$$

with $\vec{V}$ representing any of $\vec{R}$, $\vec{P}$, and $\vec{S}_A$. After λ_2 increases by $\Delta\lambda_2 = 2\pi$, the spin and orbital phase-space variables will close the loop. Thirdly, with $d/d\lambda_3 \equiv \{-, J^2\}$, all vectors rigidly rotate around the constant $\hat{J}$,

$$\frac{d\vec{V}}{d\lambda_3} = 2\vec{J} \times \vec{V}\,, \tag{2.23}$$

with $\vec{V}$ again representing any of $\vec{R}$, $\vec{P}$, and $\vec{S}_A$. The phase-space flow under $d/d\lambda_3$ closes after the parameter λ_3 increases by $\Delta\lambda_3 = 2\pi/|2\vec{J}|$.

All three of these flows can be treated with the same method. Since the symplectic forms on orbital and spin phase spaces simply add, we treat the orbital and spin components one at a time and add the final results,

$$\mathcal{J} = \mathcal{J}^{\rm orb} + \mathcal{J}^{\rm spin}\,, \tag{2.24}$$

$$\mathcal{J}^{\rm orb} \equiv \frac{1}{2\pi} \oint_C \sum_i P_i dR^i\,, \tag{2.25}$$

and similarly for the spin sector, except that the spin integral is 'capped' so as to become an area integral of $\Omega^{\rm spin}$.

We write $d/d\lambda$ for any of the three flows, and use $\vec{n}$ to denote the fixed vector about which others rotate, $\vec{n}$ being one of $\{2\vec{L}, \hat{z}, 2\vec{J}\}$. The loop closes after the parameter change of $\Delta\lambda = 2\pi/|\vec{n}|$. This is illustrated in Fig. 2.2. The only exception is that the spin vectors are not moved by $d/d\lambda_1$, but since we break the action integral up as in Eq. (2.24), this is simple to implement. First, when we parameterize C using λ, the $\mathcal{J}^{\rm orb}$ integral becomes

$$\mathcal{J}^{\rm orb} = \frac{1}{2\pi} \int_0^{\Delta\lambda} P_i \frac{dR^i}{d\lambda}\, d\lambda = \frac{1}{2\pi} \int_0^{\Delta\lambda} \vec{P} \cdot (\vec{n} \times \vec{R})\, d\lambda$$

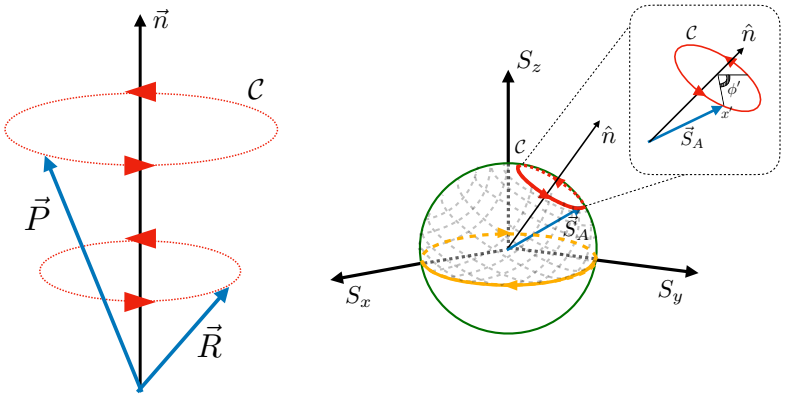

Figure 2.2: Configuring the integration paths for the action integrals.

$$= \frac{1}{2\pi} \int_0^{\Delta\lambda} \vec{n} \cdot \vec{L} \, d\lambda \quad = \hat{n} \cdot \vec{L} \, . \tag{2.26}$$

The second equality comes from evaluating the flow for $dR^i/d\lambda$; the third equality comes from permuting the triple product. The last equality arises since in all three cases, $\vec{L}$ rigidly rotates around $\vec{n}$ (because $\vec{R}$ and $\vec{P}$ also rigidly rotate around $\vec{n}$), so the dot product is constant around the loop.

For the spin sector, we choose to cap each curve C by the equatorial plane (in spin space), i.e., the oriented area integral will be bounded between the $S_A^z = 0$ plane and C. One can show that this gives the same result as the ordinary integral (for one of the two spins)

$$\mathcal{J}_A^{\text{spin}} = \frac{1}{2\pi} \oint S_A^z \, d\phi_A \, . \tag{2.27}$$

While this integral does not seem to be SO(3) covariant, recall that the symplectic form does have this symmetry, as seen in Eq. (2.8). To take advantage of this symmetry, we call $\hat{n}$ a new axis $\hat{z}'$, and instead compute $\frac{1}{2\pi} \oint S_A^{z'} d\phi'_A$. Since each $\vec{S}_A$ rigidly rotates around $\hat{n}$, the integral in one spin sector will simply be

$$\mathcal{J}_A^{\text{spin}} = S_A^{z'} = \hat{n} \cdot \vec{S}_A \, . \tag{2.28}$$

Combining, we see for the generators J^2 and J_z,

$$\mathcal{J} = \hat{n} \cdot (\vec{L} + \vec{S}_1 + \vec{S}_2) = \hat{n} \cdot \vec{J} \,. \tag{2.29}$$

Meanwhile, for L^2, only the orbital sector contributes, and we have $\mathcal{J} = \hat{n} \cdot \vec{L}$. This gives us our first three action integrals,

$$\mathcal{J}_1 = |\vec{J}| \,, \qquad \mathcal{J}_2 = J_z \,, \qquad \mathcal{J}_3 = |\vec{L}| \,. \tag{2.30}$$

2.3.2 Loop in R-P_R space

To compute a fourth action variable, we find a loop on the five-torus (of constant values of the F_i mutually-commuting phase-space functions) in a plane parallel to the R-P_R plane. We will denote the constant values of the F_i functions with overbars, i.e., taking the values $H = \bar{\mathcal{E}}$, $L^2 = \bar{\mathcal{L}}^2$, and $\overline{L \cdot S_{\rm eff}}$. We define P_R to be the momentum conjugate to the radial separation R,

$$P_R \equiv \vec{P} \cdot \hat{R} \,. \tag{2.31}$$

To show how to construct this loop, we eliminate from the 1.5PN Hamiltonian all dependence except for R, P_R, and the values of constants. This starts from the definition of $\vec{L} = \vec{R} \times \vec{P}$, to get

$$L^2 = R^2 P^2 - (\vec{P} \cdot \vec{R})^2 \,, \tag{2.32}$$

$$P^2 = P_R^2 + \frac{\bar{\mathcal{L}}^2}{R^2} \,. \tag{2.33}$$

Replacing P^2 using this relation will eliminate the angular components of $\vec{P}$ from the 1.5PN Hamiltonian. To compact the notation, we will again use the scaled variables r, p, with $p_r \equiv P_R/\mu$,

and define the shorthand

$$e_k \equiv \frac{p_r^2}{2} + \frac{\bar{\mathcal{L}}^2}{2\mu^2 R^2}\,, \tag{2.34}$$

which is the Newtonian kinetic energy per reduced mass (and also has units of v^2). Then evaluating the 1.5PN Hamiltonian on this torus, we find

$$\frac{\bar{\mathcal{E}}}{\mu} = e_k - \frac{1}{r} + \frac{1}{c^2}\left\{\frac{1}{2r^2} - (\nu+3)\frac{e_k}{r} - \frac{\nu\, p_r^2}{2r} + \frac{1}{2}(3\nu-1)e_k^2\right\} + \frac{2G}{c^2\mu R^3}\overline{L\cdot S_{\rm eff}}\,. \tag{2.35}$$

This equality demonstrates that we can solve for $P_R(R)$ in terms of $R, \bar{\mathcal{E}}, \bar{\mathcal{L}}$, and $\overline{L\cdot S_{\rm eff}}$ – thus making a loop while staying tangent to the torus. We solve for P_R^2 perturbatively in powers of $1/c^2$, finding

$$P_R^2 = 2\mu\bar{\mathcal{E}} + \frac{(1-3\nu)}{c^2}\bar{\mathcal{E}}^2 + \frac{2GM\mu\left[\mu + (4-\nu)\frac{\bar{\mathcal{E}}}{c^2}\right]}{R} + \frac{\left[-\bar{\mathcal{L}}^2 + \frac{(GM\mu)^2}{c^2}(\nu+6)\right]}{R^2} - \frac{\mu G(\bar{\mathcal{L}}^2 + 4\overline{L\cdot S_{\rm eff}})}{R^3 c^2} + O(c^{-4})\,. \tag{2.36}$$

Here we have collected terms by powers of R^{-1}, in anticipation of performing a Sommerfeld integral, following Damour and Schäfer [27]. This momentum enters into the action integral, where the loop is restricted to the (R, P_R) plane,

$$\mathcal{J}_4 = \frac{1}{2\pi}\oint P_R\, dR \qquad\qquad = \frac{2}{2\pi}\int_{R_{\rm min}}^{R_{\rm max}}\left(A + \frac{2B}{R} + \frac{C}{R^2} + \frac{D}{R^3}\right)^{1/2} dR\,, \tag{2.37}$$

where the coefficients A, B, C, D are *constants* along this loop, to be read directly from Eq. (2.36). The factor of 2 comes since the loop runs from one turning point, $R_{\rm min}$, to the other, $R_{\rm max}$, and then back.

To evaluate this integral, we can use the results from Sec. 3 and Appendix B of [27]. The result is in terms of the torus constants $\bar{\mathcal{E}}$, $\bar{\mathcal{L}}$, and $\overline{L\cdot S_{\rm eff}}$. We promote these back to their respective

phase-space functions, giving

$$\mathcal{J}_4 = -L + \frac{GM\mu^{3/2}}{\sqrt{-2H}} + \frac{GM}{c^2}\left[\frac{3GM\mu^2}{L} + \frac{\sqrt{-H}\,\mu^{1/2}(\nu-15)}{\sqrt{32}} - \frac{2G\mu^3}{L^3}\vec{S}_{\rm eff}\cdot\vec{L}\right] + O(c^{-4})\,. \quad (2.38)$$

Unlike the first three actions, the fourth action is not "exact" at 1.5PN, but rather we have presented it as a PN series, just like the radial action in Ref. [27]. This is consistent with the 1.5PN Hamiltonian itself being a truncated PN series.

The four action integrals we computed are functionally independent, as can be seen by their different dependence on the original mutually-commuting phase-space functions H, J^2, J_z, L^2, and $\vec{S}_{\rm eff}\cdot\vec{L}$. This corresponds to their loops (all of which are tangent to a torus) being in linearly-independent homology classes. The calculations for the fifth action (both as a PN series and "exact" at the 1.5PN order) are quite lengthy, so we will present in the next chapter.

It is worth noting that at 1.5PN order, spin effects enter the action integrals, as can be easily seen in Eqs. (2.30) and (2.38). This is relevant to the method of torus-averaging, which is used in canonical perturbation theory [22, 31]. Since the actions depend on spin, it is easy to see that torus-averaging will differ from orbit-averaging (over Newtonian orbits) which has been used extensively in the literature [29, 40–43]. We expect torus-averaging to be more accurate at 1PN and higher orders.

2.4 Frequencies and angle variables

2.4.1 Computing the frequencies

Since we have an integrable Hamiltonian system, the Hamiltonian is a function of the actions, though it may not be possible to write H explicitly in terms of the actions. In terms of the actions, the equations of motion for the respective angle variables are trivial,

$$\dot{\theta}_i = \frac{\partial H}{\partial \mathcal{J}_i} = \omega_i(\vec{\mathcal{J}})\,. \quad (2.39)$$

As a consequence, the usual phase space variables are all multiply-periodic functions of all of the angle variables. Concretely, this means a Fourier transform of some regular coordinate would consist of a forest of delta function peaks at $\mathbb{Z}$-linear combinations of the fundamental frequencies ω_i [44]. Additionally, if we know the frequencies, we can locate resonances — where the ratio of two frequencies is a rational number — which are key to the KAM theorem and the onset of chaos.

With $\vec{C}$ standing for the vector of all five mutually commuting constants, H being one of these C_i's, H is automatically a function of $\vec{C}$. In principle once can invert $\vec{\mathcal{J}}(\vec{C})$ (at least locally, via the inverse function theorem) for $\vec{C}(\vec{\mathcal{J}})$, and thus find an explicit expression for $H(\vec{\mathcal{J}})$ paving the road for the computation of the frequencies ω_i. But this is not necessary.

Instead, we follow the approach given in Appendix A of Ref. [45] to find the frequencies as functions of the constants of motion, via the Jacobian matrix between the five C_i's and the five $\mathcal{J}_i$'s. For the purpose of frequency computations, we take our C_i's to be (in this specific order) $\vec{C} = \{J, J_z, L, H, S_{\text{eff}} \cdot L\}$. As showed in Ref. [21], the first three of these are already action variables. We take the order of the actions to be $\vec{\mathcal{J}} = \{J, J_z, L, \mathcal{J}_4, \mathcal{J}_5\}$. The expression for $\mathcal{J}_4$ was given as an explicit function of $(H, L, S_{\text{eff}} \cdot L)$ in Ref. [21]. The Jacobian matrix $\partial \mathcal{J}^i / \partial C^j$ can be found explicitly, since we have analytical expressions for $\vec{\mathcal{J}}(\vec{C})$. This matrix is somewhat sparse, given by

$$\frac{\partial \mathcal{J}^i}{\partial C^j} = \begin{bmatrix} 1 & 0 & 0 & 0 & 0 \\ 0 & 1 & 0 & 0 & 0 \\ 0 & 0 & 1 & 0 & 0 \\ 0 & 0 & \frac{\partial \mathcal{J}_4}{\partial L} & \frac{\partial \mathcal{J}_4}{\partial H} & \frac{\partial \mathcal{J}_4}{\partial (S_{\text{eff}} \cdot L)} \\ \frac{\partial \mathcal{J}_5}{\partial J} & 0 & \frac{\partial \mathcal{J}_5}{\partial L} & 0 & \frac{\partial \mathcal{J}_5}{\partial (S_{\text{eff}} \cdot L)} \end{bmatrix} . \tag{2.40}$$

Now we use the simple fact that the Jacobian $\partial C^i / \partial \mathcal{J}^j$ is the inverse of this matrix (assuming it is full rank),

$$\frac{\partial \mathcal{J}^i}{\partial C^j} \frac{\partial C^j}{\partial \mathcal{J}^k} = \delta^i{}_k \,, \tag{2.41}$$

$$\frac{\partial \vec{C}}{\partial \vec{\mathcal{J}}} = \left[\frac{\partial \vec{\mathcal{J}}}{\partial \vec{C}}\right]^{-1} . \tag{2.42}$$

Because of the sparsity of the matrix in Eq. (2.40), we directly invert and find the only nonvanishing coefficients in the inverse are

$$\frac{\partial C^i}{\partial \mathcal{J}^j} = \begin{bmatrix} 1 & 0 & 0 & 0 & 0 \\ 0 & 1 & 0 & 0 & 0 \\ 0 & 0 & 1 & 0 & 0 \\ \frac{\partial H}{\partial J} & 0 & \frac{\partial H}{\partial L} & \frac{\partial H}{\partial \mathcal{J}_4} & \frac{\partial H}{\partial \mathcal{J}_5} \\ \frac{\partial (S_{\rm eff}\cdot L)}{\partial J} & 0 & \frac{\partial (S_{\rm eff}\cdot L)}{\partial L} & 0 & \frac{\partial (S_{\rm eff}\cdot L)}{\partial \mathcal{J}_5} \end{bmatrix} . \tag{2.43}$$

The frequencies we seek are in the fourth row of this matrix. Matrix inversion yields the following expressions for the frequencies:

$$\frac{\partial H}{\partial J} = \omega_1 = \frac{(\partial \mathcal{J}_4/\partial (S_{\rm eff}\cdot L))(\partial \mathcal{J}_5/\partial J)}{(\partial \mathcal{J}_4/\partial H)(\partial \mathcal{J}_5/\partial (S_{\rm eff}\cdot L))} , \tag{2.44a}$$

$$\frac{\partial H}{\partial J_z} = \omega_2 = 0, \tag{2.44b}$$

$$\begin{aligned} \frac{\partial H}{\partial L} = \omega_3 = \Big[&(\partial \mathcal{J}_4/\partial (S_{\rm eff}\cdot L))(\partial \mathcal{J}_5/\partial L) \\ &- (\partial \mathcal{J}_4/\partial L)(\partial \mathcal{J}_5/\partial (S_{\rm eff}\cdot L))\Big] \\ &\times (\partial \mathcal{J}_4/\partial H)^{-1}(\partial \mathcal{J}_5/\partial (S_{\rm eff}\cdot L)^{-1} , \end{aligned} \tag{2.44c}$$

$$\frac{\partial H}{\partial \mathcal{J}_4} = \omega_4 = (\partial \mathcal{J}_4/\partial H)^{-1} , \tag{2.44d}$$

$$\frac{\partial H}{\partial \mathcal{J}_5} = \omega_5 = -\frac{\partial \mathcal{J}_4/\partial (S_{\rm eff}\cdot L)}{(\partial \mathcal{J}_4/\partial H)(\partial \mathcal{J}_5/\partial (S_{\rm eff}\cdot L))}. \tag{2.44e}$$

The frequency $\omega_2 = \partial H/\partial J_z$ vanishes since H cannot depend on J_z, to preserve SO(3) symmetry. The derivatives of $\mathcal{J}_4$ with respect to $(H, L, S_{\rm eff}\cdot L)$ are easy to compute from the explicit expression given in Eq. (38) of Ref. [21].

2.4.2 The angle variables

For the purpose of canonical perturbation theory [22, 31], we want to be able to express perturbations to the Hamiltonian (namely, higher PN order terms) as functions of the angle variables which are canonically conjugate to the actions. One of these angles — the mean anomaly, which is conjugate to our $\mathcal{J}_4$ — has been presented previously in the literature, in pieces. We have explicitly checked that the Poisson bracket between $\mathcal{J}_4$ the 1.5PN mean anomaly (combining 1PN and 1.5PN inputs from Refs. [23] and [46]) is 1, up to 1.5PN order.

We now lay out a roadmap on how to implicitly construct the rest of the angle variables on the invariant tori of constant $\vec{\mathcal{J}}$ (or constant $\vec{C}$). To be more precise, we show how to obtain the standard phase-space coordinates $(\vec{\mathcal{P}}, \vec{\mathcal{Q}})$ as explicit functions of action-angle variables $(\vec{\mathcal{J}}, \vec{\theta})$. This is in fact the more useful transformation for canonical perturbation theory, since we will need to transform the 2PN and higher Hamiltonian into action-angle variables.

In action-angle variables, the flows generated by the actions $\{\cdot, \mathcal{J}_i\} = \partial/\partial\theta^i$ give the coordinate basis vector fields for flowing along the angles θ^i. Pick a fiducial point P_0 on an invariant torus, and give it angle coordinates $(0, \ldots, 0)$. Then every other point on this same torus, with angle coordinates θ^i, is reached by integrating a flow from P_0 by parameter amounts θ^i under each of the generators $\{\cdot, \mathcal{J}_i\}$, since $\left\{\theta^i, \mathcal{J}_j\right\} = \delta^i_j$. Since the actions commute, the order of these flows doesn't matter.

The construction explained above was only on an individual torus. The only requirement for extending these variables to being full phase space variables is that the choice of fiducial point $P_0(\vec{\mathcal{J}})$ is smooth in $\vec{\mathcal{J}}$. Given any choice of angle variables, we can always re-parameterize them by adding a constant that is a smooth function of $\vec{\mathcal{J}}$. That is, if θ^i are angle variables, then so are $\bar{\theta}^i = \theta^i + \delta\theta^i(\vec{\mathcal{J}})$, with smooth $\delta\theta^i$, which can be verified by taking Poisson brackets. Some of these angle variables may be simpler than others, but here we are only interested in finding one such construction.

To integrate the equations under the flow associated with any of the five actions, we start

with

$$\begin{aligned}\frac{d\vec{V}}{d\lambda} &= \left\{\vec{V}, \mathcal{J}_i(\vec{C})\right\}, \\ &= \left\{\vec{V}, C_j\right\} \frac{\partial \mathcal{J}_i}{\partial C_j},\end{aligned} \tag{2.45}$$

where use has been made of the chain rule for Poisson brackets. This is the same sparse matrix $\partial \mathcal{J}_i / \partial C_j$ which appeared in the previous section in Eq. (2.40). The matrix $\partial \mathcal{J}_i / \partial C_j$ is a function of only the $\vec{C}$, and thus is constant on each torus and each of the flows we consider. Hence, integrating the above equation boils down to integrating under the flow of the C_i's. But, this is exactly the tool that we used to construct our integral loop for $\mathcal{J}_5$ in this work as well as the three integral curves for (J^2, J_z, L^2) in Ref. [21]; and as mentioned before, the angle variable conjugate to $\mathcal{J}_4$ is the mean anomaly, which has been previously constructed. We will now deal with each of the $C_i's$ one by one.

Integration under the flow of $S_{\rm eff} \cdot L$ was performed in Sec. 3.3, whereas integration under the Hamiltonian was performed in Ref. [20].[4] It now remains to show how to integrate under the remaining three C_i's, (J^2, J_z and L^2). Sec. III (specifically Eqs. (21)-(23)) of Ref. [21] showed that the equations for a flow under any of these quantities can be concisely written in a generalized form as

$$\frac{d\vec{V}}{d\lambda} = \left\{\vec{V}, \mathcal{J}_i\right\} = \vec{U} \times \vec{V}. \tag{2.46}$$

Here $\vec{U}$ is the constant vector $2\vec{J}$, $\hat{z}$, or $2\vec{L}$ when C_i is J^2, J_z, or L^2 respectively. Meanwhile $\vec{V}$ stands for all of $\vec{R}$, $\vec{P}$, $\vec{S}_1$, and $\vec{S}_2$, with the exception that under the flow of L^2, spin vectors aren't moved, so $\vec{V}$ only stands for $\vec{R}$ and $\vec{P}$ in this case. This basically means that the $\vec{V}$ rotates around the fixed vector $\vec{U}$ with an angular velocity whose magnitude it simply U.

Computing these flows in terms of Cartesian components is somewhat cumbersome. Recall

[4]Reference [20] ignored the 1PN Hamiltonian throughout for brevity since the authors deemed it straightforward. Note that Eqs. (3.28-c,d) of this article have typos.

that instead of specifying the state of the BBH system by writing out the vectors $(\vec{R}, \vec{P}, \vec{S}_1, \vec{S}_2)$ explicitly, we can instead just use the relative angles introduced in Sec. 3.3, $\theta_{JL}, \phi_L, \phi$, etc., along with the magnitudes of various vectors. The first two angles define the direction of $\vec{L}$ and the third one defines the direction of $\vec{R}$ in the NIF. Now in light of Eq. (2.46), it is a simple matter to see that the equations for flow under J^2 and L^2 (Eqs. (21) and (23) of Ref. [21] or Eq. (2.46)) imply that

- Under the flow of J^2 by an amount θ_{J^2}, ϕ_L changes by $\Delta\phi_L = 2J\ \theta_{J^2}$.
- Under the flow of L^2 by an amount θ_{L^2}, ϕ changes by $\Delta\phi = 2L\ \theta_{L^2}$.

The flow under J_z can be handled similarly.

With all the individual pieces now identified, it is now straightforward (though lengthy) to find each standard phase space variable as an explicit function of the angle variables θ^i, on any invariant torus.

2.4.3 Action-angle based solution at 1.5PN and higher PN orders

Now there are two approaches to solving the real dynamics of the system, i.e. a flow under H. The approach in Ref. [20] was to directly integrate the flow,[4] yielding a quasi-Keplerian parameterization. Although this method is very direct, it seems difficult or impossible to extend the method to higher PN orders. The second approach is to transform all standard phase space variables $(\vec{\mathcal{P}}, \vec{\mathcal{Q}})$ to explicit functions of angles θ^i. Then these angles have a trivial real time evolution, each one increasing linearly with time $\dot{\theta}^i = \omega_i(\vec{\mathcal{J}})$. This has the great advantage that evaluating the state of the system (or its derivatives, as needed for computing gravitational waveforms) can be trivially parallelized by evaluating each time independently.

Moreover, our action-angle based solution allows for the possibility of using non-degenerate perturbation theory [22, 31] to extend our solution to higher PN orders. The procedure of Sec. 2.4.2 will yield the standard phase-space variables $(\vec{\mathcal{P}}, \vec{\mathcal{Q}})$ as explicit functions of $(\vec{\mathcal{J}}, \vec{\theta})$. This is exactly what's required for computing perturbed action-angle variables at higher PN order with canonical perturbation theory. Higher-PN terms in the Hamiltonian are given in terms of $(\vec{R}, \vec{P}, \vec{S}_1, \vec{S}_2)$, and

one must transform them to action-angle variables to apply perturbation theory. If successful, our method can be seen as the foundation of closed-form solutions of BBHs with arbitrary masses, eccentricity, and spins to high PN orders under the conservative Hamiltonian (excluding radiation-reaction for now). This is in the same spirit as Damour and Deruelle's quasi-Keplerian solution method for non-spinning BBHs given in Ref. [23], which has been pushed to 4PN order recently [47]. We are currently working to find the 2PN action-angle based solution via canonical perturbation theory.

Note that we could not have applied non-degenerate perturbation theory to a lower PN order (say 1PN) to arrive at 1.5PN or higher PN action-angle variables, because the lower PN systems are degenerate in the full phase space. This is because the spin variables are not dynamical until the 1.5PN order; so at lower orders, there are fewer than four action variables and frequencies.[5] At 1.5PN, the system becomes non-degenerate, and can be used as a starting point for perturbing to higher order. We therefore view our construction of the action-angle variables as quite significant for finding closed-form solutions of the complicated spin-precession dynamics of BBHs with arbitrary eccentricity, masses, and spin.

2.5 Summary and next steps

In this chapter, we perform the action-angle variables study of the most general BBH system (both spinning in arbitrary directions, with arbitrary masses and eccentricity). We have derived the expressions of the first four action variables of the system; the last one is derived in the next chapter. We then showed how to compute the fundamental frequencies of the system without needing to write the Hamiltonian explicitly in terms of the actions. Finally, we presented a recipe for computing the five angle variables implicitly, by finding $(\vec{R}, \vec{P}, \vec{S}_1, \vec{S}_2)$ as explicit functions of action-angle variables. We leave deriving the full expressions to future work. We also sketched how the 1.5PN action-angle variables can be used to construct solutions to the BBH system at higher PN orders via canonical perturbation theory.

[5] There can at most be 4 different non-zero frequencies of this system, since H must be independent of J_z to preserve SO(3) symmetry.

Typically, action-angle variables are found by separating the Hamilton-Jacobi (HJ) equation [22], though we were able to work them out without separating the HJ equation. Finally from this vantage point, we summarize the major ingredients which went into computing the action-angle variables of a spinning BBH with arbitrary masses and eccentricity at the leading 1.5PN order: (1) the classic complex contour integration method for the Newtonian system proposed by Sommerfeld [22]; (2) its PN extension by Damour and Schäfer [24]; (3) the integration techniques worked out in the context of the 1.5PN Hamiltonian flow in Ref. [20]; and finally (4) the method of extending the phase space by inventing the unmeasurable extended phase-space variables.

A couple of extensions of the present work are possible in the near future. Since the integrable nature (existence of action-angle variables) has already been shown in Ref. [21] (subject of Chapter 4), constructing the 2PN action-angle variables (via canonical perturbation theory) and an action-angle based solution should be the next natural line of work. With the motivation behind these action-angle variables study of the BBH systems being having closed-form solution to the system, it would be an interesting challenge to incorporate the radiation-reaction effects at 2.5PN into the to-be-constructed 2PN action-angle based solution. There is also hope that the action-angle variables at 1.5PN can also be used to re-present the effective one-body (EOB) approach to spinning binary of Ref. [25] (via a mapping of action variables between the one-body and the two-body pictures) as was originally done for non-spinning binaries in Ref. [48]. Also, it would be interesting to try to compare our action-angle and frequency results in the limit of extreme mass-ratios with similar work on Kerr extreme mass-ratio inspirals (EMRIs) [49] in some selected EMRI parameter space region where PN approximation is also valid. Lastly, there a possibility of a mathematically oriented study of our novel method of introducing the unmeasurable sub-spin variables to compute the fifth action. A few pertinent questions along this line could be (1) Is there a way to compute the fifth action without introducing the unmeasurable variables? (2) Are there other situations (with other topologically nontrivial symplectic manifolds) where an otherwise intractable action computation can be made possible using this new method? (3) What is the deeper geometrical reason that makes this method work?

CHAPTER 3

THE FIFTH ACTION VARIABLE OF BINARY BLACK HOLES AT 1.5PN

The contents of this chapter can be found at Ref. [5].

3.1 Introduction

In this chapter, we continue the action-angle variables program of the previous chapter. There we computed all but one action variables and showed how to construct the usual canonical positions and momenta coordinates as functions of actions and angles. Here we compute the fifth remaining action variable. This entire chapter has been devoted to the fifth action variable computation due to the complexity and the length of the calculations.

3.2 The extended phase space

The setup and the mathematical backdrop for this chapter is the same as the last chapter except for some additional concepts which we introduce now.

3.2.1 Introducing extra phase-space variables

In the last chapter, we succeeded in evaluating four of the five action integrals for the 1.5PN BBH system (using area integrals, since the spin two-sphere does not admit a global potential one-form Θ). We could not yet evaluate the fifth integral, associated with precessional motion, due to the complicated area integrals on the spin two-spheres.

To circumvent this problem, we invent the "extended phase space" (EPS) which has fictitious, unmeasurable variables that are related to the standard phase space (SPS) variables. The inspiration for this extended phase space comes from the observation that components of the orbital angular momentum vector $\vec{L}$ satisfy the Poisson algebra $\left\{L^i, L^j\right\} = \epsilon^{ijk} L^k$, the same as the spin variables;

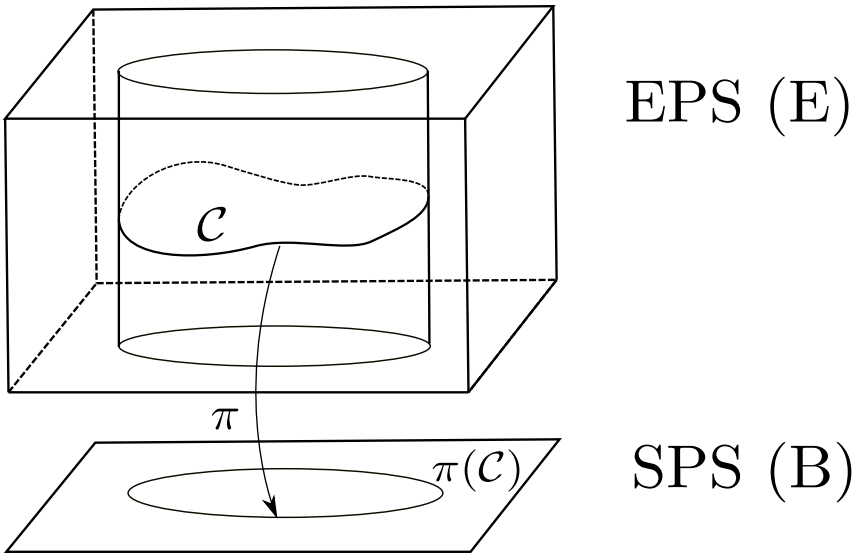

Figure 3.1: EPS E can be viewed as a fiber bundle with projection $\pi : E \to B$ down to SPS P.

but unlike spin, $\vec{L}$ is determined by $\vec{R}$ and $\vec{P}$ which live in $T^*\mathbb{R}^3$, which has an exact symplectic form (admits a global potential Θ). Therefore we create a new 18-dimensional manifold $E = (T^*\mathbb{R}^3)^3$ with canonical coordinates R^i, P_i, R^i_a, P_{ai} with $a = 1, 2$, with canonical Poisson algebra

$$\left\{R^i, P_j\right\}_E = \delta^i_j\,, \qquad \left\{R^i_a, P_{bj}\right\}_E = \delta_{ab}\delta^i_j\,. \tag{3.1}$$

Here we use the subscript E to distinguish the Poisson bracket in the EPS from the bracket in SPS. We may call the $\vec{R}_a, \vec{P}_a$ variables the "sub-spin" (SS) variables. The relationship between the E coordinates and the B spin coordinates is

$$\vec{S}_a \equiv \vec{R}_a \times \vec{P}_a\,, \qquad a = 1, 2\,. \tag{3.2}$$

This means the B is a quotient of E by the above relation. We can think of this as a fiber bundle (with non-compact fibers) with projection

$$\pi : E \to B\,, \tag{3.3}$$

which takes a point in E and sends it to the point in B where its spin coordinates are determined via Eq. (3.2). This is depicted in Fig. 3.1. We comment here that if we think of the three-dimensional spin manifold with coordinates S^i as $\mathfrak{so}(3)^*$, which has a Lie-Poisson structure, then the projection $T^*\mathbb{R}^3 \to \mathfrak{so}(3)^*$ is the *momentum map*.

Any function on B can be pulled back with $\pi^\star$ to a function on E, so we can "evolve" the SS variables with the 1.5PN Hamiltonian H. While the SS variables can appear in intermediate calculations, they are a mathematical convenience for the purpose of computing $\mathcal{J}_5$; thus in the end, physical quantities must only depend on $\vec{S}_a$ and not $\vec{R}_a$ or $\vec{P}_a$.

3.2.2 Comparing the EPS and SPS pictures

We now have two PBs, $\{,\}_B$ in the base symplectic manifold, and $\{,\}_E$ in the EPS. It is easy to check that, when acting on functions that only depend on SPS variables, the two PBs agree, since Eqs. (3.1) imply Eq. (2.6). Because of this crucial observation, that we conclude that the SPS picture and the EPS picture are equivalent for the evolution of any function f under the flow of another function g, when both f and g depend only on SPS variables; loosely,

$$\{f, g\}_B = \{f, g\}_E \ . \tag{3.4}$$

This implies that either of the two pictures can be used to evolve the system.

We can state this compatibility more precisely in the language of differential geometry. Given some symplectic form Ω, its associated Poisson bracket $\{f, g\}$ is found from

$$\{f, g\} = \Omega^{-1}(df, dg) \,, \tag{3.5}$$

where Ω^{-1} is the bivector that is the inverse of Ω, $[\Omega^{-1}]^{ij}\Omega_{jk} = \delta^i_k$. In our setting we have a symplectic form Ω_B in the SPS and Ω_E in the EPS. The compatibility condition between the two

Poisson brackets is

$$\pi^\star\left(\Omega_B^{-1}(df,dg)\right) = \Omega_E^{-1}(\pi^\star df, \pi^\star dg)\,, \tag{3.6}$$

where $\pi^\star$ is the pullback induced by the projection map, and $f, g : B \to \mathbb{R}$. Since the LHS is fiberwise constant, so is the RHS; and so we can also consistently push this equality forward to B. Since f and g are arbitrary, this compatibility implies

$$\pi_\star(\Omega_E^{-1}) = \Omega_B^{-1}\,, \tag{3.7}$$

where $\pi_\star$ is the pushforward.

The two pictures are also equivalent when we investigate the integrability of the system, following the LA theorem [21, 31–33, 50].[1] In the base manifold, we have the required $10/2 = 5$ mutually commuting constants to establish integrability: $H, J^2, J_z, L^2, S_{\rm eff}\cdot L$ (we omit the vector arrows on vectors when there is no confusion). In the EPS picture, we also have the requisite $18/2 = 9$ commuting constants required for integrability. Those are the five constants already listed above, plus $S_a^2, R_a\cdot P_a$ for $(a = 1, 2)$. These nine constants are viewed as functions in the 18-dimensional EPS rather than the SPS. Because of integrability, there are five (nine) action variables in the SPS (EPS), and similarly for the angle variables.

There is however a very important difference in the two spaces. In the base manifold, the symplectic form of Eq. (2.9) is only closed, but not exact (essentially due to the hairy ball theorem). Contrast this with the EPS, which is topologically $(T^*\mathbb{R}^3)^3$ and therefore exact,

$$\Omega_E = dP_i \wedge dR^i + dP_{ai} \wedge dR_a^i \tag{3.8}$$

$$\Omega_E = d(P_i \wedge dR^i + P_{ai} \wedge dR_a^i)\,. \tag{3.9}$$

[1]The theorem states that, on a $2n$-dimensional symplectic manifold, if $\partial_t H = 0$ and there are n independent phase-space functions F_i in mutual involution, and if level sets of these functions form a compact and connected manifold, then the system is integrable.

3.2.3 Strategy to compute the action

Since the EPS and SPS are equivalent for physical quantities (which only depend on SPS variables), we can use either space for calculations. In particular, since the EPS has an exact symplectic form, we can compute the actions there using

$$\mathcal{J}_k = \frac{1}{2\pi} \oint_{C_k} \left(\vec{P} \cdot d\vec{R} + \vec{P}_1 \cdot d\vec{R}_1 + \vec{P}_2 \cdot d\vec{R}_2 \right). \tag{3.10}$$

Even though we were not able to compute the fifth action in the SPS, this integral becomes quite simple in the EPS. Crucially, when computing the fifth action in the EPS, the result is fiberwise constant, meaning it can be written with only observable variables $(\vec{R}, \vec{P}, \vec{S}_1, \vec{S}_2)$. In other words, the dependence of this action on the unmeasurable variables occurs only through the combinations $\vec{S}_1 = \vec{R}_1 \times \vec{P}_1$ and $\vec{S}_2 = \vec{R}_2 \times \vec{P}_2$. This makes it possible to treat the fifth action as a function of only the SPS variables.

To see that the function $\mathcal{J}_5$ on the base manifold is indeed an action, we need to show that the flow in B generated by $\mathcal{J}_5$ recurs with period 2π. What is the relationship between the flow in B and in E? For every point $b \in B$, there is an entire fiber $\pi^{-1}(b) \in E$, and there is a different integral curve starting at every point on the fiber. By construction, the flow in E along each of these integral curves recurs with period 2π. What is not obvious is that after flowing by parameter λ, these points (on any given fiber) do not end up on different fibers, but rather on one single fiber. This is a consequence of Eq. (3.7), which ensures that there is a consistent sense of horizontal vector fields. We denote the vector field generated by f with

$$X_f^B \equiv \{f, \cdot\}_B = \Omega_B^{-1}(df, \cdot)\,, \tag{3.11}$$

and similarly $X_f^E \equiv \{f, \cdot\}_E$. The compatibility of the brackets tells us that

$$\pi_\star(X^E_{(\pi^\star f)}) = X_f^B\,, \tag{3.12}$$

which is that the horizontal component of $X^E_{(\pi^\star f)}$ is fiberwise constant. This ensures that flows starting from all initial conditions along a fiber stay "synchronized" in the horizontal direction, and always in the fiber over the flow in the base manifold. Finally, since any flow in E recurs after parameter 2π, so does the flow in B.

While the flow recurs in both E and B with period 2π, one might worry that there is a shorter period in B, some fraction $2\pi/k$ for $k > 1$. This could happen if the simple loop $C \in E$ is a k-fold covering of a simple loop in B. While we are not aware of any topological obstruction to this possibility, we argue that our specific construction below does not generate this situation. As we will see in Sec. 3.3, we construct a piecewise closed curve $C \in E$ by following the flow under several generators, one of which is $X^E_{S_{\rm eff}\cdot L}$. By construction this curve is homotopic to the flow under $X^E_{\mathcal{J}_5}$, which generates the closed curve $\tilde{C} \in E$. The homotopy $C \sim \tilde{C}$ is mapped to the homotopy of the images, $\pi(C) \sim \pi(\tilde{C})$. So, it suffices to argue that C is not a multiple covering of a simple loop. Here we can use the fact that the only generator of our piecewise curve that changes the mutual angles between the three angular momenta (e.g. $\hat{L}\cdot\hat{S}_1$; see Sec. 3.3) is $S_{\rm eff}\cdot L$, and we flow by exactly one precession period of $S_{\rm eff}\cdot L$. Thus $\pi(\tilde{C})$ cannot traverse a loop more than once.

We make a few closing remarks before we turn to evaluating the fifth action integral. Because of the nonstandard EPS procedure, we numerically verified that flowing by 2π under the fifth action derived from Eq. (3.10) yields a closed loop (as required for the flow along an action variable), within numerical errors, whether treated as an SPS function or EPS function. Also, the first four action integrals computed in Ref. [21] via area integrals in B, when pulled back to E, are the same as the ones derived from the loop integral Eq. (3.10) in E. In summary, the equivalence of the two pictures (in terms of integrability, action-angle variables, and most importantly, the evolution under a flow associated with any observable), the global exactness of the symplectic form Ω_E, and the ease of evaluation of the action variables, make us prefer the EPS for the action computation.

3.3 Computing the fifth action

Four out of the five actions were already presented in Ref. [21]. Here we compute the fifth one. None of the previously-computed actions pertained to the spin-orbit precession of the BBH. Therefore, we generate a curve on the invariant torus by flowing under $S_{\rm eff} \cdot L$ for one precession cycle. Although the mutual angles between $(\vec{L}, \vec{S}_1, \vec{S}_2)$ return to their original values, the frame has been rotated, so the curve is not a closed loop. However, flowing under (J^2, L^2, S_1^2, S_2^2) can close the loop, without affecting the previously-mentioned mutual angles (and therefore ensuring that the loop we constructed is in a different homotopy class than the four associated to the other actions; note that we do not need to flow along H or J_z).

So, to compute the action in Eq. (2.10), we will flow under each of $(S_{\rm eff} \cdot L, J^2, L^2, S_1^2, S_2^2)$ by different parameter amounts $\Delta\lambda_k$, forming a closed loop. The integral can be computed piecewise as five integrals,

$$\mathcal{J}_5 = \mathcal{J}_{S_{\rm eff}\cdot L} + \mathcal{J}_{J^2} + \mathcal{J}_{L^2} + \mathcal{J}_{S_1^2} + \mathcal{J}_{S_2^2}, \tag{3.13}$$

where each part corresponds to the segment generated by flowing under the quantity in the subscript. The main difficulty is determining the appropriate parameter amounts $\Delta\lambda_k$.

Focusing on $\mathcal{J}_{S_{\rm eff}\cdot L}$, we will need the evolution equations under the flow of $S_{\rm eff} \cdot L$ which read

$$\frac{d\vec{R}}{d\lambda} = \vec{S}_{\rm eff} \times \vec{R}, \tag{3.14a}$$

$$\frac{d\vec{P}}{d\lambda} = \vec{S}_{\rm eff} \times \vec{P}, \tag{3.14b}$$

$$\frac{d\vec{R}_a}{d\lambda} = \sigma_a \left(\vec{L} \times \vec{R}_a\right), \tag{3.14c}$$

$$\frac{d\vec{P}_a}{d\lambda} = \sigma_a \left(\vec{L} \times \vec{P}_a\right), \tag{3.14d}$$

and they imply

$$\frac{d\vec{L}}{d\lambda} = \vec{S}_{\rm eff} \times \vec{L}, \tag{3.15a}$$

$$\frac{d\vec{S}_a}{d\lambda} = \sigma_a \left(\vec{L} \times \vec{S}_a \right). \tag{3.15b}$$

From these evolution equations we have

$$2\pi \mathcal{J}_{S_{\rm eff}\cdot L} = 2\pi(\mathcal{J}^{\rm orb} + \mathcal{J}^{\rm spin}) \tag{3.16}$$

$$= \int_{\lambda_i}^{\lambda_f} \left(P_i \frac{dR^i}{d\lambda} + P_{1i} \frac{dR_1^i}{d\lambda} + P_{2i} \frac{dR_2^i}{d\lambda} \right) d\lambda$$

$$= \int_{\lambda_i}^{\lambda_f} \Big(\vec{P} \cdot (\vec{S}_{\rm eff} \times \vec{R}) + \vec{P}_1 \cdot (\sigma_1 \vec{L} \times \vec{R}_1)$$

$$+ \vec{P}_2 \cdot (\sigma_2 \vec{L} \times \vec{R}_2) \Big) \, d\lambda \tag{3.17}$$

$$= 2 \int_{\lambda_i}^{\lambda_f} (S_{\rm eff} \cdot L) \, d\lambda = 2(S_{\rm eff} \cdot L) \Delta\lambda_{S_{\rm eff}\cdot L}, \tag{3.18}$$

$$\mathcal{J}_{S_{\rm eff}\cdot L} = \frac{(S_{\rm eff} \cdot L)\Delta\lambda_{S_{\rm eff}\cdot L}}{\pi} \tag{3.19}$$

with $\Delta\lambda_{S_{\rm eff}\cdot L}$ being the amount of flow required under $S_{\rm eff} \cdot L$. We could pull $S_{\rm eff} \cdot L$ out of the integral since it is a constant under the flow of $S_{\rm eff} \cdot L$. After performing similar calculations, we can also show that (see also Sec. III-A of Ref. [21])

$$\mathcal{J}_{J^2} = \frac{J^2 \Delta\lambda_{J^2}}{\pi}, \tag{3.20a}$$

$$\mathcal{J}_{L^2} = \frac{L^2 \Delta\lambda_{L^2}}{\pi}, \tag{3.20b}$$

$$\mathcal{J}_{S_1^2} = \frac{S_1^2 \Delta\lambda_{S_1^2}}{\pi}, \tag{3.20c}$$

$$\mathcal{J}_{S_2^2} = \frac{S_2^2 \Delta\lambda_{S_2^2}}{\pi}, \tag{3.20d}$$

where the quantities $\Delta\lambda$ are the flow amounts required under the corresponding commuting constant

in the subscript. This finally renders the fifth action to be

$$\mathcal{J}_5 = \frac{1}{\pi}\Big\{(S_{\rm eff}\cdot L)\Delta\lambda_{S_{\rm eff}\cdot L} + J^2\Delta\lambda_{J^2} + L^2\Delta\lambda_{L^2} + S_1^2\Delta\lambda_{S_1^2} + S_2^2\Delta\lambda_{S_2^2}\Big\}. \tag{3.21}$$

Evaluating the five parameter flow amounts will occupy the remainder of this section.

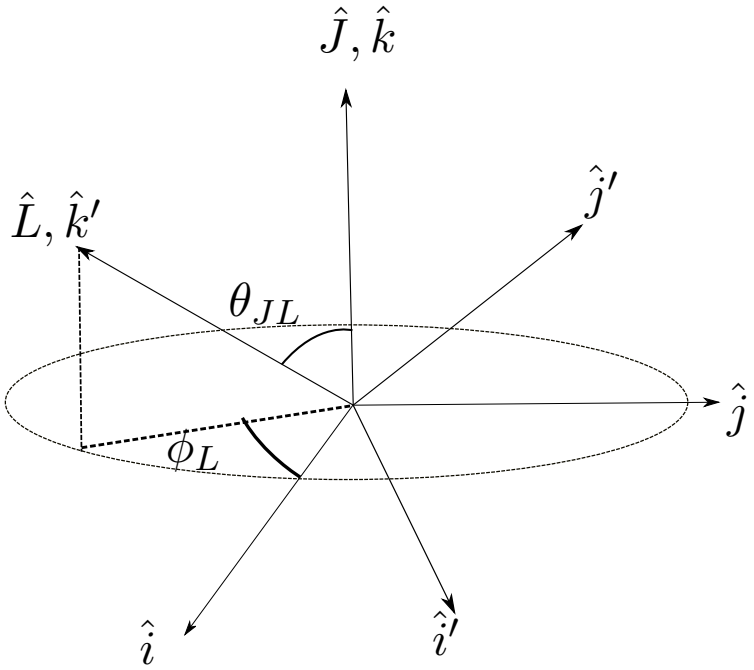

Figure 3.2: Frame $(i'j'k')$ triad is displayed along with the inertial (ijk) triad .

Evaluating the flow amounts $\Delta\lambda$'s

In this subsection, we will rely heavily on the methods of integration first presented in Ref. [20], while trying to integrate the evolution equations for flow under H, with the 1PN Hamiltonian terms omitted. We first need to set up some vector bases before we can integrate the equations of motion. Fig. 3.2 displays two sets of bases. The one in which the components of a vector will be assumed to be written in this chapter is the inertial triad (ijk), unless stated otherwise. Since

vector derivatives (as geometrical objects) depend on the frame in which the derivatives are taken, we mention here that this (ijk) triad is also the frame in which all the derivatives of any general vector will be assumed to be taken.[2]

3.3.0.1 Evaluating $\Delta\lambda_{S_{\rm eff}\cdot L}$

The evaluation of $\Delta\lambda_{S_{\rm eff}\cdot L}$ can happen only when we can compute the mutual angles between $\vec{L}, \vec{S}_1$ and $\vec{S}_2$ as a function of the flow parameter under the flow of $S_{\rm eff}\cdot L$. Therefore, most of 3.3.0.1 deals with how to do this calculation and only towards the end we arrive at the expression of $\Delta\lambda_{S_{\rm eff}\cdot L}$.

Under the flow of $S_{\rm eff}\cdot L$, a generic quantity g evolves as $dg/d\lambda = \{g, S_{\rm eff}\cdot L\}$ which implies the following evolution equations for the dot products between the three angular momenta under the flow of $S_{\rm eff}\cdot L$

$$\begin{aligned}&\frac{1}{\sigma_2}\frac{d(\vec{L}\cdot\vec{S}_1)}{d\lambda} = -\frac{1}{\sigma_1}\frac{d(\vec{L}\cdot\vec{S}_2)}{d\lambda}\\ =&\frac{1}{(\sigma_1-\sigma_2)}\frac{d(\vec{S}_1\cdot\vec{S}_2)}{d\lambda} = \vec{L}\cdot(\vec{S}_1\times\vec{S}_2),\end{aligned} \tag{3.22}$$

which means that we can easily construct three constants of motion (dependent on the 5 basic constants). These are the differences between the three quantities

$$\left\{\frac{\vec{L}\cdot\vec{S}_1}{\sigma_2}\,,\ -\frac{\vec{L}\cdot\vec{S}_2}{\sigma_1}\,,\ \frac{\vec{S}_1\cdot\vec{S}_2}{\sigma_1-\sigma_2}\right\}\,. \tag{3.23}$$

whose λ derivatives are all equal to the triple product $\vec{L}\cdot(\vec{S}_1\times\vec{S}_2)$. Namely, these constants of motion are

$$\begin{aligned}\Delta_1 &= \frac{\vec{S}_1\cdot\vec{S}_2}{\sigma_1-\sigma_2} - \frac{\vec{L}\cdot\vec{S}_1}{\sigma_2}\\ &= \frac{1}{\sigma_1-\sigma_2}\left[\frac{1}{2}(J^2-L^2-S_1^2-S_2^2) - \frac{\vec{L}\cdot\vec{S}_{\rm eff}}{\sigma_2}\right],\end{aligned} \tag{3.24}$$

[2]Recall that in general, the derivative of a vector as seen in a frame is a different geometrical object from the derivative of the vector as seen in a different frame [22].

$$\Delta_2 = \frac{\vec{S}_1 \cdot \vec{S}_2}{\sigma_1 - \sigma_2} + \frac{\vec{L} \cdot \vec{S}_2}{\sigma_1}$$
$$= \frac{1}{\sigma_1 - \sigma_2}\left[\frac{1}{2}(J^2 - L^2 - S_1^2 - S_2^2) - \frac{\vec{L} \cdot \vec{S}_{\rm eff}}{\sigma_1}\right], \tag{3.25}$$
$$\Delta_{21} = \frac{\vec{L} \cdot \vec{S}_1}{\sigma_2} + \frac{\vec{L} \cdot \vec{S}_2}{\sigma_1}$$
$$= \frac{\vec{L} \cdot \vec{S}_{\rm eff}}{\sigma_1 \sigma_2}. \tag{3.26}$$

Stated differently, all this means that the three mutual angles between $\vec{L}$, $\vec{S}_1$, and $\vec{S}_2$ satisfy linear relationships. If we define the mutual angles as $\cos\kappa_1 \equiv \hat{L} \cdot \hat{S}_1$, $\cos\kappa_2 \equiv \hat{L} \cdot \hat{S}_2$, and $\cos\gamma \equiv \hat{S}_1 \cdot \hat{S}_2$, their relations are

$$\cos\gamma = \Sigma_1 + \frac{L}{S_2}\frac{\sigma_1 - \sigma_2}{\sigma_2}\cos\kappa_1 \tag{3.27}$$
$$\cos\kappa_2 = \Sigma_2 - \frac{\sigma_1 S_1}{\sigma_2 S_2}\cos\kappa_1, \tag{3.28}$$

where

$$\Sigma_1 = \frac{(\sigma_1 - \sigma_2)\Delta_1}{S_1 S_2} = \frac{\sigma_2(J^2 - L^2 - S_1^2 - S_2^2) - 2S_{\rm eff} \cdot L}{2\sigma_2 S_1 S_2}, \tag{3.29}$$
$$\Sigma_2 = \frac{S_{\rm eff} \cdot L}{\sigma_2 L S_2} = \frac{\Delta_{21}\sigma_1}{L S_2}. \tag{3.30}$$

We will integrate the solution for

$$f \equiv \frac{\vec{S}_1 \cdot \vec{S}_2}{\sigma_1 - \sigma_2} = \frac{S_1 S_2 \cos\gamma}{\sigma_1 - \sigma_2}, \tag{3.31}$$
$$\frac{df}{d\lambda} = \vec{L} \cdot (\vec{S}_1 \times \vec{S}_2), \tag{3.32}$$

which is the most symmetrical of the three dot products given above. Thus if we have a solution for $f(\lambda)$, we automatically have solutions for the three dot products,

$$\vec{S}_1 \cdot \vec{S}_2 = (\sigma_1 - \sigma_2) f, \tag{3.33}$$

$$\vec{L} \cdot \vec{S}_1 = \sigma_2(f - \Delta_1), \tag{3.34}$$

$$\vec{L} \cdot \vec{S}_2 = -\sigma_1(f - \Delta_2). \tag{3.35}$$

The triple product on the RHS of Eq. (3.32) is the signed volume of the parallelepiped with ordered sides $\vec{L}, \vec{S}_1, \vec{S}_2$. In general, for a parallelepiped with sides $\vec{\mathcal{A}}, \vec{\mathcal{B}}, \vec{C}$, and dot products

$$\vec{\mathcal{A}} \cdot \vec{\mathcal{B}} = \mathcal{A}\,\mathcal{B}\cos\gamma', \tag{3.36}$$

$$\vec{\mathcal{A}} \cdot \vec{C} = \mathcal{A}\,C\cos\beta', \tag{3.37}$$

$$\vec{\mathcal{B}} \cdot \vec{C} = \mathcal{B}\,C\cos\alpha', \tag{3.38}$$

a standard result from analytical geometry is that the signed volume of this parallelepiped can be written as

$$V = \vec{\mathcal{A}} \cdot (\vec{\mathcal{B}} \times \vec{C}) = \pm\mathcal{A}\mathcal{B}C\left[1 + 2(\cos\alpha')(\cos\beta')(\cos\gamma') - \cos^2\alpha' - \cos^2\beta' - \cos^2\gamma'\right]^{1/2}, \tag{3.39}$$

where the sign is decided on the basis of the handedness of the $(\vec{\mathcal{A}}, \vec{\mathcal{B}}, \vec{C})$ triad. The radicand is always non-negative. We can use this equation to write the evolution equation for f as

$$\frac{df}{d\lambda} = \pm\sqrt{P(f)}\,, \tag{3.40}$$

where the cubic $P(f) \geq 0$ and is given by

$$P(f) = L^2S_1^2S_2^2 + 2(\vec{L}\cdot\vec{S}_1)(\vec{L}\cdot\vec{S}_2)(\vec{S}_1\cdot\vec{S}_2) - L^2(\vec{S}_1\cdot\vec{S}_2)^2 - S_1^2(\vec{L}\cdot\vec{S}_2)^2 - S_2^2(\vec{L}\cdot\vec{S}_1)^2\,, \tag{3.41}$$

$$= L^2S_1^2S_2^2 - 2\sigma_1\sigma_2(\sigma_1 - \sigma_2)f(f - \Delta_1)(f - \Delta_2) - L^2(\sigma_1 - \sigma_2)^2f^2$$
$$- S_2^2\sigma_2^2(f - \Delta_1)^2 - S_1^2\sigma_1^2(f - \Delta_2)^2\,, \tag{3.42}$$

where we have used Eq. (3.33)-(3.35) to rewrite in terms of f and constants. This is a general

cubic, which we will write as

$$P(f) = a_3 f^3 + a_2 f^2 + a_1 f + a_0 \,, \tag{3.43}$$

with the coefficients

$$a_3 = 2\sigma_1\sigma_2 \left(\sigma_2 - \sigma_1\right) \,, \tag{3.44a}$$

$$a_2 = 2\left(\Delta_1 + \Delta_2\right)\left(\sigma_1 - \sigma_2\right)\sigma_1\sigma_2 - L^2\left(\sigma_1 - \sigma_2\right)^2 - \sigma_1^2 S_1^2 - \sigma_2^2 S_2^2 \,, \tag{3.44b}$$

$$a_1 = 2\left[\sigma_1^2 S_1^2 \Delta_2 + \sigma_2^2 S_2^2 \Delta_1 + \sigma_1\sigma_2\Delta_1\Delta_2(\sigma_2 - \sigma_1)\right] \,, \tag{3.44c}$$

$$a_0 = L^2 S_1^2 S_2^2 - \sigma_1^2 S_1^2 \Delta_2^2 - \sigma_2^2 S_2^2 \Delta_1^2 \,. \tag{3.44d}$$

It is important here to note the sign of a_3,

$$\mathrm{sgn}(a_3) = \begin{cases} +1 \,, & m_1 > m_2 \,, \\ 0 \,, & m_1 = m_2 \,, \\ -1 \,, & m_1 < m_2 \,. \end{cases} \tag{3.45}$$

The fact that the cubic degenerates to a quadratic when $m_1 = m_2$ is the reason to treat the equal mass case separately.

Now we rewrite the cubic in terms of its roots,

$$P(f) = A(f - f_1)(f - f_2)(f - f_3) \,, \tag{3.46}$$

where $A = a_3$ is the leading term, and when all three roots are real, we assume the ordering $f_1 \leq f_2 \leq f_3$.

For completeness, we state the roots in the trigonometric form. The cubic can be depressed

by defining $g \equiv f + a_2/(3a_3)$ in terms of which P becomes $P = a_3(g^3 + pg + q)$ with the coefficients

$$p = \frac{3a_1a_3 - a_2^2}{3a_3^2}\,, \qquad\qquad q = \frac{2a_2^3 - 9a_1a_2a_3 + 27a_0a_3^2}{27a_3^3}\,. \tag{3.47}$$

When there are three real solutions, $p < 0$, and the argument to the arccos below will be in $[-1, +1]$. In terms of these depressed coefficients, the trigonometric solutions for the roots are

$$f_k = -\frac{a_2}{3a_3} + 2\sqrt{\frac{-p}{3}}\cos\left[\frac{1}{3}\arccos\left(\frac{3q}{2p}\sqrt{\frac{-3}{p}}\right) + \frac{2\pi k}{3}\right]\,. \tag{3.48}$$

This form yields the desired ordering $f_1 \le f_2 \le f_3$.

Whenever any two of the vectors $\{\vec{L}, \vec{S}_1, \vec{S}_2\}$ are collinear, the triple product on the RHS of Eq. (3.32) vanishes. A less drastic degeneracy is if two roots coincide. Here we will restrict ourselves to the case of three simple roots (at the end of Sec. 3.4, we will argue that the cubic has three real roots for the cases of interest). Since $P(f) \ge 0$, we have

$$\begin{cases} f_1 \le f \le f_2\,, & m_1 > m_2\,, \\ f_2 \le f \le f_3\,, & m_1 < m_2\,. \end{cases} \tag{3.49}$$

That is, f will lie between the two roots where $P(f) > 0$. Without loss of generality we will take $m_1 > m_2$ and handle only this case. Below, we treat $\sqrt{P(f)}$ as an analytic function on a Riemann surface with two sheets and branch points at the roots, which we avoid. With an appropriate contour we will integrate

$$\frac{df}{\sqrt{(f - f_1)(f - f_2)(f - f_3)}} = \sqrt{A}\,d\lambda\,. \tag{3.50}$$

Reparameterize this integral via

$$f = f_1 + (f_2 - f_1)\sin^2\phi_p \tag{3.51}$$

$$df = 2(f_2 - f_1)\sin\phi_p \cos\phi_p \, d\phi_p \, . \tag{3.52}$$

We define ϕ_p so it increases monotonically with λ as

$$\frac{2\, d\phi_p}{\sqrt{(f_3 - f_1) - (f_2 - f_1)\sin^2\phi_p}} = \sqrt{A} d\lambda \, . \tag{3.53}$$

Now factor out $(f_3 - f_1)$ from the radicand in the denominator to give

$$\frac{d\phi_p}{\sqrt{1 - k^2 \sin^2\phi_p}} = \frac{1}{2}\sqrt{A(f_3 - f_1)} d\lambda \, , \tag{3.54}$$

where we have defined

$$k \equiv \sqrt{\frac{f_2 - f_1}{f_3 - f_1}}. \tag{3.55}$$

Note that $0 < k < 1$, because of the ordering of the roots. Equation (3.54) can be integrated to give

$$u \equiv F(\phi_p, k) = \frac{1}{2}\sqrt{A(f_3 - f_1)}(\alpha + [\lambda - \lambda_0]) \, , \tag{3.56}$$

where $F(\phi_p, k)$ is the incomplete elliptic integral of the first kind defined as [51]

$$F(\phi, k) \equiv \int_0^\phi \frac{\mathrm{d}\theta}{\sqrt{1 - k^2 \sin^2\theta}}. \tag{3.57}$$

In Eq. (3.56), λ_0 is the initial value of the flow parameter and α is an integration constant,[3]

$$\alpha = \frac{2}{\sqrt{A\,(f_3 - f_1)}} F\left(\arcsin\sqrt{\frac{f\,(\lambda_0) - f_1}{f_2 - f_1}}, k\right). \tag{3.58}$$

[3]In Eq. (3.58), the branch choice of arcsin depends on the initial sign of $df/d\lambda$. When $df/d\lambda > 0$, take the principal branch of arcsin; if $df/d\lambda < 0$, use the next branch.

We can now rewrite the parameterization in terms of the Jacobi sn and amplitude am functions [51],

$$\mathrm{sn}(u,k) \equiv \sin(\mathrm{am}(u,k)) \equiv \sin\phi_p\,. \tag{3.59}$$

This turns our original parameterization into

$$f(\lambda) = f_1 + (f_2 - f_1)\,\mathrm{sn}^2(u(\lambda),k). \tag{3.60}$$

The solution for f is thus given by Eq. (3.60) accompanied by Eqs. (3.56) and (3.58).

From this solution for $f(\lambda)$, we recover solutions for the three dot products $\vec{S}_1\cdot\vec{S}_2$, $\vec{L}\cdot\vec{S}_1$, and $\vec{L}\cdot\vec{S}_2$, by using Eqs. (3.33)-(3.35). We also immediately get the λ-period of the precession. One precession cycle occurs when ϕ_p goes from 0 to π, or when f starts from f_1, goes to f_2 and then returns back to f_1 (see parameterization in Eq. (3.51)). Integrating on this interval via Eq. (3.56) gives the equation for the λ-period of precession, which we call Λ, in terms of the complete elliptic integral of the first kind $K(k) \equiv F(\pi/2,k) = F(\pi,k)/2$,

$$\Lambda\sqrt{A(f_3 - f_1)} = 2F(\pi,k) = 4K(k). \tag{3.61}$$

Recall that our goal is to close a loop in the EPS by successively flowing under $S_{\mathrm{eff}}\cdot L, J^2, L^2, S_1^2$, and S_2^2. A necessary condition for the phase-space loop to close is that the mutual angles between $\vec{L}, \vec{S}_1$, and $\vec{S}_2$ recur at the end of the flow. Since the flows under J^2, L^2, S_1^2, and S_2^2 do not change these mutual angles, we flow under $S_{\mathrm{eff}}\cdot L$ by exactly the precession period,

$$\Delta\lambda_{S_{\mathrm{eff}}\cdot L} = \Lambda. \tag{3.62}$$

3.3.0.2 Evaluating $\Delta\lambda_{J^2}$

After flowing under $S_{\mathrm{eff}}\cdot L$ by parameter $\Delta\lambda_{S_{\mathrm{eff}}\cdot L}$, the mutual angles between $\vec{L}, \vec{S}_1$, and $\vec{S}_2$ have recurred, but $\vec{L}$ and other quantities have been moved. We now plan to flow under J^2 by $\Delta\lambda_{J^2}$

so that $\vec{L}$ is restored; this restoration is a necessary condition for closing the phase space loop. To find the required amount of flow under J^2 so that $\vec{L}$ is restored, we need to find the final state of $\vec{L}$ after flowing under $S_{\rm eff} \cdot L$ by $\Delta\lambda_{S_{\rm eff}\cdot L}$. Instead of working with Cartesian components, we find it more convenient to work with the angles $\vec{L}$ makes in a new frame.

Without loss of generality, we choose the z-axis along the $\vec{J}$ vector. Now there are two angles to find: the "polar" θ_{JL}, where $\cos\theta_{JL} = \vec{J}\cdot\vec{L}/(JL)$, and an "azimuthal" ϕ_L. This ϕ_L is only defined up to an overall global (time-independent) rotation about $\vec{J}$.

Since we have already solved for the angles between $\vec{L}, \vec{S}_1$, and $\vec{S}_2$, in Sec. 3.3.0.1, we also have the angle θ_{JL},

$$\vec{J}\cdot\vec{L} = JL\cos\theta_{JL} = L^2 + \vec{S}_1\cdot\vec{L} + \vec{S}_2\cdot\vec{L}\,. \tag{3.63}$$

This shows that θ_{JL} has recurred after the $S_{\rm eff}\cdot L$ flow, because all the mutual angles between $\vec{L}, \vec{S}_1$, and $\vec{S}_2$ have. So, what remains to be tackled is the azimuthal angle ϕ_L. Since ϕ_L is only defined up to an overall constant, we get a differential equation for $d\phi_L/d\lambda$ (which is the rate of precession of the *line of nodes*). $\vec{L}$ in component form is

$$\vec{L} = L(\sin\theta_{JL}\cos\phi_L, \sin\theta_{JL}\sin\phi_L, \cos\theta_{JL})\,, \tag{3.64}$$

and therefore it follows that

$$\begin{aligned}\frac{d\vec{L}}{d\lambda} =& L\left(\cos\theta_{JL}\cos\phi_L\frac{d\theta_{JL}}{d\lambda} - \sin\theta_{JL}\sin\phi_L\frac{d\phi_L}{d\lambda}, \cos\theta_{JL}\sin\phi_L\frac{d\theta_{JL}}{d\lambda} + \sin\theta_{JL}\cos\phi_L\frac{d\phi_L}{d\lambda},\right.\\ &\left. -\sin\theta_{JL}\frac{d\theta_{JL}}{d\lambda}\right)\,.\end{aligned} \tag{3.65}$$

With the aid of the instantaneous azimuthal direction vector given by

$$\hat{\phi} = \frac{\vec{J}\times\vec{L}}{|\vec{J}\times\vec{L}|} = \frac{\vec{J}\times\vec{L}}{JL\sin\theta_{JL}} = \frac{\hat{z}\times\vec{L}}{L\sin\theta_{JL}}\,, \tag{3.66}$$

we can extract $d\phi_L/d\lambda$ via an elementary result involving the dot product $\hat{\phi}\cdot(d\vec{L}/d\lambda)$

$$\hat{\phi}\cdot\frac{d\vec{L}}{d\lambda} = L\sin\theta_{JL}\frac{d\phi_L}{d\lambda}\,. \tag{3.67}$$

This leads to

$$\frac{d\phi_L}{d\lambda} = \frac{\hat{\phi}\cdot(d\vec{L}/d\lambda)}{L\sin\theta_{JL}} = \frac{\vec{J}\times\vec{L}}{JL^2\sin^2\theta_{JL}}\cdot\frac{d\vec{L}}{d\lambda}\,. \tag{3.68}$$

Now using $d\vec{L}/d\lambda = -d\vec{S}_1/d\lambda - d\vec{S}_2/d\lambda$, and inserting the precession equations for the two spins,

$$\frac{d\phi_L}{d\lambda} = \frac{1}{JL^2\sin^2\theta_{JL}}(\vec{J}\times\vec{L})\cdot(\vec{S}_{\rm eff}\times\vec{L}) = \frac{J}{J^2L^2-(\vec{J}\cdot\vec{L})^2}\left[(\vec{J}\cdot\vec{S}_{\rm eff})L^2-(\vec{J}\cdot\vec{L})(\vec{L}\cdot\vec{S}_{\rm eff})\right] \tag{3.69}$$

$$= \frac{J\left[(\sigma_1S_1^2+\sigma_2S_2^2+(\sigma_1+\sigma_2)\vec{S}_1\cdot\vec{S}_2)L^2-(\vec{S}_1\cdot\vec{L}+\vec{S}_2\cdot\vec{L})(\vec{L}\cdot\vec{S}_{\rm eff})\right]}{J^2L^2-(L^2+\vec{S}_1\cdot\vec{L}+\vec{S}_2\cdot\vec{L})^2}\,. \tag{3.70}$$

We see that everything on the RHS is given in terms of constants of motion ($J, L, \vec{L}\cdot\vec{S}_{\rm eff}$) and the inner products between the three angular momenta (which can be found from $f(\lambda)$ in the previous section). Put everything in terms of f using Eqs. (3.33)-(3.35) and separate into partial fractions,

$$\frac{d\phi_L}{d\lambda} = \frac{J\left[(\sigma_1S_1^2+\sigma_2S_2^2+(\sigma_1^2-\sigma_2^2)f)L^2-(\sigma_2(f-\Delta_1)-\sigma_1(f-\Delta_2))(\vec{L}\cdot\vec{S}_{\rm eff})\right]}{J^2L^2-(L^2+\sigma_2(f-\Delta_1)-\sigma_1(f-\Delta_2))^2} \tag{3.71}$$

$$= \frac{B_1}{D_1-(\sigma_1-\sigma_2)f}+\frac{B_2}{D_2-(\sigma_1-\sigma_2)f}\,, \tag{3.72}$$

where we have defined

$$B_1 = \frac{1}{2}\left[(\vec{L}\cdot\vec{S}_{\rm eff}+L^2(\sigma_1+\sigma_2))(J+L)+L\left(\sigma_1S_1^2+\sigma_2S_2^2+(\sigma_1+\sigma_2)(\Delta_2\sigma_1-\Delta_1\sigma_2)\right)\right]\,, \tag{3.73}$$

$$B_2 = \frac{1}{2}\left[(\vec{L}\cdot\vec{S}_{\rm eff} + L^2(\sigma_1+\sigma_2))(J-L) - L\left(\sigma_1 S_1^2 + \sigma_2 S_2^2 + (\sigma_1+\sigma_2)(\Delta_2\sigma_1 - \Delta_1\sigma_2)\right)\right], \tag{3.74}$$

$$D_1 = L(L+J) + \Delta_2\sigma_1 - \Delta_1\sigma_2\,, \tag{3.75}$$

$$D_2 = L(L-J) + \Delta_2\sigma_1 - \Delta_1\sigma_2\,. \tag{3.76}$$

So we need to be able to perform the two integrals (with $i = 1, 2$)

$$I_i \equiv \int \frac{B_i}{D_i - (\sigma_1-\sigma_2)f} d\lambda = \int \frac{B_i}{D_i - (\sigma_1-\sigma_2)f}\frac{d\lambda}{df} df \tag{3.77}$$

$$= \int \frac{\pm B_i}{D_i - (\sigma_1-\sigma_2)f} \frac{df}{\sqrt{A(f-f_1)(f-f_2)(f-f_3)}}\,, \tag{3.78}$$

where the last equality is due to Eq. (3.40). With these integrals, we will have

$$\int \frac{d\phi_L}{d\lambda} d\lambda = \phi_L(f) - \phi_{L,0} = I_1 + I_2\,. \tag{3.79}$$

The integrals I_i are another type of incomplete elliptic integral (defined below). Using the parameterization of Eqs. (3.51) and (3.52), I_i becomes

$$I_i(\lambda) = \int^{\phi_p} \frac{B_i}{D_i - (\sigma_1-\sigma_2)(f_1 + (f_2-f_1)\sin^2\phi_p)} \frac{2d\phi_p}{\sqrt{A(f_3-f_1)(1-k^2\sin^2\phi_p)}} \tag{3.80}$$

$$= \frac{2B_i}{\sqrt{A(f_3-f_1)}} \frac{1}{D_i - f_1(\sigma_1-\sigma_2)} \int^{\phi_p} \frac{1}{1-\alpha_i^2\sin^2\phi_p} \frac{d\phi_p}{\sqrt{1-k^2\sin^2\phi_p}}\,, \tag{3.81}$$

where we have defined

$$\alpha_i^2 \equiv \frac{(\sigma_1-\sigma_2)(f_2-f_1)}{D_i - f_1(\sigma_1-\sigma_2)}\,. \tag{3.82}$$

Thus we can identify the I_i's in terms of the incomplete elliptic integral of the third kind, which is

defined as [51]

$$\Pi(a,b,c) \equiv \int_0^b \frac{1}{\sqrt{1-c^2\sin^2\theta}} \frac{d\theta}{1-a\sin^2\theta}\,. \tag{3.83}$$

I_i thus becomes

$$I_i(\lambda) = \frac{2B_i}{\sqrt{A(f_3-f_1)}} \frac{\Pi(\alpha_i^2, \mathrm{am}(u(\lambda),k),k)}{D_i - f_1(\sigma_1-\sigma_2)}\,, \tag{3.84}$$

and we get the solution for $\phi_L(\phi_p)$

$$\phi_L(\lambda) - \phi_{L,0} = \frac{2}{\sqrt{A(f_3-f_1)}} \left[\frac{B_1\Pi(\alpha_1^2,\phi_p,k)}{D_1 - f_1(\sigma_1-\sigma_2)} + \frac{B_2\Pi(\alpha_2^2,\phi_p,k)}{D_2 - f_1(\sigma_1-\sigma_2)} \right]. \tag{3.85}$$

Here $\phi_{L,0}$ is an integration constant to be determined by inserting $\lambda = \lambda_0$ and $\phi_L = \phi_L(\lambda_0)$ into the equation.

To close the loop, we need to know the angle $\Delta\phi_L$ that ϕ_L goes through under one period of the precession cycle (when flowing under $\vec{L}\cdot\vec{S}_{\mathrm{eff}}$), that is, when ϕ_p advances by π. This is given in terms of the *complete* elliptic integral of the third kind, $\Pi(\alpha^2,k) \equiv \Pi(\alpha^2,\pi/2,k)$ yielding

$$\Delta\phi_L \equiv \phi_L(\lambda_0+\Lambda) - \phi_L(\lambda_0) = \frac{4}{\sqrt{A(f_3-f_1)}} \left[\frac{B_1\Pi(\alpha_1^2,k)}{D_1 - f_1(\sigma_1-\sigma_2)} + \frac{B_2\Pi(\alpha_2^2,k)}{D_2 - f_1(\sigma_1-\sigma_2)} \right], \tag{3.86}$$

where we have used the fact that $\Pi(\alpha^2,\pi,k) = 2\Pi(\alpha^2,k)$.

To negate this angular offset caused by flowing under $S_{\mathrm{eff}}\cdot L$ and thereby closing the loop, we need to flow under J^2 by

$$\Delta\lambda_{J^2} = -\frac{\Delta\phi_L}{2J}. \tag{3.87}$$

Note that this flow does not alter the mutual angles between $\vec{L}$, $\vec{S}_1$, and $\vec{S}_2$, as necessary to close the loop in the phase space. Now that the angles within the triad $(\vec{L},\vec{S}_1,\vec{S}_2)$ have recurred and the full vector $\vec{L}$ has recurred, the concern is if the spin vectors have recurred. The spin vectors constrained

not only by their mutual angles within the $(\vec{L}, \vec{S}_1, \vec{S}_2)$ triad, but also with $\vec{J}$. Their angles with $\vec{J}$ are algebraically related to the previous mutual angles, e.g. $\vec{J} \cdot \vec{S}_2 = \vec{L} \cdot \vec{S}_1 + \vec{S}_1 \cdot \vec{S}_2 + S_2^2$. All of the angle cosines have recurred, which narrows down to two solutions: the original configuration for $(\vec{L}, \vec{S}_1, \vec{S}_2)$, and its reflection in the J-L plane. We can rule out the reflected solution with the following observation. The original configuration and its reflection have opposite signs for the signed volume $\vec{L} \cdot (\vec{S}_1 \times \vec{S}_2)$, and thus opposite signs for the radical $\sqrt{P(f)}$. The two different signs correspond to the two different sheets of the Riemann surface, and by integrating in f space from f_1 to f_2 and back to f_1, we have gone around two branch points, ending up on the same sheet, with the same original orientation. Therefore, after the flows by $S_{\text{eff}} \cdot L$ and J^2, each of the three vectors $(\vec{L}, \vec{S}_1, \vec{S}_2)$ have recurred.

3.3.0.3 Evaluating $\Delta\lambda_{L^2}$

After flowing under $S_{\text{eff}} \cdot L$ and J^2, all the three angular momenta $\vec{L}$, $\vec{S}_1$, and $\vec{S}_2$ have recurred, but the orbital vectors $(\vec{R}, \vec{P})$ and sub-spin vectors have not. We will now restore $\vec{R}$ and $\vec{P}$ by flowing under L^2 by $\Delta\lambda_{L^2}$, to be determined in this section. At this point we introduce a non-inertial frame (NIF) with $(i'j'k')$ axes whose basis vectors are unit vectors along $\vec{J} \times \vec{L}, \vec{L} \times (\vec{J} \times \vec{L})$ and $\vec{L}$ respectively, as depicted pictorially in Fig. 3.2.

Now, $\vec{R}$ has to be in the $i'j'$ plane because $\vec{R} \perp \vec{L}$. Denote by ϕ the angle made by $\vec{R}$ with the i' axis. The key point is that after successively flowing under $S_{\text{eff}} \cdot L$ (with $S_{\text{eff}} \cdot L \equiv \vec{S}_{\text{eff}} \cdot \vec{L}$) by $\lambda_{S_{\text{eff}} \cdot L}$, J^2 by λ_{J^2}, and L^2 by a certain amount λ_{L^2} (to be calculated), if ϕ is restored, then so are $\vec{R}$ and $\vec{P}$. This is so because under these three flows, R, P and $\vec{R} \cdot \vec{P}$ do not change. Hence the restoration of ϕ after the above three flows by the above stated amounts restores both $\vec{R}$ and $\vec{P}$.

Our strategy is to compute ϕ under the flow of $S_{\text{eff}} \cdot L$. The flow under J^2 does not change the NIF angle ϕ, since J^2 rigidly rotates all vectors together. And in the end, we will undo the change to ϕ (caused by the $S_{\text{eff}} \cdot L$ flow) by flowing under L^2.

Under the flow of $S_{\text{eff}} \cdot L$, we have

$$\dot{\vec{R}} = \left\{ \vec{R}, S_{\text{eff}} \cdot L \right\} = \vec{S}_{\text{eff}} \times \vec{R}. \tag{3.88}$$

To write the components of this equation in the NIF, we need the components of all the individual vectors involved in the same frame which are given by

$$\vec{R} = \begin{bmatrix} R\cos\phi \\ R\sin\phi \\ 0 \end{bmatrix}_n , \ \vec{L} = \begin{bmatrix} 0 \\ 0 \\ L \end{bmatrix}_n ,$$
$$\vec{J} = \begin{bmatrix} 0 \\ J\sin\theta_{JL} \\ J\cos\theta_{JL} \end{bmatrix}_n , \ \vec{S}_1 = S_1 \begin{bmatrix} \sin\kappa_1\cos\xi_1 \\ \sin\kappa_1\sin\xi_1 \\ \cos\kappa_1 \end{bmatrix}_n ,$$
$$\vec{S}_2 = S_2 \begin{bmatrix} \sin\kappa_2\cos\xi_2 \\ \sin\kappa_2\sin\xi_2 \\ \cos\kappa_2 \end{bmatrix}_n , \tag{3.89}$$

where ϕ is the azimuthal angle of $\vec{R}$ in the NIF. Here the letter 'n' beside these columns indicate that the components are in the NIF and ξ_i's are the azimuthal angles of $\vec{S}_i$ in the NIF.

The Euler matrix $\tilde{\Lambda}$ which when multiplied with the column consisting of a vector's components in the inertial frame gives its components in the NIF is

$$\tilde{\Lambda} = \begin{pmatrix} \cos\phi_L & \sin\phi_L & 0 \\ -\sin\phi_L\cos\theta_{JL} & \cos\phi_L\cos\theta_{JL} & \sin\theta_{JL} \\ \sin\phi_L\sin\theta_{JL} & -\cos\phi_L\sin\theta_{JL} & \cos\theta_{JL} \end{pmatrix} \tag{3.90}$$

Now we take the $\vec{R}$ in Eq. (3.89), evaluate its components in the inertial frame using $\tilde{\Lambda}^{-1}$. We then differentiate each of these components with respect to λ (the flow parameter under $S_{\text{eff}} \cdot L$) and transform these components back to the NIF using $\tilde{\Lambda}$, thus finally yielding the components (in the non-inertial frame) of the derivative of $\vec{R}$. The result comes out to be (keeping in mind that

$dR/d\lambda = 0$)

$$\dot{\vec{R}} = \begin{bmatrix} -R\sin\phi(\dot{\phi_L}\cos\theta_{JL} + \dot{\phi}) \\ R\cos\phi(\dot{\phi_L}\cos\theta_{JL} + \dot{\phi}) \\ R(-\dot{\phi_L}\sin\theta_{JL}\cos\phi + \dot{\theta}_{JL}\sin\phi) \end{bmatrix}_n . \tag{3.91}$$

Plugging Eqs. (3.89) and (3.91) in Eq. (3.88) and using the first two components of the resulting matrix equation gives us

$$\frac{d\phi}{d\lambda} = \sigma_1 S_1 \cos\kappa_1 + \sigma_2 S_2 \cos\kappa_2 - \cos\theta_{JL}\frac{d\phi_L}{d\lambda} \tag{3.92}$$

Note that since simply replacing $\cos\phi$ and $\sin\phi$ in Eqs. (3.89) for $\vec{R}$ with their derivatives would have yielded the derivative of NIF components of $\vec{R}$, whereas we need the NIF components of the inertial-frame derivative, which forms the LHS of Eq. (3.88).

We digress a bit to write $\vec{J} = \vec{L} + \vec{S}_1 + \vec{S}_2$ in component form in the NIF using Eqs. (3.89). Only the third component is of interest to us,

$$J\cos\theta_{JL} = L + S_1\cos\kappa_1 + S_2\cos\kappa_2 . \tag{3.93}$$

We use this equation for θ_{JL}, and Eqs. (3.72) for $d\phi_L/d\lambda$, to write $d\phi/d\lambda$ in terms of κ_1, κ_2, and γ. Finally using Eqs. (3.33)-(3.35) to express everything in terms of f, we get

$$\frac{d\phi}{d\lambda} = \frac{B_1}{D_1 - (\sigma_1 - \sigma_2)\,f} - \frac{B_2}{D_2 - (\sigma_1 - \sigma_2)\,f} - \frac{S_{\text{eff}}\cdot L + (\Delta_1 - \Delta_2)\sigma_1\sigma_2 + L^2(\sigma_1 + \sigma_2)}{L}. \tag{3.94}$$

This is the equivalent of Eq. (3.72) for $d\phi_L/d\lambda$, and therefore its solution can be found in a totally parallel way to what led us to $\phi_L(\lambda)$ in Eq. (3.85). This gives us

$$\phi(\lambda) - \phi_0 = \frac{2}{\sqrt{A\,(f_3 - f_1)}}\left[\frac{B_1\Pi\left(\alpha_1^2, \phi_p, k\right)}{D_1 - f_1\,(\sigma_1 - \sigma_2)} - \frac{B_2\Pi\left(\alpha_2^2, \phi_p, k\right)}{D_2 - f_1\,(\sigma_1 - \sigma_2)}\right]$$

$$- \left(S_{\text{eff}} \cdot L + (\Delta_1 - \Delta_2)\, \sigma_1 \sigma_2 + L^2\, (\sigma_1 + \sigma_2) \right) \frac{(\lambda - \lambda_0)}{L}\,, \tag{3.95}$$

where again the integration constant ϕ_0 is determined by inserting $\lambda = \lambda_0$ and $\phi = \phi(\lambda_0)$ into this equation.

The angle $\Delta\phi$ that ϕ goes through under one period of the precession cycle when flowing under $\vec{L} \cdot \vec{S}_{\text{eff}}$, is given in a similar manner as we arrived at Eq. (3.86). We get

$$\begin{aligned} \Delta\phi \equiv \phi(\lambda_0 + \Lambda) - \phi(\lambda_0) = \frac{4}{\sqrt{A(f_3 - f_1)}} \left[\frac{B_1 \Pi(\alpha_1^2, k)}{D_1 - f_1(\sigma_1 - \sigma_2)} - \frac{B_2 \Pi(\alpha_2^2, k)}{D_2 - f_1(\sigma_1 - \sigma_2)} \right] \\ - \left(S_{\text{eff}} \cdot L + (\Delta_1 - \Delta_2)\, \sigma_1 \sigma_2 + L^2\, (\sigma_1 + \sigma_2) \right) \frac{\Lambda}{L}\,. \end{aligned} \tag{3.96}$$

To negate this angular offset caused by flowing under $S_{\text{eff}} \cdot L$, we need to flow under L^2 by

$$\Delta\lambda_{L^2} = -\frac{\Delta\phi}{2L}. \tag{3.97}$$

Note that this flow does not change any of the three angular momenta $\vec{L}$, $\vec{S}_1$, or $\vec{S}_2$, which is necessary for closing the loop in the phase space.

3.3.0.4 Evaluating $\Delta\lambda_{S_1^2}$ and $\Delta\lambda_{S_2^2}$

Once we have made sure that $\vec{R}$, $\vec{P}$, $\vec{S}_1$, $\vec{S}_2$ and hence also $\vec{L}$ have been restored by successively flowing under $S_{\text{eff}} \cdot L$, J^2, and L^2 by $\Delta\lambda_{S_{\text{eff}} \cdot L}$, $\Delta\lambda_{J^2}$ and $\Delta\lambda_{L^2}$ respectively, now is the time to restore the sub-spin vectors $\vec{R}_{1/2}$ and $\vec{P}_{1/2}$. The strategy and calculations are analogous to the ones for $\vec{R}$ and $\vec{P}$, so we won't explicate them in full detail. We will show the basic roadmap and the final results.

For the purposes of these calculations, the relevant figure is Fig. 3.3, which shows a second non-inertial frame $(i'' j'' k'')$ centered around $\vec{S}_1$. Its axes point along $\vec{J} \times \vec{S}_1$, $\vec{S}_1 \times (\vec{J} \times \vec{S}_1)$ and $\vec{S}_1$, respectively. We also use this figure to introduce the definitions of the azimuthal angle ϕ_{S_1} and polar angle θ_{JS_1} pictorially. Also, just like ϕ was the angle between $\vec{R}$ and the i' axis in 3.3.0.3, we define ϕ_1 to be the angle between $\vec{R}_1$ and i'' axis, with the understanding that $\vec{R}_1$ must lie in the

$i''j''$ plane.

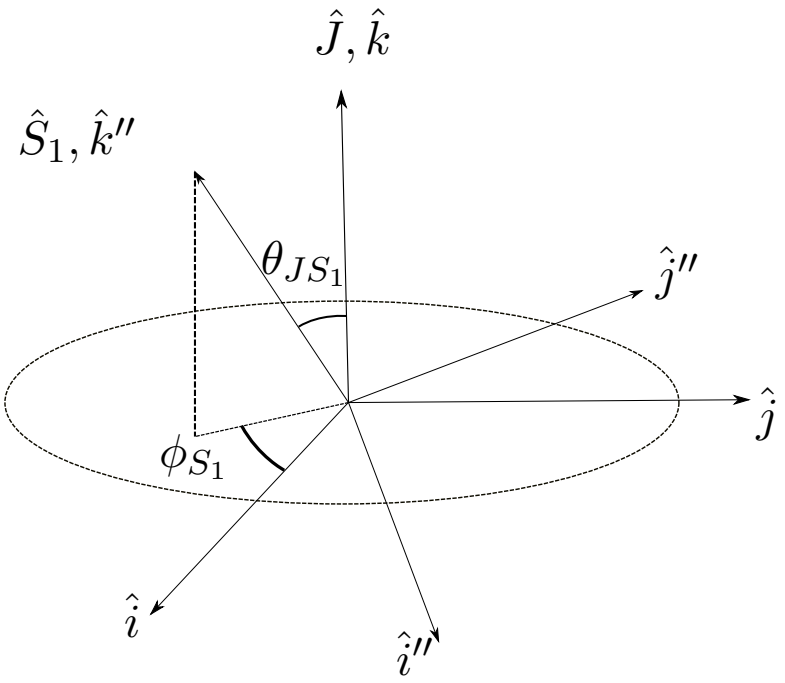

Figure 3.3: Frame $(i''j''k'')$ is displayed along with the inertial (ijk) frame.

Now, just like in Secs. 3.3.0.2 and 3.3.0.3, all we have to worry about is to restore the change in ϕ_1 which an $S_{\rm eff} \cdot L$ flow (by $\lambda_{S_{\rm eff} \cdot L}$) brings about, for doing so would imply that both $\vec{R}_1$ and $\vec{P}_1$ have been restored. The justifications are analogous to those presented in Secs. 3.3.0.2 and 3.3.0.3 while dealing with the orbital sector. We won't do the calculations for the sub-spin variables for the other black hole because the calculations are of the same nature of that for the first one. Now we proceed to compute the change in ϕ_1 brought about by the $S_{\rm eff} \cdot L$ flow.

We denote components in the $(i''j''k'')$ frame by using the subscript $n2$. In this frame we have

$$\vec{J} = \begin{bmatrix} 0 \\ J \sin\theta_{JS_1} \\ J \cos\theta_{JS_1} \end{bmatrix}_{n2} , \ \vec{S}_1 = \begin{bmatrix} 0 \\ 0 \\ S_1 \end{bmatrix}_{n2} . \tag{3.98}$$

We also have

$$\vec{L} = L \begin{bmatrix} \sin\kappa_1 \cos\xi_3 \\ \sin\kappa_1 \sin\xi_3 \\ \cos\kappa_1 \end{bmatrix}_{n2} , \vec{S}_2 = S_2 \begin{bmatrix} \sin\gamma \cos\xi_4 \\ \sin\gamma \sin\xi_4 \\ \cos\gamma \end{bmatrix}_{n2} . \tag{3.99}$$

Here ξ_3 and ξ_4 are the azimuthal angles of $\vec{L}$ and $\vec{S}_2$, respectively, in the $(i''j''k'')$ frame. We now write the third component of $\vec{J} \equiv \vec{L} + \vec{S}_1 + \vec{S}_2$ in the (i'', j'', k'') frame as

$$J\cos\theta_{JS_1} = S_1 + L\cos\kappa_1 + S_2\cos\gamma\,. \tag{3.100}$$

The derivative of $\vec{S}_1$ along the flow of $S_{\rm eff}\cdot L$ (denoted by a dot) is

$$\dot{\vec{S}}_1 \equiv \frac{d\vec{S}_1}{d\lambda} = \left\{\vec{S}_1, \vec{S}_{\rm eff}\cdot\vec{L}\right\} = \sigma_1\vec{L}\times\vec{S}_1. \tag{3.101}$$

The analog of $d\phi/d\lambda$ given in Eq. (3.68) becomes

$$\frac{d\phi_{S_1}}{d\lambda} = \frac{\vec{J}\times\vec{S}_1}{JS_1^2\sin^2\theta_{JS_1}}\cdot\frac{d\vec{S}_1}{d\lambda}\,. \tag{3.102}$$

Using Eq. (3.101), we can arrive at the analog of $d\phi/d\lambda$ as a function of f [Eq. (3.72)],

$$\frac{d\phi_{S_1}}{d\lambda} = J\sigma_2 + \frac{B_{1S}}{D_{1S}+\sigma_1 f} + \frac{B_{2S}}{D_{2S}+\sigma_1 f}\,, \tag{3.103}$$

where we have defined

$$B_{1S} = \frac{1}{2}\left[-S_1\sigma_1(L^2 - JS_1 + S_1^2 + \Delta_2\sigma_1) + (J-S_1)^2S_1\sigma_2 - (J-2S_1)\Delta_1\sigma_1\sigma_2 + (J-S_1)\Delta_1\sigma_2^2\right] \tag{3.104}$$

$$B_{2S} = \frac{1}{2}\left[S_1\sigma_1(L^2 + JS_1 + S_1^2 + \Delta_2\sigma_1) - (J+S_1)^2S_1\sigma_2 - (J+2S_1)\Delta_1\sigma_1\sigma_2 + (J+S_1)\Delta_1\sigma_2^2\right] \tag{3.105}$$

$$D_{1S} = (S_1 - J)S_1 - \Delta_1\sigma_2\,, \tag{3.106}$$

$$D_{2S} = (S_1 + J)S_1 - \Delta_1\sigma_2\,. \tag{3.107}$$

Analogous to matrix equations for $\vec{R}$ and $\dot{\vec{R}}$ in Eqs. (3.89) and (3.91), we can write $\vec{R}_1$ in the component form as

$$\vec{R}_1 = \begin{pmatrix} R_1\cos\phi_1 \\ R_1\sin\phi_1 \\ 0 \end{pmatrix}_{n2}\,, \tag{3.108}$$

and its derivative as (keeping in mind that $dR_1/d\lambda = 0$ along the flow under $S_{\text{eff}}\cdot L$)

$$\dot{\vec{R}}_1 = \begin{pmatrix} -R_1\sin\phi_1\left(\dot{\phi}_{S1}\cos\theta_{JS_1} + \dot{\phi}_1\right) \\ R_1\cos\phi_1\left(\dot{\phi}_{S_1}\cos\theta_{JS_1} + \dot{\phi}_1\right) \\ R_1\left(-\dot{\phi}_{S_1}\sin\theta_{JS_1}\cos\phi_1 + \dot{\theta}_{JS_1}\sin\phi_1\right) \end{pmatrix}_{n2} \tag{3.109}$$

Also, along the flow under $S_{\text{eff}}\cdot L$, $\vec{R}_1$ evolves as

$$\dot{\vec{R}}_1 = \sigma_1\vec{L}\times\vec{R}_1. \tag{3.110}$$

Using Eqs. (3.99), (3.108), and (3.109) to express Eq. (3.110) in component form and either the first or the second component of the equation when supplemented with Eqs. (3.100) and (3.103) to eliminate $\cos\theta_{JS_1}$ and $d\phi_{S_1}/d\lambda$ gives us $\dot{\phi}_1$. We again write the partial fraction form (analogous to Eq. (3.94))

$$\dot{\phi}_1 = S_1(\sigma_2 - \sigma_1) - \left(\frac{B_{1S}}{D_{1S} + \sigma_1 f} - \frac{B_{2S}}{D_{2S} + \sigma_1 f}\right). \tag{3.111}$$

We have also used Eqs. (3.27), (3.28), and (3.31) to write the cosines of κ_1, κ_2, and γ in terms of f.

Finally, in a way very similar to how $\Delta\phi$ in Eq. (3.96) was found, we find the angle $\Delta\phi_1$ that

ϕ_1 goes through under one period of the precession cycle when flowing under $\vec{L} \cdot \vec{S}_{\text{eff}}$. We get

$$\Delta\phi_1 = \frac{-4}{\sqrt{A\,(f_3 - f_1)}} \left[\frac{B_{1S}\Pi\left(\alpha_{1S}^2, k\right)}{D_{1S} + f_1\sigma_1} - \frac{B_{2S}\Pi\left(\alpha_{2S}^2, k\right)}{D_{2S} + f_1\sigma_1} \right] + S_1(\sigma_2 - \sigma_1)\Lambda, \tag{3.112}$$

where we have defined

$$\alpha_{iS}^2 \equiv \frac{-\sigma_1(f_2 - f_1)}{D_{iS} + f_1\sigma_1}\,. \tag{3.113}$$

To negate this angular offset brought about flowing under $S_{\text{eff}} \cdot L$, we need to flow under S_1^2 by

$$\Delta\lambda_{S_1^2} = -\frac{\Delta\phi_1}{2S_1}, \tag{3.114}$$

And similarly, $\Delta\lambda_{S_2^2}$ can also be arrived at using calculations of the same nature as for $\Delta\lambda_{S_1^2}$. So, we won't present them here.

At long last, the fifth action is given by Eq. (3.21), where the $\Delta\lambda$'s are presented in Eqs. (3.62), (3.87), (3.97), (3.114) and the expression for $\Delta\lambda_{S_2^2}$ (not presented here). It is this action variable under whose flow (by an amount of 2π), we numerically verified that we get a closed loop (within numerical errors), whether we view this action as a function of the SPS variables or the EPS variables. We point out that unlike the previously computed actions in Ref. [21], we had to invoke the EPS picture to compute the fifth action, though it would be interesting to see if it can be computed purely in the SPS. There is another difference to highlight between the computation of the fifth action as compared to the first three [21]. The flows under J^2, J_z, and L^2 already individually form closed loops, which translates to their associated actions being functions of just these individual conserved quantities. Meanwhile the flow of $S_{\text{eff}} \cdot L$ does not form a closed loop by itself, so the fifth action ended up being a function of all of $J, L, S_{\text{eff}} \cdot L, S_1$, and S_2, since we needed all of these additional flows to form a closed loop.

Fifth action in the equal mass case

The above result for the fifth action (Eq. (3.21)) is not manifestly finite in the equal mass limit: there are many factors of $(\sigma_1 - \sigma_2)$ which vanish in this limit, including some in denominators, and one which makes the cubic $P(f)$ degenerate to a quadratic. We have checked numerically that the equal mass limit of $\mathcal{J}_5$ is finite, but trying to take this limit analytically is cumbersome. There is however a simpler way, and the solvability of the equal-mass case has been independently investigated in the literature, albeit in the orbit- and precession-averaged approach [52].

For $\sigma_1 = \sigma_2$, it is easy to check that $\vec{S}_1 \cdot \vec{S}_2$, along with H, J^2, L^2, and J_z forms a set of five mutually commuting constants. In fact, $S_{\rm eff} \cdot L$ can then be seen as a function of these five constants, and is therefore no longer an independent constant. It can be checked that under the flow of $\vec{S}_1 \cdot \vec{S}_2$ we have the flow equations

$$\left\{\vec{S}_1, \vec{S}_1 \cdot \vec{S}_2\right\} = \vec{S} \times \vec{S}_1 = \left\{\vec{S}_1 \cdot \vec{S}_2, \vec{S}_2\right\} = \vec{S}_2 \times \vec{S}, \tag{3.115}$$

and these imply that both the spin vectors rotate around $\vec{S} \equiv \vec{S}_1 + \vec{S}_2$ which itself remains fixed. At this point we can simply use the result of Eq. (28) of Ref. [21] with $\hat{n} = \vec{S}/S$, which gives our fifth action variable for the equal mass case as

$$\widetilde{\mathcal{J}}_{5(m_1=m_2)} = (\vec{S}_1 + \vec{S}_2) \cdot \vec{S}/S = S, \tag{3.116}$$

without needing to do any integral in the orbital sector, since $\vec{R}$ and $\vec{P}$ don't evolve when flowing under $\vec{S}_1 \cdot \vec{S}_2$. The reason we used a tilde in the above equation is because $\widetilde{\mathcal{J}}_{5(m_1=m_2)}$ need not be the equal mass limit of $\mathcal{J}_5$, since action variables of a system are not unique; see Proposition 11.3 of Ref. [33].

Finally, using the equal mass relations

$$J^2 = L^2 + S_1^2 + S_2^2 + 2(\vec{L} \cdot \vec{S} + \vec{S}_1 \cdot \vec{S}_2), \tag{3.117}$$

$$S_{\rm eff} \cdot L = \frac{7}{4}\vec{L} \cdot \vec{S}, \tag{3.118}$$

$$S^2 = S_1^2 + S_2^2 + 2\vec{S}_1 \cdot \vec{S}_2, \tag{3.119}$$

in Eq. (38) of Ref. [21], it is possible to arrive at an equation connecting the Hamiltonian with the actions. Performing a PN series inversion, one can write an explicit expression for the Hamiltonian in terms of the actions, up to 1.5PN. This can be used to explicitly obtain the frequencies of the system via $\omega_i = \partial H/\partial \mathcal{J}_i$.

3.4 Fifth action at the leading PN order

The action variable given by Eq. (3.21) is in exact form with respect to the 1.5PN Hamiltonian H. It is a worthwhile exercise to write the leading order contribution of this action because it is a much shorter expression than the exact one. This is in the same spirit as the expression of the fourth action variable which was presented in Eq. (38) of Ref. [21]. Another advantage is that we can then write $S_{\rm eff} \cdot L$ in terms of the actions, including the fifth one (discussed below), which when used in Eq. (38) of Ref. [21] can give an expression for Hamiltonian in terms of the actions.

Note that out of the five actions: $J, L, J_z, \mathcal{J}_4$, and $\mathcal{J}_5$ (see Ref. [21] for the first four), the first two coincide with each other at 1PN order due to the absence of spins. The next important action variable at 1PN is the analog of $\mathcal{J}_4$ [24] since the 1PN Hamiltonian does not depend on J_z. This explains the presence of only two frequencies (resulting from effectively two actions) at 1PN. Since $\mathcal{J}_5$ comes into play for the first time only at the 1.5PN order, we can sensibly seek only its leading PN order contribution, which we turn to now.

We now sketch the plan for how to obtain the leading PN contribution to $\mathcal{J}_5$. It comprises a couple of steps which were performed in MATHEMATICA.

Step 1: To start with, instead of writing the various quantities which make up $\mathcal{J}_5$ in terms of the five commuting constants, write them only in terms of $\vec{L}, \vec{S}_1, \vec{S}_2, \sigma_1$ and σ_2 with the understanding that $\vec{S}_1$ and $\vec{S}_2$ are 0.5PN order higher than $\vec{L}$ (see Ref. [21] for more details on this). Attach a formal

PN order counting parameter ϵ to $\vec{S}_1$ and $\vec{S}_2$. This ϵ will be used as a PN perturbative expansion parameter: every power of ϵ stands for an extra 0.5PN order. At the end of the calculation, ϵ will be set equal to 1. Writing various quantities of interest in terms of $\vec{L}, \vec{S}_1$, and $\vec{S}_2$ is imperative since it serves to expose the PN powers explicitly. For example, $J^2 - L^2 = O(\epsilon)$, though both J^2 and L^2 are $O(\epsilon^0)$.

Step 2: Instead of trying to series expand $\mathcal{J}_5$ directly in terms of ϵ in one go, we first series expand various quantities that make up $\mathcal{J}_5$, and then use these expanded versions to finally build up the series-expanded version of $\mathcal{J}_5$. As a first step, series expand the cubic expression of Eq. (3.42) and its roots, keeping terms at $O(\epsilon^2)$. Expansion of the roots up to $O(\epsilon^2)$ is necessary because the turning points f_1 and f_2 coincide at lower orders.

Step 3: Series expand various other quantities that make up $\mathcal{J}_5$, such as $k^2, B_1, B_2, D_1, D_2, \alpha_1$ and α_2 in ϵ such that the resulting expansions have two non-zero post-Newtonian terms. We don't have to worry about series expanding certain other quantities which make up $\Delta\lambda_4$ and $\Delta\lambda_5$, since they don't contribute to the fifth action variable at the leading order.

Step 4: Using these series-expanded ingredients, build up $\mathcal{J}_5$ of Eq. (3.21). The PN orders of the five additive parts of $\mathcal{J}_5$ (as shown in Eq. (3.13)) are schematically shown here as

$$\mathcal{J}_{S_{\rm eff}\cdot L} = O(\epsilon), \tag{3.120}$$

$$\mathcal{J}_{J^2} = \mathcal{J}_0\epsilon^0 + O(\epsilon), \tag{3.121}$$

$$\mathcal{J}_{L^2} = -\mathcal{J}_0\epsilon^0 + O(\epsilon), \tag{3.122}$$

$$\mathcal{J}_{S_1^2} = O(\epsilon^2), \tag{3.123}$$

$$\mathcal{J}_{S_2^2} = O(\epsilon^2), \tag{3.124}$$

where we have indicated that the leading order components of $\mathcal{J}_{J^2}$ and $\mathcal{J}_{L^2}$ cancel each other. Our leading order $\mathcal{J}_5$ is thus the sum of the first three contributions. The last two contributions being at

sub-leading orders can be dropped. At this point we can set $\epsilon = 1$.

Step 5: At this point the resulting perturbative $\mathcal{J}_5$ is a function of $\vec{L}, \vec{S}_1, \vec{S}_2, \sigma_1, \sigma_2$ and dot products formed out of them. We still want to write this as a function of the commuting constants only, keeping in line with the tradition followed in the action-angle variables formalism. To do so, we eliminate $\vec{L} \cdot \vec{S}_1$ and $\vec{L} \cdot \vec{S}_2$ using the following results valid up to the leading PN order

$$\vec{L} \cdot \vec{S}_1 \sim + \frac{2S_{\rm eff} \cdot L - (J^2 - L^2 - S_1^2 - S_2^2)\sigma_2}{2(\sigma_1 - \sigma_2)}, \tag{3.125a}$$

$$\vec{L} \cdot \vec{S}_2 \sim - \frac{2S_{\rm eff} \cdot L - (J^2 - L^2 - S_1^2 - S_2^2)\sigma_1}{2(\sigma_1 - \sigma_2)}, \tag{3.125b}$$

which finally yields the leading PN order contribution to $\mathcal{J}_5$ as

$$\begin{aligned}\mathcal{J}_5 \sim & \frac{1}{4L|\sigma_1 - \sigma_2| \left(C_1^2 - 4L^2 \left({S_1}^2 + {S_2}^2\right)\right)} \times \\ & \Big[C_1^3 C_2(\sigma_1 + \sigma_2) - 4C_1^2 C_2(S_{\rm eff} \cdot L) + 4C_1 L^2 \left\{{S_1}^2(C_2(\sigma_1 - \sigma_2) + 2\sigma_1)\right. \\ & \left. + {S_2}^2(C_2(\sigma_2 - \sigma_1) + 2\sigma_2)\right\} - 16L^2(S_{\rm eff} \cdot L)\left({S_1}^2 + {S_2}^2\right)\Big],\end{aligned} \tag{3.126}$$

where the following definitions have been assumed

$$C_1 = J^2 - L^2 - S_1^2 - S_2^2, \tag{3.127}$$

$$C_2 = \left[1 - \frac{4(C_1\sigma_1 - 2S_{\rm eff} \cdot L)(C_1\sigma_2 - 2S_{\rm eff} \cdot L)}{(C_1(\sigma_1 + \sigma_2) - 4S_{\rm eff} \cdot L)^2 - 4L^2(\sigma_1 - \sigma_2)^2\left({S_1}^2 + {S_2}^2\right)}\right]^{1/2} - 1. \tag{3.128}$$

We could have chosen to eliminate $\vec{L} \cdot \vec{S}_1$ and $\vec{L} \cdot \vec{S}_2$ using slightly modified forms of Eqs. (3.125) by simply ignoring S_1^2 and S_2^2 terms in the numerator. These modified forms of Eqs. (3.125) and the resulting modified form of the leading order contribution to the fifth action would still agree with the original results (Eqs. (3.125) and Eq. (3.126)) up to the leading PN order.

We note that the expression of the leading PN order contribution to the fifth action in

Eq. (3.126) is much shorter than that of the exact 1.5PN fifth action (when both are expressed in terms of the commuting constants). This could be used in an efficient implementation of the evaluation of the fifth action on a computer.

We also note that Eq. (3.126) can be used to arrive at a quartic equation in $S_{\rm eff} \cdot L$ with other action variables as parameters of this quartic equation. This means it is in principle possible to solve for $S_{\rm eff} \cdot L$ as a function of the actions. By inserting this into Eq. (38) of Ref. [21], we can explicitly find the 1.5PN $H(\vec{\mathcal{J}})$ as a function of all of the actions (after a PN series inversion). This gives an alternative approach for computing the frequencies $\omega_i = \partial H/\partial \mathcal{J}_i$ which can be compared with the approach in Sec. 2.4.

We have numerically verified that $\mathcal{J}_5$ as presented in Eq. (3.126) above converges to the exact 1.5PN version in the limit of small PN parameter ($S_1, S_2 \ll L$).

Now we try to address the issue of the nature of roots of the cubic $P(f)$ of Eq. (3.43). It is predicated on the nature of the discriminant D, with a positive D implying three real roots, negative D implying one real and two distinct complex roots, and $D = 0$ implies repeated roots. The discriminant of the exact cubic $P(f)$ is too complicated for us to investigate its sign. We rather choose to investigate the sign of its leading order PN contribution. It is in the same spirit as the calculation of the leading PN order contribution of $\mathcal{J}_5$ above. We write D in terms of $\vec{L}$, $\vec{S}_1$, and $\vec{S}_2$ while attaching a formal power counting parameter ϵ to both $\vec{S}_1$ and $\vec{S}_2$. Then series-expand D in ϵ and keep only the leading order term which comes out to be

$$\begin{aligned} D \sim\ & 4L^4 \left[L^2 S_1^2 - \left(\vec{L}\cdot\vec{S}_1\right)^2\right]\left[L^2 S_2^2 - \left(\vec{L}\cdot\vec{S}_2\right)^2\right] \\ & \times (\sigma_1 - \sigma_2)^6 \epsilon^4 + O(\epsilon^5)\,. \end{aligned} \tag{3.129}$$

In "general position" this is positive. If both spins are aligned or anti-aligned with $\vec{L}$, we will have repeated roots, and the spins will remain aligned or anti-aligned with $\vec{L}$ as the system evolves under the flows of $S_{\rm eff} \cdot L$ or H. Aside from this special case, the PN limit suggests that the $D < 0$ case of only one real root is disallowed. This is necessary on physical grounds, as there must be two

turning points for the mutual angle variable f.

3.5 Conclusions

We finally finish the action-angle variables line of work by computing the fifth action in this chapter. Typically, action-angle variables are found by separating the Hamilton-Jacobi (HJ) equation [22], though we were able to work them out without separating the HJ equation. Finally from this vantage point, we summarize the major ingredients which went into computing the action-angle variables of a spinning BBH with arbitrary masses and eccentricity at the leading 1.5PN order (the subject of this and the last chapter): (1) the classic complex contour integration method for the Newtonian system proposed by Sommerfeld [22]; (2) its PN extension by Damour and Schäfer [24]; (3) the integration techniques worked out in the context of the 1.5PN Hamiltonian flow in Ref. [20]; and finally (4) the method of extending the phase space by inventing the unmeasurable extended phase-space variables.

In the context of our new mathematical method of computing action variables via the introduction of the unmeasurable sub-spin variables, there is a possibility of a mathematically oriented study of this method. A few pertinent questions along this line could be (1) Is there a way to compute the fifth action without introducing the unmeasurable variables? (2) Are there other situations (with other topologically nontrivial symplectic manifolds) where an otherwise intractable action computation can be made possible using this new method? (3) What is the deeper geometrical reason that makes this method work?

CHAPTER 4

INTEGRABILITY OF BINARY BLACK HOLES AT 2PN

The contents of this chapter can be found at Ref. [4].

4.1 Introduction

This chapter will try to address the challenge of determining whether the "generic" BBH systems (two BHs, with their spins misaligned from the orbital angular momentum, in an eccentric orbit) are integrable or not. Integrability is defined as a condition when a dynamical system possesses action-angle variables. Integrable systems are nice in that they cannot be chaotic and are more amenable to analytical modeling or numerical simulations. Eccentricity leads to apsidal precession, and spin-orbit coupling leads to precession of both the spins and the orbital plane. Such complicated nonlinear dynamics in a high dimensional phase space leads to the fear of chaos. One ultimate goal of studying the BBH problem is to produce rapid gravitational-wave predictions—and chaos would obstruct the possibility of analytical waveforms. Showing the integrability of the system and the existence of action-angle variables opens the door to constructing a closed-form analytical waveform model. The study of chaos and integrability in the spinning, eccentric BBH system has an interesting history [19, 36, 41, 53–63]. We will recap some of the highlights below. Some of the claims in the literature seem at odds with each other. Besides our main results, we will also explain these apparent contradictions and correct some misstatements in the literature regarding integrability of the BBH system.

The generic BBH system, in Hamiltonian form, has long been known to be integrable at the 1.5 post-Newtonian (PN) order [28]. This comes from the Liouville-Arnold theorem [31, 32]: the ten-dimensional phase space has five independent constants of motion, which all pairwise commute

under the Poisson bracket. This integrability leads to the existence of an analytic solution [26]. At 2PN, Levin [53, 54] performed numerical simulations and concluded that the generic BBH system is chaotic. Schnittman and Rasio [56] also simulated generic systems at 2PN, and by measuring the Lyapunov exponent, found either no chaos, or weak chaos with a Lyapunov time which was many times greater than the inspiral time. Soon after, Cornish and Levin [57] found the Lyapunov and inspiral time-scale could be comparable to each other, though they warned that the Lyapunov time is coordinate-dependent. Hartl and Buonanno [36] performed a survey of generic orbits, simulating them at 2PN (and including some PN terms that previous authors had not). For the most part, they found regular (i.e. non-chaotic) orbits, though they did report chaos in some cases, which they reported to be astrophysically disfavored. Though not discussed in any of these works, the coexistence of regular and chaotic orbits in phase space is a typical characteristic of a nearly-integrable system, proven in the KAM theorem [31, 32]. This applies to the second and higher PN Hamiltonians, when treated as a perturbation to the integrable 1.5PN Hamiltonian.

There have also been a number of analytical studies of integrability. Damour [28] pointed out the additional constants of motion, though did not emphasize that they commute or that the generic BBH is integrable. Königsdörffer and Gopakumar [19, 64] suggested integrability at higher PN order, by constructing an analytic solution for two specific mass/spin configurations, and removing all spin terms in the Hamiltonian except for the leading order spin-orbit interaction. Beyond the 1.5PN spin-orbit effect, the next non-trivial effect on integrability is the spin-spin interactions at 2PN, which is conjectured to source chaotic behavior [53]. Let us also mention that some analytic work [58–63] has discussed integrability by only counting the number of constants of motion, which is not enough for the Liouville-Arnold theorem: the constants must be mutually commuting. For example, while each of the three components J_i are constants, they do not commute with each other.

Along independent lines, a large body of literature has been developed by taking advantage of orbit-averaging and precession-averaging. The principle at work is that there is a large separation of timescales, $t_{\rm orb} \ll t_{\rm prec} \ll t_{\rm rad}$; so the orbital variables' influence on precession dynamics may

be approximated by averaging, and similarly for precession-averaging. Early post-Newtonian works invoking orbit-averaging to study spin effects include [29, 40, 41], and precession-averaging followed in [42, 43]. An important milestone was Racine's discovery that a quantity $\vec{L} \cdot \vec{S}_0$ (to be introduced later) is constant under the *Newtonian-orbit-average* of the 2PN equations of motion (EOMs), despite not being constant under the full 2PN equations. We will briefly comment on the relation of our results to the averaged results.

In this chapter, we show integrability at 2PN. These are both part of the larger program to eventually build analytical waveform models for the generic spinning, eccentric BBH system. The known integrability at 1.5PN implies the existence of action-angle variables. We then proceed to 2PN, where in the spirit of perturbation theory, we add an ansatz for PN corrections to the 1.5PN exactly-commuting constants, and solve for these corrections to find the 2PN-valid constants. We work with the full 2PN Hamiltonian rather than removing the spin-spin interaction. This shows (via the Liouville-Arnold theorem to be discussed later) that the generic BBH is integrable at 2PN, in the sense of perturbation theory. That is, these 2PN constants only mutually commute up to sufficiently-high-order errors. This also implies that the action variables can be pushed to 2PN, so an analytical orbital solution is possible at this order. We finally revisit the criteria for integrability by analyzing the timescales for "constants" to vary when evolved with the next order Hamiltonian. With this more physical criterion, $\vec{S}_{\rm eff} \cdot \vec{L}$ actually varies at the 1PN timescale, despite being a 1.5PN constant of motion. The 2PN constants we construct only vary at 2.5PN order, justifying that the BBH system is integrable at 2PN order.

The existence of these perturbative constants is not in conflict with the presence of chaos in phase space. From the KAM theorem, most invariant tori will remain unbroken under a sufficiently small perturbation. Resonant tori will be the first to break up into chaotic regions. Our constants are applicable to unbroken tori, which according to Ref. [36] fill the vast majority of phase space.

The layout of this chapter is as follows. In Sec. 2.2 the mathematical preliminaries like post-Newtonian power counting, Liouville integrability, the Hamiltonian phase space and Poisson bracket structure for the BBH problem, and the 2PN Hamiltonian, have already been introduced.

In Sec. 4.2, we give an algebraic definition of PN involution and integrability. We then describe how to systematically construct appropriate ansätze for corrections to add to constants of motion, reducing the problem to linear algebra. Finally we solve for the corrections and present the five approximate constants of motion, which are in involution up to errors that can be ignored at 2PN. In Sec. 4.3, we present our discussion, ideas for future work, and conclude.

4.2 Integrability at 2PN

The spirit of the post-Newtonian method is perturbation theory in powers of $1/c$, which opens the door for canonical perturbation theory applied to Hamiltonian dynamics. As the KAM theorem dictates [22, 31], when we add a small perturbation to an integrable system, and this perturbation breaks integrability, the perturbed motion is still multiply-periodic and restricted to n-tori, except for resonant tori where chaos ensues.[1]

We can take advantage of perturbation theory by treating the 2PN system as a perturbation upon the 1.5PN Hamiltonian. We find deformations to the 1.5PN constants of motion such that the 2PN system is integrable in the perturbative sense. This method can be pushed to higher PN order, but here we only demonstrate it at the first order where "exact" integrability is broken, namely at the 2PN order. In Sec. 4.2.1 we explain what we mean by perturbative integrability, and in Sec. 4.2.2 the method for finding the deformations to the constants. In Sec. 4.2.3 we give the results for the deformed constants, and discuss some subtle issues in PN integrability in Sec. 4.2.4.

4.2.1 Perturbative integrability

To make the definition of perturbative integrability precise, we will introduce the "dominant PN order of" symbol $[-]$. If a phase-space quantity is asymptotic to c^{-2m}, then it has dominant PN order m, i.e.,

$$f \sim F(R, P, \chi)c^{-2m} \qquad \longleftrightarrow \qquad [f] \equiv m\,, \tag{4.1}$$

[1]The KAM theorem actually gives more precise estimates for the ϵ dependence of the chaotic component of phase space; see Ref. [31] for more details.

where $F(R, P, \chi)$ is a c-independent phase-space function, and we employ the $\sim$ symbol of asymptotic analysis [65]. The algebra of formal power series tells us how $[-]$ interacts with multiplication, addition, and thus Poisson brackets. Multiplication is simple,

$$[f\, g] = [f] + [g]\,. \tag{4.2}$$

When two phase-space functions have different dominant orders, addition is also simple,

$$[f + g] = \min([f], [g]) \qquad \text{if } [f] \neq [g]\,. \tag{4.3}$$

However, if $f \sim -g$, then there will be a cancellation in the dominant order of $f + g$, and the dominant order of the sum will be higher than $\min([f], [g])$. Such cancellation can happen in Poisson brackets, and is necessary for our algebraic definition of perturbative integrability.

In perturbation theory, equalities only need to be satisfied up to some sufficiently-small error terms. Thus for perturbative integrability, we will replace $\{F_i, F_j\} = 0$ with conditions $\{F_i, F_j\} = O(c^{-2p})$, for some appropriate PN orders p. If we want perturbative integrability at relative qPN order, we know we want each $\{F_i, F_j\}$ to be at least a factor of $c^{-2(q+1/2)}$ higher than some phase-space quantity, but what is that quantity?

To answer this question, we define the function $\mathrm{DNC}(f, g)$ which measures what would be the "expected" dominant PN order of $\{f, g\}$ if there was no cancellation in the leading order ("dominant non-commutation"). This expected order has two cases, corresponding to the leading orders of f and g both contain a common spin vector or not. This is because the (inverse) symplectic form for spins itself carries a power of S and thus c^{-1} [see Eq. (2.8)]. Thus we define

$$\mathrm{DNC}(f, g) = \begin{cases} [f] + [g] - \frac{1}{2}\,, & \text{both } f \text{ and } g \text{ contain} \\ & \text{spin at dominant order,} \\ [f] + [g]\,, & \text{otherwise.} \end{cases}$$

If f and g do not have cancellation at the leading order, we see that $\mathrm{DNC}(f, g) = [\{f, g\}]$. For

example, $\mathrm{DNC}(R^i, P_i) = 0$, but $\mathrm{DNC}(S_A^i, S_A^j) = 1/2$ for $i \neq j$.

If $\{f, g\} = 0$ exactly, then f and g are said to be in involution up to infinite order. Otherwise we say that f and g are in involution "up to qPN order" when the two equivalent conditions hold,

$$\{f, g\} \sim O\left(c^{-2(\mathrm{DNC}(f,g)+q+\frac{1}{2})}\right), \tag{4.4a}$$

$$[\{f, g\}] > \mathrm{DNC}(f, g) + q\,. \tag{4.4b}$$

As a consistency check, notice that for the previous examples (R^i, P_i) and (S_A^i, S_A^j) with $i \neq j$, each pair is not in involution even at the leading (0PN) order, as would be expected. Now we define a "qPN constant of motion" to be a quantity which is in involution with the qPN Hamiltonian up to at least qPN order. Finally, we define qPN perturbative integrability in a $2n$-dimensional phase space when we have n independent phase-space functions (including the qPN Hamiltonian) which are in mutual involution up to at least qPN order with one additional condition. This condition demands that the n independent phase-space functions (including the $(q+1/2)$PN Hamiltonian) must be such that in the extreme PN limit $(1/c \to 0)$, they must reduce to n independent phase-space functions in exact mutual involution. The justification of this additional condition can be found in Appendix B of [66]. We will revisit this definition further in Sec. 4.2.4, and see that it still has a shortcoming.

4.2.2 Method of finding deformations

We now construct perturbative constants of motion up to 2PN. Note that J^2 and J_z always remain exact constants of motion, at any order, for an SO(3)-invariant Hamiltonian. Along with the Hamiltonian, they form a set of three independent mutually commuting constants of motion. We need to add two more quantities to this list to establish integrability. We propose that the two required constants of motion are perturbative deformations of the 1.5PN constants of motion, L^2 and $\vec{S}_{\mathrm{eff}} \cdot \vec{L}$, namely

$$\widetilde{L^2} = L^2 + \delta L^2, \tag{4.5}$$

$$\widetilde{S_{\rm eff}\cdot L} = \vec{S}_{\rm eff}\cdot\vec{L} + \delta(\vec{S}_{\rm eff}\cdot\vec{L})\,, \tag{4.6}$$

where δL^2 and $\delta(\vec{S}_{\rm eff}\cdot\vec{L})$ are higher-PN corrections that we must find. For every pair, we want involution up to 2PN order [$q = 2$ in Eq. (4.4)]. The dominant orders of each of these functions are $\left[\widetilde{L^2}\right] = [H] = 0$ and $\left[\widetilde{S_{\rm eff}\cdot L}\right] = \frac{1}{2}$. Therefore, to satisfy 2PN perturbative integrability, we require

$$\left\{\widetilde{L^2}, H\right\} \sim O(c^{-5}), \tag{4.7a}$$

$$\left\{\widetilde{S_{\rm eff}\cdot L}, H\right\} \sim O(c^{-6}), \tag{4.7b}$$

$$\left\{\widetilde{S_{\rm eff}\cdot L}, \widetilde{L^2}\right\} \sim O(c^{-6}), \tag{4.7c}$$

where H is the 2PN Hamiltonian.

Satisfying these integrability conditions amounts to finding the deformations δL^2 and $\delta(\vec{S}_{\rm eff}\cdot\vec{L})$, which both proceed following the same approach. First, the PN orders that are required to appear in a deformation are identified. Then we construct an ansatz for the deformation out of geometrical objects at these required PN orders, times some coefficients to be determined by Eqs. (4.7). This turns the problem into a systematic enumerative algebra problem.

At first glance it may seem that this procedure is not systematic, as there are an infinite number of terms that could appear in such an ansatz at fixed PN order, but this is not true. First, the only quantities that may appear are geometric objects transforming covariantly under SO(3) rigid rotations:

- the metric tensor δ_{ij} (Kronecker delta),
- Levi-Civita tensor (not the symbol) ϵ_{ijk},
- the position vector $\vec{R}$, its norm R and unit radial vector $\hat{R} \equiv \vec{R}/R$,
- momentum vector $\vec{P}$, and
- spin vectors ($\vec{S}_1$, $\vec{S}_2$).

In practice, it is simpler to construct such ansätze from $\hat{R}$ and powers of the scalar R, rather than considering $\vec{R}$. SO(3) covariance requires that these objects automatically commute with J^2 and J_z. The types of terms allowed in a deformation have the same tensorial character and parity (scalar, pseudoscalar, vector, etc.) as the quantity being corrected. While negative powers R^{-k} can appear in PN expressions, negative powers of P or S do not. Now, if we choose a maximum operator order (number of tensors multiplied together), there are only a finite number of combinations that can be built at each PN order and operator order. Now the problem is indeed enumerative: if a solution is not found, increase the operator order and try again.

Let us demonstrate by using $\widetilde{L^2}$ as an example. First, we determine the PN orders necessary for the ansatz of the deformation δL^2. Expanding Eq. (4.7a),

$$\begin{aligned}\left\{\widetilde{L^2}, H\right\} &= \left\{L^2, H_{\rm 2PN}\right\} + \left\{\delta L^2, H_{\rm N}\right\} \\ &\quad + \left\{\delta L^2, H_{\rm 1PN} + H_{\rm 1.5PN} + H_{\rm 2PN}\right\} , \\ &\sim O(c^{-5}) . \end{aligned} \tag{4.8}$$

The noncommutation in the first term on the RHS is only with the spin-spin term, since L^2 commutes with the orbital part,

$$\begin{aligned}\left\{L^2, H_{\rm 2PN}\right\} &= \left\{L^2, H_{\rm SS,2PN}\right\} \\ &\sim O(S^2\, c^{-2}) \sim O(c^{-4}) . \end{aligned} \tag{4.9}$$

This is the dominant error that must be cancelled by the terms involving δL^2, which we see must involve spins. The bracket of δL^2 with the Hamiltonian also follows PN ordering and is dominated by $\left\{\delta L^2, H_{\rm N}\right\}$, with the other terms being higher-PN. One must be careful to check what happens with the spin terms, which potentially reduce PN orders: for example since δL^2 has spins in its leading order, $\left\{\delta L^2, H_{\rm 1.5PN}\right\}$ is only 1PN order higher than $\left\{\delta L^2, H_{\rm N}\right\}$, rather than 1.5PN. Therefore

this condition simplifies to

$$\left\{L^2, H_{\rm SS,2PN}\right\} + \left\{\delta L^2, H_{\rm N}\right\} = 0\,, \tag{4.10}$$

with the equality being exact. To satisfy this, δL^2 will need to contain two spin in the leading order, which by inspection must be $\delta L^2 \sim O(S^2 c^{-2})$.

To build an appropriate $O(S^2 c^{-2})$ ansatz for δL^2, we note from Eq. (2.3) that a factor of $1/c^2$ should accompany either two powers of $\vec{p} \equiv \vec{P}/\mu$, or one power of $1/R$, and any number of powers of $\hat{R}$. Since L^2 is parity even, we will not use ϵ_{ijk} to construct the ansatz for δL^2: an odd number of ϵ's makes a parity odd term, and an even number can be written in terms of δ^i_j. This yields an ansatz containing terms of the form

$$\delta L^2 \supset \left(\frac{1}{c^2} \underbrace{S^i_A S^j_B P^k P^l \hat{R}^m \hat{R}^n}_{\text{19 contractions}}\,, \frac{1}{Rc^2} \underbrace{S^i_A S^j_B \hat{R}^k \hat{R}^l}_{\text{6 contractions}} \right). \tag{4.11}$$

Here we mean to take all possible contractions of the two tensorial forms, where the indices (A, B) label spins in the same way as in Sec. 2.2. This leads to 19 possible contractions involving two factors of $\vec{P}$, and 6 contractions without $\vec{P}$, giving us altogether 25 terms in our most general ansatz for δL^2. Since we are taking contractions, the use of the metric tensor δ_{ij} is implicit in our ansatz construction. Our ansatz for δL^2 then consists of a sum of all these 25 terms with coefficients to be solved for demanding that Eq. (4.10) be true.

One can employ similar lines of reasoning to construct an ansatz for $\delta(\vec{S}_{\rm eff} \cdot \vec{L})$ and solve for the coefficients so that Eq. (4.7b) is satisfied, although it is a more complicated case than for δL^2. Instead of Eq. (4.10), this time we demand that Eq. (4.19) be satisfied in the next section. Finally, there may be additional constraints on the terms in the ansätze arising from the requirement that the Poisson bracket $\left\{\widetilde{L^2}, \widetilde{S_{\rm eff} \cdot L}\right\}$ must also vanish to the required order, Eq. (4.7c). That is how we finally arrive at the desired $\widetilde{L^2}$ and $\widetilde{S_{\rm eff} \cdot L}$. We formed sufficiently general ansätze using the `AllContractions` and `MakeAnsatz` commands of the MATHEMATICA package xTRAS [67],

which works in the xAct/xTensor suite [39, 68]. Our result may be verified by the Mathematica notebook which can be found at [38].

4.2.3 The deformed constants

Following the above procedure to find a deformation to L^2, we write this deformation as

$$\widetilde{L^2} = \underbrace{L^2}_{\text{0PN}} + \underbrace{\delta L^2}_{\text{2PN}} . \tag{4.12}$$

For brevity we will define the symmetric tensor

$$h^{ij} \equiv \frac{p^i p^j}{2} - \frac{r^i r^j}{r^3} , \tag{4.13}$$

where we again used the scaled variables $\vec{p} \equiv \vec{P}/\mu$, $r = R/GM$. Notice that h^{ij} has units of v^2, and that the trace is

$$h \equiv \delta_{ij} h^{ij} = H_N/\mu . \tag{4.14}$$

Then we can write our deformation as

$$\delta L^2 = \frac{-2\nu}{c^2}\left[\frac{m_2}{m_1} S_1^i S_1^j h_{ij} + S_1^i S_2^j \left(h_{ij} - \delta_{ij}\frac{h}{2}\right) + (1 \leftrightarrow 2)\right] . \tag{4.15}$$

We are also free to add arbitrary constants times $S_1^2 h/c^2$ and $S_2^2 h/c^2$ without affecting integrability.

Proceeding similarly for $\vec{S}_{\text{eff}} \cdot \vec{L}$, we decompose the deformation as

$$\widetilde{S_{\text{eff}} \cdot L} = \underbrace{\vec{S}_{\text{eff}} \cdot \vec{L}}_{\text{0PN}} + \underbrace{\delta_1(\vec{S}_{\text{eff}} \cdot \vec{L})}_{\text{0.5PN}} + \underbrace{\delta_2(\vec{S}_{\text{eff}} \cdot \vec{L})}_{\text{1.5PN}} . \tag{4.16}$$

The two deformations are

$$\delta_1(\vec{S}_{\text{eff}} \cdot \vec{L}) = \frac{1}{4}\vec{S}_1 \cdot \vec{S}_2 , \tag{4.17}$$

$$\delta_2(\vec{S}_{\rm eff}\cdot\vec{L}) = \frac{1}{c^2}\left[\sigma_1\frac{m_2^2}{M^2}S_1^iS_1^jh_{ij} + \frac{1}{8}(3+2\nu)S_1^iS_2^jh_{ij} + (1\leftrightarrow 2)\right]. \tag{4.18}$$

We are also free to add arbitrary constants times S_1^2h/c^2, S_2^2h/c^2, and $(\vec{S}_1\cdot\vec{S}_2)h/c^2$ without affecting integrability. The cancellations happen as

$$\underbrace{\left\{\vec{S}_{\rm eff}\cdot\vec{L}, H_{\rm SS,2PN}\right\}}_{\substack{\text{both orbital and spin PBs;}\\ O(c^{-4})\text{ and }O(c^{-5})}} + \underbrace{\left\{\delta_1(\vec{S}_{\rm eff}\cdot\vec{L}), H_{\rm 1.5PN}\right\}}_{\substack{\text{spin PBs;}\\ O(c^{-4})}} + \underbrace{\left\{\delta_1(\vec{S}_{\rm eff}\cdot\vec{L}), H_{\rm SS,2PN}\right\}}_{\substack{\text{spin PBs;}\\ O(c^{-5})}} + \underbrace{\left\{\delta_2(\vec{S}_{\rm eff}\cdot\vec{L}), H_{\rm N}\right\}}_{\substack{\text{orbital PBs;}\\ O(c^{-4})}} = 0\,, \tag{4.19}$$

with the equality being exact, where $H_{\rm SS,2PN}$ is defined in Eq. (2.16). Below every Poisson bracket, we indicate both the PN orders arising, and what kind of PBs (orbital or spin) are needed to expand each term. With these corrections, we have fulfilled the required level of commutation given in Eqs. (4.7). In fact, we slightly exceeded this goal, achieving

$$\left\{\widetilde{L^2}, H\right\} \sim O(c^{-6})\,, \tag{4.20a}$$

$$\left\{\widetilde{S_{\rm eff}\cdot L}, H\right\} \sim O(c^{-6})\,, \tag{4.20b}$$

$$\left\{\widetilde{S_{\rm eff}\cdot L}, \widetilde{L^2}\right\} \sim O(c^{-7})\,. \tag{4.20c}$$

Therefore, along with the 2PN Hamiltonian H, J^2, and J_z, the deformed constants $\widetilde{L^2}$ and $\widetilde{S_{\rm eff}\cdot L}$ now form a set of 5 independent, mutually commuting constants of motion at 2PN order, thereby establishing the integrable nature of the BBH system at this order.

It is worth comparing our results to the widely-used results based on orbit-averaging (over a Newtonian orbit) [29, 40–43]. Racine found [29] that the combination $\vec{S}_0\cdot\vec{L}$ is conserved by what we call $\langle d/dt\rangle_N$, the Newtonian-orbit average of the 2PN EOMs. Here $\vec{S}_0 \equiv (1+m_2/m_1)\vec{S}_1 + (1+m_1/m_2)\vec{S}_2$ was introduced by Damour [28]. Two comments are in order. First, $\vec{S}_0\cdot\vec{L}$ differs at its leading order from $\vec{S}_{\rm eff}\cdot\vec{L}$ and therefore $\widetilde{S_{\rm eff}\cdot L}$. Since spins and $\vec{L}$ are all constants at Newtonian

order, applying the Newtonian-orbit-average to form $\left\langle \vec{S}_{\rm eff} \cdot \vec{L} \right\rangle_N = \vec{S}_{\rm eff} \cdot \vec{L}$ does not recover $\vec{S}_0 \cdot \vec{L}$. Second, as mentioned at the end of Sec. 2.3, a more accurate average is not over the Newtonian orbit, but on the phase-space torus formed by level sets of the five constants of motion. The torus-average will already differ at 1PN order from the Newtonian-orbit average. We can confirm using the 2PN Hamiltonian and averaging over the Newtonian orbit the two independent equalities,

$$\left\langle \frac{d}{dt} \right\rangle_N \vec{S}_0 \cdot \vec{L} = 0\,, \qquad\qquad \left\langle \frac{d}{dt} \vec{S}_0 \cdot \vec{L} \right\rangle_N = 0\,. \tag{4.21}$$

However, we should expect that the torus-average will differ. More precisely, with the 2PN Hamiltonian and no averaging,

$$\frac{d}{dt} \vec{S}_0 \cdot \vec{L} = O(S^2 c^{-2}) = O(c^{-4})\,. \tag{4.22}$$

Thus while Newtonian-orbit averaging gives a cancellation of this leading order, we expect the more accurate torus average to be nonzero at the order

$$\left\langle \frac{d}{dt} \vec{S}_0 \cdot \vec{L} \right\rangle_T = O(c^{-6})\,. \tag{4.23}$$

Notice this is the same level of conservation that we achieved in Eq. (4.20b), but our result is valid instantaneously, that is, without resorting to averaging.

4.2.4 PN constancy and integrability revisited

Our algebraic definition of PN involution and integrability introduced in Sec. 4.2.1 has a shortcoming. To understand this, let's examine the timescales on which phase-space quantities vary. For some quantity f, when evolved with the full nPN Hamiltonian $H^{n\rm PN}$ (not the nPN contribution to the Hamiltonian), we can approximate the timescale of variation with

$$T_n(f) \equiv \frac{f}{\left\{ f, H^{n\rm PN} \right\}}\,. \tag{4.24}$$

For example, the orbital (or Newtonian) timescale is

$$T_N \equiv T_0(R^i) \approx \sqrt{\frac{R^3}{GM}}\,. \tag{4.25}$$

Now, with the algebraic definition of PN integrability given in Sec. 4.2.1, $\vec{S}_{\rm eff}\cdot\vec{L}$ is a 1.5PN constant of motion. But let us examine the timescale of its variation, in units of the orbital time. We cannot use $H^{1.5\rm PN}$ for this, since $\vec{S}_{\rm eff}\cdot\vec{L}$ and $H^{1.5\rm PN}$ commute. The timescale of variation is controlled by the 2PN Hamiltonian, and one can check

$$T_2(\vec{S}_{\rm eff}\cdot\vec{L}) \sim O\left(\left(\frac{v}{c}\right)^{-3} T_N\right)\,, \tag{4.26}$$

implying that $\vec{S}_{\rm eff}\cdot\vec{L}$ varies on a timescale that is only 1.5PN longer than T_N, rather than the expected 2PN orders longer. Therefore, $\vec{S}_{\rm eff}\cdot\vec{L}$ is not a 1.5PN constant from the criterion of comparing timescales, and the BBH system cannot yet be called integrable at 1.5PN order despite the existence of five exactly commuting constants at this order.

The key point is that $H_{n\rm PN}$ may sometimes induce variations in a quantity f at a timescale which is only $(n-1/2)$PN orders larger than T_N, rather than nPN orders larger. As was emphasized in Secs. 2.2.1, 2.2.2, and 4.2.1, this happens because of the factor of c^{-1} in spin, and the form of the spin Poisson bracket. Therefore, to establish if a quantity is a constant of motion on an nPN timescale will generally involve examining the $(n+1/2)$PN Hamiltonian.

To conservatively satisfy the timescale analysis, we revise the earlier definition of qPN constancy and integrability by using the next order, $(q+1/2)$PN, Hamiltonian, instead of the qPN Hamiltonian. However, we only introduce relative qPN corrections to our deformed constants. We have checked that the five quantities $H, J_z, J^2, \widetilde{L^2}$ and $\widetilde{S_{\rm eff}\cdot L}$ (H now being the 2.5PN Hamiltonian [37]) are also in mutual involution up to 2PN according to our revised definition, even though the last two quantities were derived in Sec. 4.2.2 by only considering the 2PN Hamiltonian. This calculation is also verified in the supplement to this article [38]. In terms of timescales, we now

satisfy

$$T_{2.5}\left(\widetilde{S_{\rm eff}\cdot L}\right) \sim O\left(\left(\frac{v}{c}\right)^{-5} T_N\right) . \tag{4.27}$$

Hence, we have established the integrable nature of the BBH system at one PN order higher (2PN) than what was earlier known (1PN) on the basis of timescale of variation.

4.3 Discussion

In this chapter, we studied the problem of integrability at 2PN. By adding corrections to the 1.5PN mutually commuting constants of motion, we constructed 2PN perturbatively commuting quantities. This proves the integrable nature of the BBH system at 2PN in a perturbative sense. Our construction required us to propose appropriate definitions of PN involution and integrability. Proving perturbative integrability at 2PN and higher is more delicate than at 1.5PN, since the 1.5PN commutation does not require perturbation theory. We presented a systematic method to find higher-PN corrections to mutually commuting constants of motion, forming an ansatz by enumerating possible tensor expressions, turning the problem into linear algebra. We therefore expect our method to be useful in extending integrability to even higher PN orders.

By now a large number of authors have studied the problems of integrability or chaos in the BBH system in post-Newtonian theory, either numerically or analytically. Importantly, while Hartl and Buonanno [36] did find chaos in the PN BBH system, they found it is only present in a small component of phase space. The constants of motion we have constructed apply to the invariant tori in the non-chaotic regions of phase space, i.e. the majority of the volume. This improves the outlook for using perturbative integrability as a tool for generating highly-accurate and efficient waveform models.

To employ integrability for efficient waveform modeling, the current work will have to be extended in a number of natural ways. We can try to extend our current work to 3PN order. The 2PN integrability of the system encourages us to push our derivation of 1.5PN action-angle variables (of

the last chapter) to 2PN too. This opens the possibility to construct an analytic waveform model for the completely generic system, without needing to e.g. orbit-average [29, 40, 41], precession-averaging [42, 43, 69, 70], or expand in powers of eccentricity [71, 72]. As discussed at the end of Sec. 4.2.3, we expect the time derivatives of the orbit-averaged constants to have errors at relative 2.5PN order, when averaged over the true orbits, rather than over Newtonian orbits. This is the same level of error in the time derivatives of our instantaneous constants, i.e. without needing to average. We hope to see our integrability results applied to future analytical waveform models such as the `Phenom` family.

A difficulty will arise at 2.5PN order, where the dynamics are no longer conservative. Starting at this order, the "constants" of motion will now vary with time. One possible approach will be the formalism of non-conservative classical dynamics [73–76], which has a Hamiltonian version. Even if the non-conservative approach proves difficult, the conservative sector of the dynamics can still be pushed to higher PN order, and the time-evolution of the "constants" imposed afterwards through order reduction.

CHAPTER 5

GENERALIZED QUASI-KEPLERIAN SOLUTION FOR ECCENTRIC, NON-SPINNING COMPACT BINARIES AT 4PN ORDER AND THE ASSOCIATED IMR WAVEFORM

The contents of this chapter can be found at Ref. [77].

5.1 Introduction

The subject of this chapter won't be the most general BBH system (one with arbitrary masses, spins and eccentricity). We will specialize to a system with arbitrary masses and eccentricity but no spins.

It turns out that PN-accurate Keplerian type parametric solution is a key ingredient to implement GW phasing for eccentric inspirals. Such solutions were presented in Refs. [78] and [79] at 2PN and 3PN orders, respectively. The solution of Ref. [79] that solves 3PN-accurate conservative orbital dynamics, detailed in Refs. [80, 81], is crucial to model the inspiral part of two IMR families, available in Refs. [2, 82]. Further, the Keplerian type parametric solution is also important to compute GW emission induced secular evolution of the orbital elements [1, 83–85]. This chapter computes 4PN order corrections to the 3PN-accurate generalized quasi-Keplerian parametric solution of Ref. [79] in the Arnowitt, Deser, and Misner (ADM) coordinates. We have dropped certain zero-average oscillatory terms from our solution arising due to 4PN tail effects due to them being relatively unimportant in GW data analysis. It was demonstrated that the total 4PN-accurate conservative Hamiltonian is the sum of instantaneous (local-in-time) near-zone Hamiltonian [86] and time-symmetric but nonlocal-in-time tail Hamiltonian [87]. These instantaneous contributions in the center-of-mass frame are similar in structure to 3PN-accurate Hamiltonian, as is evident from Eqs. (8.40) and (8.41) of Ref. [86]. Therefore, it is reasonable

to expect that this part should admit Keplerian type parametric solution. Unfortunately, 4PN contributions to the time-symmetric but nonlocal-in-time tail Hamiltonian, given by Eq. (8.32) of Ref. [86], do not support any closed-form exact-in-e_t (e_t stands for an eccentricity) expression. Instead, we compute the approximate-in-e_t (valid up to $e_t \lesssim 0.9$), secular dynamics (ignoring the oscillatory ones) of the tail effect by employing canonical perturbation theory. This is reflected in corrections to the mean motion and the periastron advance, using Padé-like approximants. We perform detailed consistency checks to ensure the correctness of our lengthy solution. Further, we have verified that our local and non-local 4PN order expressions for the rate of periastron advance is consistent with similar expressions that are present in Refs. [88, 89].

We employ our 4PN order results to obtain an improved version of a restricted class of time-domain eccentric IMR family, detailed in Ref. [2]. This IMR family invokes PN approximation and employs temporally evolving quadrupolar order $h_{\times,+}$ associated with compact binaries inspiralling along 3PN-accurate eccentric orbits while being under the effects of 4.5PN-accurate (or relative 2PN order) GW damping. As for the merger-ringdown part, we implement the approach of Ref. [2] exactly (as a blackbox), explained in some detail in Sec. 5.3.2. This approach rests on identifying certain epochs during the inspiral-merger of the binary such as $t_{\rm blend} < t_{\rm circ} < t_{\rm peak}$. For $t < t_{\rm blend}$, PN equations of motion are used and for $t > t_{\rm circ}$ we use the circular merger model (CMM) which is based on the assumption that the binary is essentially circular for $t > t_{\rm circ}$. The CMM model is got via interpolation between circular numerical relativity (NR) waveforms for different q (mass ratio) values. To build the waveform between $t_{\rm blend}$ and $t_{\rm circ}$, a certain 'blending' procedure is employed which just like the CMM model, rests on the ideas of interpolation although of a different nature than the one employed to construct the CMM model. Ref. [2] used 23 NR simulations (with various mass ratios and initial eccentricities) as a basis for these interpolations which finally give the CMM and the blended waveforms.

We adapt the publicly available MATHEMATICA package [90] of Ref. [2] to obtain an updated eccentric IMR family using our 4PN-order parametric solution which can be found at Ref. [91, 92]. Moreover, we improve their inspiral description in a number of ways which results in a

computationally more efficient (and higher PN order accurate) implementation of the eccentric inspiral dynamics of the binary. This includes the use of closed-form expressions to model orbital time scale variations and an improved way to tackle the PN-accurate Kepler equation (Mikkola method in conjuction with an 'auxiliary eccentric anomaly'). We also pursue preliminary data analysis implications of our approximant to assess the importance of the 4PN order contributions to the inspiral part.

We expect our IMR waveform to be valid across a slightly larger parameter range than that for the waveform of Ref. [2], although we have not checked it; see the end of Sec. 5.3 for more details. Apart from our main IMR MATHEMATICA package, we also present a derived package which makes use of only the PN equations of motion to produce the waveforms and hence can be trusted only for the inspiral part. Because this PN package has nothing to do with the CMM, it should be valid for a much higher range of e_t ($e_t \lesssim 0.85$) than our main IMR package.

The plan of the chapter is as follows. In Sec. 5.2, we detail the derivation of 4PN order generalized quasi-Keplerian parametric solution after giving a brief introduction to the approach. We then discuss how to incorporate the tail effect into it. In Sec. 5.3, we describe how we employed our parametric solution to develop an accurate and efficient eccentric inspiral waveform and obtain its IMR version, influenced by Ref. [2]. Some preliminary data analysis explorations are also discussed. Some of the computational details and lengthy expressions are provided in the appendices.

Convention: From Sec. 5.3 onwards, t denotes the ADM coordinate time, whereas in Sec. 5.2, it denotes the ADM coordinate time scaled down by a factor of GM, with G and M standing for the gravitational constant and the total mass of the binary; more details below.

5.2 Keplerian type solution at 4PN order

We begin by summarizing Keplerian type parametric solution that describes efficiently the Newtonian dynamics of point mass binaries in eccentric orbits and its PN-accurate extensions. These extensions, detailed in Refs. [78, 79, 93, 94], may be referred to as the 'generalized quasi-

Keplerian' parametric solution for describing PN-accurate orbital dynamics of compact binaries in eccentric orbits. How we derive Keplerian type parametric solution associated with the 4PN-accurate near-zone local-in-time Hamiltonian $\mathcal{H}^{\rm local}_{\rm 4PN}$, given by Eq. (8.41) of Ref. [86], is detailed in Sec. 5.2.2.

5.2.1 Keplerian type solution and its 3PN extensions

The classical Keplerian parametric solution provides a semi-analytic description for the temporal evolution of a point mass binary in non-circular orbits under the influence of Newtonian dynamics [95]. It other words, it provides a parametric description for the relative separation vector $\mathbf{R} \equiv R(\cos\phi, \sin\phi, 0)$ in the usual center-of-mass reference frame of the binary. These angular and radial variables describe the position of the reduced mass $\mu = m_1\, m_2/M$ around the total mass $M = m_1 + m_2$ (m_1 and m_2 being the individual masses). We parametrize R and ϕ by

$$r = a(1 - e\cos u)\,, \tag{5.1a}$$

$$\phi - \phi_0 = v \equiv 2\arctan\left[\left(\frac{1+e}{1-e}\right)^{1/2} \tan\frac{u}{2}\right], \tag{5.1b}$$

where $r = R/(GM)$ and the auxiliary angles u and v are called eccentric and true anomalies, respectively. Further, a and e denote the semi-major axis and orbital eccentricity of the Newtonian closed orbit of μ around M. The explicit temporal evolution for $\mathbf{R}$ is specified by the classical Kepler equation, namely

$$l \equiv n(t - t_0) = u - e\,\sin u\,, \tag{5.2}$$

where l and n are usually referred to as the mean anomaly and the mean motion, respectively. Further, $n = 2\,\pi/P$ with P being the orbital period and t_0 and ϕ_0 stand for some initial coordinate time and initial orbital phase, respectively. We reserve the symbol t for the re-scaled coordinate time $t = t'/(GM)$, where t' represents the ADM time coordinate whose unit is seconds. The

explicit expressions for these orbital elements a, e and n are given by

$$a = \frac{1}{(-2\,E)}\,, \tag{5.3a}$$

$$e^2 = 1 + 2\,E\,h^2\,, \tag{5.3b}$$

$$n = (-2\,E)^{3/2}\,, \tag{5.3c}$$

where E is the orbital energy per unit reduced mass while the reduced angular momentum h is given by $h = J/(G\,M)$ with J being the orbital angular momentum per unit reduced mass. It is customary to employ $J_s(se)$, the Bessel functions of the first kind, to express u in terms l as [96]

$$u = l + \sum_{s=1}^{\infty} \frac{2}{s} J_s(se)\,\sin(s\,l)\,. \tag{5.4}$$

Remarkably, it is also possible to find Keplerian type parametric solution to the conservative orbital dynamics of compact binaries moving in relativistic orbits in the PN approximation. It was Damour and Deruelle who first proposed certain quasi-Keplerian parametrization to tackle 1PN accurate orbital dynamics of non-spinning compact binaries [93]. Thereafter, Schäfer and his collaborators developed the generalized quasi-Keplerian parametric solution to tackle both the 2PN and 3PN-accurate orbital dynamics of compact binaries [78, 79, 94]. The fully 3PN-accurate generalized quasi-Keplerian parametrization for a compact binary in an eccentric orbit may be written as

$$r = a_r\,(1 - e_r\,\cos u)\,, \tag{5.5a}$$

$$\begin{aligned} l = n\,(t' - t'_0) &= u - e_t\,\sin u + \left(\frac{g_{4t}}{c^4} + \frac{g_{6t}}{c^6}\right)\,(v - u) \\ &+ \left(\frac{f_{4t}}{c^4} + \frac{f_{6t}}{c^6}\right)\,\sin v + \frac{i_{6t}}{c^6}\,\sin 2\,v + \frac{h_{6t}}{c^6}\,\sin 3\,v\,, \end{aligned} \tag{5.5b}$$

$$\begin{aligned} \frac{2\,\pi}{\Phi}\,(\phi - \phi_0) &= v + \left(\frac{f_{4\phi}}{c^4} + \frac{f_{6\phi}}{c^6}\right)\,\sin 2v \\ &+ \left(\frac{g_{4\phi}}{c^4} + \frac{g_{6\phi}}{c^6}\right)\,\sin 3v + \frac{i_{6\phi}}{c^6}\,\sin 4v + \frac{h_{6\phi}}{c^6}\,\sin 5v\,, \end{aligned} \tag{5.5c}$$

where $v = 2\arctan[\sqrt{(1+e_\phi)/(1-e_\phi)}\,\tan(u/2)]$(see Ref. [79]). A casual comparison of Eqs. (5.5) with Eqs. (5.1a) and (5.2) reveals that at PN orders there are three different eccentricities which are denoted by e_r, e_t and e_ϕ. These radial, time and angular eccentricity parameters are introduced to ensure that the resulting PN-accurate parametric solution looks Keplerian at the first post-Newtonian order (at higher PN orders it gains additional terms as can be seen in Eqs. (5.5)). The orbital elements a_r and n provide certain PN-accurate semi-major axis and mean motion while the factor $2\pi/\Phi$ gives the angle of advance of the pericenter per orbital revolution. Further, we have many orbital functions that appear at 2PN and 3PN orders and these are denoted by $g_{4t}, g_{6t}, f_{4t}, f_{6t}, i_{6t}, h_{6t}, f_{4\phi}, f_{6\phi}, g_{4\phi}, g_{6\phi}, i_{6\phi}$, and $h_{6\phi}$. The explicit 3PN-accurate expressions for these orbital elements and functions in terms of 3PN accurate orbital energy E, angular momentum h and the symmetric mass ratio $\eta = \mu/M$ are provided in Ref. [79]. Additionally, Ref. [97] derived 3PN-accurate extension of Eq. (5.4) thereby providing a closed-form solution of the 3PN Kepler equation, namely Eq. (5.5b). Further, Ref. [98] provided hyperbolic extension of Eq. (5.5a) to model PN-accurate GWs from compact binaries in hyperbolic passages. We note in passing that the 1PN-accurate parametric solution is usually referred to as the quasi-Keplerian parameterization as it looks functionally similar to its Newtonian counterpart. However, the parametric solutions at higher PN orders are termed the generalized quasi-Keplerian parameterizations and this is mainly due to the appearances of PN-accurate orbital functions in the expressions for $(\phi - \phi_0)$ and the Kepler equation.

These PN-accurate parametric solutions are of definite interest from observational points of view. For example, the 1PN-accurate Keplerian type parametric solution is crucial to operationalize the widely employed Damour-Deruelle timing formula to time relativistic binary pulsars [99, 100]. Moreover, the above parametrization is also employed to construct accurate and efficient GW templates for compact binaries inspiralling along PN-accurate eccentric orbits [101, 102]. Very recently, the above solution was also invoked to model pulsar timing array residuals induced by nano-Hz GWs from massive BH binaries in relativistic eccentric orbits [103]. In what follows, we extend the computations of Ref. [79] to obtain 4PN order Keplerian type parametric solution for

eccentric compact binaries.

5.2.2 Incorporating local-in-time 4PN Hamiltonian: generalized quasi-Keplerian solution

We employ the local-in-time part of the 4PN accurate ADM Hamiltonian for non-spinning compact binaries, given by Eq. (8.41) of Ref. [86], for computing 4PN order Keplerian parametric solution[1]. This Hamiltonian was crucial to complete the program to derive the 4PN accurate compact binary dynamics that incorporates all the general relativity based $(v/c)^8$ corrections as detailed in Ref. [87, 104]. The above Hamiltonian included certain time-symmetric nonlocal-in-time interactions, which are connected to the dominant order tail effects in the gravitational radiation reaction [105]. The resulting compact binary dynamics extends the 3PN-accurate conservative orbital dynamics, presented in Ref. [106], with the help of lengthy 4PN order computations that employ dimensional regularization and detailed far-zone matching [86, 87, 107, 108]. Very recently, Ref. [89] provided an independent check for the 4PN-accurate Hamiltonian of Schäfer and his collaborators by recomputing it within an effective field theory (EFT) approach in harmonic coordinates. We note that there are independent efforts to obtain 4PN accurate orbital dynamics using the EFT approach [109, 110] and Fokker action computations [111]. We give below the local-in-time near-zone 4PN-accurate reduced Hamiltonian in ADM-type coordinates and in the center-of-mass frame, given by Eq. (8.41) of Ref. [86], as (see footnote 2)

$$\mathcal{H}^{\rm local}_{\rm 4PN}(\mathbf{r},\hat{\mathbf{p}}) = \frac{\hat{\mathbf{p}}^2}{2} - \frac{1}{r} + \frac{1}{c^2}\mathcal{H}_1(\mathbf{r},\hat{\mathbf{p}}) + \frac{1}{c^4}\mathcal{H}_2(\mathbf{r},\hat{\mathbf{p}}) + \frac{1}{c^6}\mathcal{H}_3(\mathbf{r},\hat{\mathbf{p}}) + \frac{1}{c^8}\mathcal{H}_4(\mathbf{r},\hat{\mathbf{p}})\,, \tag{5.6}$$

where the explicit expressions for the 1PN, 2PN and 3PN contributions are given in Eq. (7) of Ref. [79]. This reduced Hamiltonian is connected to the Hamiltonian by $\mathcal{H}^{\rm local}_{\rm 4PN}(\mathbf{r},\hat{\mathbf{p}}) = H^{\rm local}_{\rm 4PN}(\mathbf{r},\hat{\mathbf{p}})/\mu$. The 4PN order contributions, extracted from Eq. (8.41) of Ref. [86], read

[1] A masterly treatise on the PN computations for compact binary dynamics in the Hamiltonian approach to general relativity is available in Ref. [80]

$$
\begin{aligned}
\mathcal{H}_4(\mathbf{r},\hat{\mathbf{p}}) &= \left(\frac{7}{256} - \frac{63}{256}\eta + \frac{189}{256}\eta^2 - \frac{105}{128}\eta^3 + \frac{63}{256}\eta^4\right)(\hat{\mathbf{p}}^2)^5 \\
&+ \left\{\frac{45}{128}(\hat{\mathbf{p}}^2)^4 - \frac{45}{16}(\hat{\mathbf{p}}^2)^4\,\eta + \left(\frac{423}{64}(\hat{\mathbf{p}}^2)^4 - \frac{3}{32}(\mathbf{n}\cdot\hat{\mathbf{p}})^2(\hat{\mathbf{p}}^2)^3 - \frac{9}{64}(\mathbf{n}\cdot\hat{\mathbf{p}})^4(\hat{\mathbf{p}}^2)^2\right)\eta^2 \right. \\
&\left. + \left(-\frac{1013}{256}(\hat{\mathbf{p}}^2)^4 + \frac{23}{64}(\mathbf{n}\cdot\hat{\mathbf{p}})^2(\hat{\mathbf{p}}^2)^3 + \frac{69}{128}(\mathbf{n}\cdot\hat{\mathbf{p}})^4(\hat{\mathbf{p}}^2)^2 - \frac{5}{64}(\mathbf{n}\cdot\hat{\mathbf{p}})^6(\hat{\mathbf{p}}^2) + \frac{35}{256}(\mathbf{n}\cdot\hat{\mathbf{p}})^8\right)\eta^3 \right. \\
&\left. + \left(-\frac{35}{128}(\hat{\mathbf{p}}^2)^4 - \frac{5}{32}(\mathbf{n}\cdot\hat{\mathbf{p}})^2(\hat{\mathbf{p}}^2)^3 - \frac{9}{64}(\mathbf{n}\cdot\hat{\mathbf{p}})^4(\hat{\mathbf{p}}^2)^2 - \frac{5}{32}(\mathbf{n}\cdot\hat{\mathbf{p}})^6\hat{\mathbf{p}}^2 - \frac{35}{128}(\mathbf{n}\cdot\hat{\mathbf{p}})^8\right)\eta^4\right\}\frac{1}{r} \\
&+ \left\{\frac{13}{8}(\hat{\mathbf{p}}^2)^3 + \left(-\frac{791}{64}(\hat{\mathbf{p}}^2)^3 + \frac{49}{16}(\mathbf{n}\cdot\hat{\mathbf{p}})^2(\hat{\mathbf{p}}^2)^2 - \frac{889}{192}(\mathbf{n}\cdot\hat{\mathbf{p}})^4\hat{\mathbf{p}}^2 + \frac{369}{160}(\mathbf{n}\cdot\hat{\mathbf{p}})^6\right)\eta \right. \\
&\left. + \left(\frac{4857}{256}(\hat{\mathbf{p}}^2)^3 - \frac{545}{64}(\mathbf{n}\cdot\hat{\mathbf{p}})^2(\hat{\mathbf{p}}^2)^2 + \frac{9475}{768}(\mathbf{n}\cdot\hat{\mathbf{p}})^4\hat{\mathbf{p}}^2 - \frac{1151}{128}(\mathbf{n}\cdot\hat{\mathbf{p}})^6\right)\eta^2 \right. \\
&\left. + \left(\frac{2335}{256}(\hat{\mathbf{p}}^2)^3 + \frac{1135}{256}(\mathbf{n}\cdot\hat{\mathbf{p}})^2(\hat{\mathbf{p}}^2)^2 - \frac{1649}{768}(\mathbf{n}\cdot\hat{\mathbf{p}})^4\hat{\mathbf{p}}^2 + \frac{10353}{1280}(\mathbf{n}\cdot\hat{\mathbf{p}})^6\right)\eta^3\right\}\frac{1}{r^2} \\
&+ \left\{\frac{105}{32}(\hat{\mathbf{p}}^2)^2 + \left(\left(\frac{2749\pi^2}{8192} - \frac{589189}{19200}\right)(\hat{\mathbf{p}}^2)^2 + \left(\frac{63347}{1600} - \frac{1059\pi^2}{1024}\right)(\mathbf{n}\cdot\hat{\mathbf{p}})^2\hat{\mathbf{p}}^2 \right.\right. \\
&\left.\left. + \left(\frac{375\pi^2}{8192} - \frac{23533}{1280}\right)(\mathbf{n}\cdot\hat{\mathbf{p}})^4\right)\eta \right. \\
&\left. + \left(\left(\frac{18491\pi^2}{16384} - \frac{1189789}{28800}\right)(\hat{\mathbf{p}}^2)^2 + \left(-\frac{127}{3} - \frac{4035\pi^2}{2048}\right)(\mathbf{n}\cdot\hat{\mathbf{p}})^2\hat{\mathbf{p}}^2 \right.\right. \\
&\left.\left. + \left(\frac{57563}{1920} - \frac{38655\pi^2}{16384}\right)(\mathbf{n}\cdot\hat{\mathbf{p}})^4\right)\eta^2 + \left(-\frac{553}{128}(\hat{\mathbf{p}}^2)^2 - \frac{225}{64}(\mathbf{n}\cdot\hat{\mathbf{p}})^2\hat{\mathbf{p}}^2 - \frac{381}{128}(\mathbf{n}\cdot\hat{\mathbf{p}})^4\right)\eta^3\right\}\frac{1}{r^3} \\
&+ \left\{\frac{105}{32}\hat{\mathbf{p}}^2 + \left(\left(\frac{185761}{19200} - \frac{21837\pi^2}{8192}\right)\hat{\mathbf{p}}^2 + \left(\frac{3401779}{57600} - \frac{28691\pi^2}{24576}\right)(\mathbf{n}\cdot\hat{\mathbf{p}})^2\right)\eta \right. \\
&\left. + \left(\left(\frac{672811}{19200} - \frac{158177\pi^2}{49152}\right)\hat{\mathbf{p}}^2 + \left(\frac{110099\pi^2}{49152} - \frac{21827}{3840}\right)(\mathbf{n}\cdot\hat{\mathbf{p}})^2\right)\eta^2\right\}\frac{1}{r^4} \\
&+ \left\{-\frac{1}{16} + \left(\frac{6237\pi^2}{1024} - \frac{169199}{2400}\right)\eta + \left(\frac{7403\pi^2}{3072} - \frac{1256}{45}\right)\eta^2\right\}\frac{1}{r^5}. \qquad (5.7)
\end{aligned}
$$

where $\mathbf{r} = \mathbf{R}/(GM)$, $r = |\mathbf{r}|$, $\mathbf{n} = \mathbf{r}/r$ and $\hat{\mathbf{p}} = \mathbf{P}/\mu$; $\mathbf{R}$ and $\mathbf{P}$ are the relative separation vector and its conjugate momentum vector respectively. It is easy to show that the above $\mathcal{H}(\mathbf{r}, \hat{\mathbf{p}})$ admits two conserved quantities, namely the 4PN order reduced energy $E = \mathcal{H}^{local}_{\rm 4PN}$ and the reduced angular momentum $\hat{\mathbf{J}} = \mathbf{r} \times \hat{\mathbf{p}}$ of the binary in the center-of-mass frame due to its invariance under time translations and spatial rotations. These considerations allow us to restrict the motion of our non-spinning compact binary to a plane and employ polar coordinates such that $\mathbf{r} = r(\cos\phi, \sin\phi)$. Naturally, the relative motion follows the following differential equations arising from the Hamiltonian equations

$$\dot{r} = \mathbf{n} \cdot \frac{\partial \mathcal{H}}{\partial \hat{\mathbf{p}}} \ , \tag{5.8a}$$

$$r^2\, \dot{\phi} = \left| \mathbf{r} \times \frac{\partial \mathcal{H}}{\partial \hat{\mathbf{p}}} \right|, \tag{5.8b}$$

where $\dot{r} = dr/dt, \dot{\phi} = d\phi/dt$. It is convenient to introduce a variable $s = 1/r$ such that the $\dot{r}^2$ expression at the Newtonian order becomes a quadratic polynomial in s. In terms of s, we have $\dot{r}^2 = (ds/dt)^2/s^4 = \dot{s}^2/s^4$ which leads to a 4PN order expression for $\dot{s}^2$ in terms of $(-2\,E)$, $h = |\hat{\mathbf{J}}|$, η and s. This allows us to obtain PN-accurate expressions for the two turning points of an eccentric orbit, defined by Eqs. (5.8). Further, we also compute 4PN order differential equation for $d\phi/ds = \dot{\phi}/\dot{s}$ using Eqs. (5.8) to tackle the angular part of our 4PN order Keplerian type parametric solution.

We first focus on the 4PN order expression for $\dot{r}^2$ and it turns out to be a 9th degree polynomial in s. This expression may be written symbolically as

$$\begin{aligned} \dot{r}^2 = \frac{1}{s^4}\left(\frac{ds}{dt}\right)^2 &= a_0 + a_1\, s + a_2\, s^2 + a_3\, s^3 + a_4\, s^4 + a_5\, s^5 \\ &\quad + a_6\, s^6 + a_7\, s^7 + a_8\, s^8 + a_9\, s^9 \, . \end{aligned} \tag{5.9}$$

The explicit 4PN order contributions to these coefficients are provided in the accompanying MATHEMATICA file `Lengthy_Expressions.nb` [91, 92], while their 3PN-accurate contributions are

available as Eqs. (A1) in Ref. [79]. Further, the coefficients a_8 and a_9 contain only 4PN order contributions. To obtain parametric solution to Eq. (5.9), we need to follow a couple of steps. First, we compute the two positive roots of the RHS of Eq. (5.9) having finite limits as $1/c \to 0$ by demanding $\dot{r}^2 = 0$ (other roots are pushed to $\pm\infty$ in this limit). We label these 4PN order roots as s_- (pericenter) and s_+ (apocenter). They correspond to the turning points of our PN-accurate eccentric orbits and are functions of E, h and η. For illustration, we display below their 1PN accurate expressions

$$\begin{aligned} s_\pm &= \frac{1 \pm \sqrt{1+2\,h^2\,E}}{h^2} \\ &\mp \frac{1}{c^2}\frac{\left(1 \pm \sqrt{1+2\,h^2\,E}\right)^2\left[-\eta - 9 \pm 2\,(\eta-7)\,\sqrt{1+2\,h^2\,E} + (3\eta-1)\,\left(1+2\,h^2\,E\right)\right]}{8\,h^4\,\sqrt{1+2\,h^2\,E}}\,. \end{aligned} \tag{5.10}$$

The explicit 4PN order expressions for these two roots are available in the accompanying MATHEMATICA notebook `Lengthy_Expressions.nb` [91, 92]. We now parametrize the 4PN order radial motion with the help of the following ansatz:

$$r = a_r\,(1 - e_r\,\cos u), \tag{5.11}$$

where a_r and e_r are some 4PN order semi-major axis and radial eccentricity, respectively. This ansatz allows us to express both a_r and e_r in terms of s_- and s_+ as

$$a_r = \frac{1}{2}\frac{s_- + s_+}{s_-\,s_+}\,, \qquad e_r = \frac{s_- - s_+}{s_- + s_+}\,. \tag{5.12}$$

This leads in a straightforward manner to the 4PN order expressions for a_r and e_r^2 in terms of E, h and η.

We now move on to obtain an integral connecting t and s after factorizing the above $(ds/dt)^2/s^4$ expression using 4PN order s_- and s_+ expressions. The resulting 4PN order integral

may be written as

$$t - t_0 = \int_s^{s_-} \frac{A_0 + A_1\bar{s} + A_2\bar{s}^2 + A_3\bar{s}^3 + A_4\bar{s}^4 + A_5\bar{s}^5 + A_6\bar{s}^6 + A_7\bar{s}^7}{\sqrt{(s_- - \bar{s})(\bar{s} - s_+)}\,\bar{s}^2} d\bar{s}\,, \tag{5.13}$$

and how we obtain the above integral from our PN-accuate expression for ds/dt is explained in Appendix A of Ref. [112]. Additionally, we gather from the structure of the expressions of $(ds/dt)^2$, s_- and s_+ that the coefficients A_i (with $i = 1, .., 7$) should be some PN-accurate functions of E, h and η. We now compute the radial orbital period as the value of the above integral between s_- and s_+, multiplied by two. In other words, 4PN order expression for the radial period reads

$$P = 2\int_{s_+}^{s_-} \frac{A_0 + A_1\bar{s} + A_2\bar{s}^2 + A_3\bar{s}^3 + A_4\bar{s}^4 + A_5\bar{s}^5 + A_6\bar{s}^6 + A_7\bar{s}^7}{\sqrt{(s_- - \bar{s})(\bar{s} - s_+)}\,\bar{s}^2} d\bar{s}\,. \tag{5.14}$$

The explicit expression for P will be displayed when we present 4PN order Keplerian type solution. Note that PN-accurate mean motion $n = 2\pi/P$.

We now have all the necessary ingredients to obtain the 4PN order Kepler equation. This requires us to express the mean anomaly $l \equiv n(t - t_0)$ as a function of eccentric anomaly u with the help of our Eqs. (5.13) and (5.14) while employing our parametric equation for $r = a_r(1 - e_r\,\cos u)$. It is convenient to introduce an auxiliary variable $\tilde{v} = 2\arctan[\sqrt{(1+e_r)/(1-e_r)}\,\tan(u/2)]$ and with the help of a few trigonometric relations involving $\tilde{v}$, we obtain the following provisional parametrization for l as

$$\begin{aligned} l \equiv n\,(t - t_0) &= u + \kappa_0 \sin u + \frac{\kappa_1}{c^4}(\tilde{v} - u) + \frac{\kappa_2}{c^4}\sin\tilde{v} \\ &+ \frac{\kappa_3}{c^6}\sin 2\tilde{v} + \frac{\kappa_4}{c^6}\sin 3\tilde{v} + \frac{\kappa_5}{c^8}\sin 4\tilde{v} + \frac{\kappa_6}{c^8}\sin 5\tilde{v}\,. \end{aligned} \tag{5.15}$$

The steps required to obtain the above expression from Eq. (5.13) are sketched in the Appendix B of Ref. [79]. Note that these κ_i coefficients are some PN accurate functions of E, h and η and they can be had from the accompanying MATHEMATICA notebook `Lengthy_Expressions.nb` [91, 92] and some details of the underlying computations are provided in Appendices A and B of Ref. [112]. We

treat the above expression as a provisional one as it contains 1PN order corrections to the classical Kepler equation due to the presence of PN accurate κ_0 expression that multiplies $\sin u$. Recall that there exists 1PN-accurate Kepler equation that is structurally similar (by "structurally similar" we mean having no explicit 1PN additive correction terms) to the classical Kepler equation, obtained by invoking certain conchoidal transformation [93]. It will be desirable to keep such a structure while computing 4PN order Kepler equation and this will be taken up later.

We move on to tackle the angular part by first computing our 4PN order expression for $d\phi/ds$ with the help of $d\phi/ds = \dot{\phi}/\dot{s}$, where $\dot{\phi}$ expression arises from the usual Hamiltonian equations of motion. Influenced by our approach to tackle the radial motion, we obtain an expression for $d\phi/ds$ which involves a similar factorization based on s_+ and s_- as in Eqs. (5.13) and (5.14). The resulting expression may be written as

$$\frac{d\phi}{ds} = \frac{B_0 + B_1\, s + B_2\, s^2 + B_3\, s^3 + B_4\, s^4 + B_5\, s^5 + B_6\, s^6 + B_7\, s^7}{\sqrt{(s_- - s)(s - s_+)}} \tag{5.16}$$

where the coefficients B_i $(i = 1, ..., 7)$, as expected, are some 4PN order functions of E, h and η (the explicit expressions for these coefficients are listed in the accompanying MATHEMATICA notebook). Additionally, we sketch how to obtain 1PN-accurate $d\phi/ds$ expression from $\dot{\phi}$ and dt/ds in Appendix A of [112]. The above equation also allows us to compute the amount by which periastron (or pericenter) advances during the above computed 4PN order radial period P. This is obtained by integrating the above equation between our 4PN order roots s_+ and s_- and multiplying the result by two. In other words, the amount of periastron advance during one radial period is

$$\Phi = 2 \int_{s_+}^{s_-} \frac{B_0 + B_1 \bar{s} + B_2 \bar{s}^2 + B_3 \bar{s}^3 + B_4 \bar{s}^4 + B_5\, \bar{s}^5 + B_6\, \bar{s}^6 + B_7\, \bar{s}^7}{\sqrt{(s_- - \bar{s})(\bar{s} - s_+)}} d\bar{s}\,. \tag{5.17}$$

It should be obvious that the resulting 4PN order Φ expression depends on E, h and η and we have verified that our expression is consistent with Eq. (20-k) in Ref. [79]. We now invoke 4PN order expressions for Φ (got by evaluating the integral in Eq. (5.17)) and $d\phi/ds$ to obtain $(\phi - \phi_0) \times (2\,\pi/\Phi)$

which we symbolically write as

$$\frac{2\,\pi}{\Phi}\times(\phi-\phi_0)=\int_s^{s_-}\frac{B'_0+B_1\bar{s}+B'_2\bar{s}^2+B'_3\bar{s}^3+B'_4\bar{s}^4+B'_5\bar{s}^5+B'_6\bar{s}^6+B'_7\,\bar{s}^7}{\sqrt{(s_--\bar{s})(\bar{s}-s_+)}}d\bar{s}\,, \tag{5.18}$$

where the primed B'_i coefficients are got from the unprimed B_i's. It is possible to evaluate the above integral with the help of certain trigonometric relations and steps as detailed in Appendix B of Ref. [112]. This results in the following provisional parametric expression for the 4PN order angular motion

$$\begin{aligned}\frac{2\,\pi}{\Phi}\,(\phi-\phi_0)&=\tilde{v}+\frac{\lambda_1}{c^2}\sin\tilde{v}+\frac{\lambda_2}{c^4}\sin 2\tilde{v}+\frac{\lambda_3}{c^4}\sin 3\tilde{v}\\&+\frac{\lambda_4}{c^6}\sin 4\tilde{v}+\frac{\lambda_5}{c^6}\sin 5\tilde{v}+\frac{\lambda_6}{c^8}\sin 6\tilde{v}+\frac{\lambda_7}{c^8}\sin 7\tilde{v}\,,\end{aligned} \tag{5.19}$$

where λ_i are some PN accurate functions, expressible in terms of E, h and η.

Following Ref. [79], we obtain our final parametrization for l and ϕ equations with the help of some true anomaly variable $v=2\arctan[\sqrt{(1+e_\phi)/(1-e_\phi)}\tan(u/2)]$ that involves a new angular eccentricity parameter e_ϕ. The plan is to write Eq. (5.19) in terms of v rather than $\tilde{v}$ so that there are no explicit, additive $1/c^2$ corrections, while allowing e_ϕ to differ from e_r by some yet to be determined PN corrections. It is possible to write our $\tilde{v}$ in terms of v

$$\begin{aligned}\tilde{v}=v&+\frac{y}{c^2}\sin v+\frac{y^2}{4c^4}\,(-2\sin v+\sin 2v)\\&+\frac{y^3}{12c^6}\,(3\sin v-3\sin 2v+\sin 3v)\\&+\frac{y^4}{32c^8}\,(-4\sin v+6\sin 2v-4\sin 3v+\sin 4v)\end{aligned} \tag{5.20}$$

where y connects e_ϕ and e_r to 4PN order and it is natural to introduce y such that

$$y=\frac{\sqrt{(1+e_r)/(1-e_r)}}{\sqrt{(1+e_\phi)/(1-e_\phi)}}-1. \tag{5.21}$$

We now express $2\,\pi\ (\phi - \phi_0)\ /\Phi$, given by Eq. (5.19), in terms of v and demand that there are no $\sin v$ terms up to 4PN order. This requirement uniquely determines y as a PN series which connects e_ϕ to e_r. For example, the dominant 1PN contribution of y may be written as

$$y = -\frac{\eta\sqrt{1+2\,E\,h^2}}{2\,c^2\,h^2} + O\left(\frac{1}{c^4}\right). \tag{5.22}$$

It should be noted that we imposed such a restriction because 1PN-accurate parametric solution, derived in Ref. [93], supported a *Keplerian* like parametrization for the angular part with the help of v. This leads to the following parametric solution for the angular motion while incorporating 4PN order contributions:

$$\begin{aligned}\frac{2\,\pi}{\Phi}\,(\phi-\phi_0) = v &+ \left(\frac{f_{4\phi}}{c^4} + \frac{f_{6\phi}}{c^6} + \frac{f_{8\phi}}{c^8}\right)\sin 2v + \left(\frac{g_{4\phi}}{c^4} + \frac{g_{6\phi}}{c^6} + \frac{g_{8\phi}}{c^8}\right)\sin 3v \\ &+ \left(\frac{i_{6\phi}}{c^6} + \frac{i_{8\phi}}{c^8}\right)\sin 4v + \left(\frac{h_{6\phi}}{c^6} + \frac{h_{8\phi}}{c^8}\right)\sin 5v + \frac{k_{8\phi}}{c^8}\,\sin 6\,v + \frac{j_{8\phi}}{c^8}\,\sin 7\,v\,,\end{aligned} \tag{5.23}$$

where $v = 2\arctan[\sqrt{(1+e_\phi)/(1-e_\phi)}\tan(u/2)]$. Interestingly, the contributions at 2PN, 3PN and 4PN orders are supplemented by other trigonometric functions of v and this is why we term the resulting solution as the generalized quasi-Keplerian parametric solution. We will display shortly the explicit 4PN order expressions for these orbital elements and functions.

We now move to finalize the provisional expression for our 4PN order Kepler equation, given by Eq. (5.15). The idea is to express $\tilde{v}$ in terms of v with the help of the above listed PN-accurate relation of Eq. (5.20). This leads to the following Kepler equation that includes 4PN order contributions in terms of $u, e_t, v(u)$ and its trigonometric functions as

$$\begin{aligned}l = n\,(t-t_0) = u - e_t\,\sin u &+ \left(\frac{g_{4t}}{c^4} + \frac{g_{6t}}{c^6} + \frac{g_{8t}}{c^8}\right)(v-u) + \left(\frac{f_{4t}}{c^4} + \frac{f_{6t}}{c^6} + \frac{f_{8t}}{c^8}\right)\sin v \\ &+ \left(\frac{i_{6t}}{c^6} + \frac{i_{8t}}{c^8}\right)\sin 2\,v + \left(\frac{h_{6t}}{c^6} + \frac{h_{8t}}{c^8}\right)\sin 3\,v + \frac{k_{8t}}{c^8}\,\sin 4\,v + \frac{j_{8t}}{c^8}\,\sin 5\,v\,.\end{aligned} \tag{5.24}$$

The PN accurate expressions for n, e_t and the orbital functions appearing in the above PN-accurate

Kepler equation will be listed below.

We now have all the parts to display, in its entirety, the fourth post-Newtonian order generalized quasi-Keplerian parametrization for an eccentric compact binary in ADM-type coordinates as

$$r = a_r\,(1 - e_r\,\cos u)\ , \tag{5.25}$$

$$\begin{aligned} l = n\,(t-t_0) = u - e_t\,\sin u + \left(\frac{g_{4t}}{c^4} + \frac{g_{6t}}{c^6} + \frac{g_{8t}}{c^8}\right)\,(v-u) + \left(\frac{f_{4t}}{c^4} + \frac{f_{6t}}{c^6} + \frac{f_{8t}}{c^8}\right)\,\sin v \\ + \left(\frac{i_{6t}}{c^6} + \frac{i_{8t}}{c^8}\right)\,\sin 2\,v + \left(\frac{h_{6t}}{c^6} + \frac{h_{8t}}{c^8}\right)\,\sin 3\,v + \frac{k_{8t}}{c^8}\,\sin 4\,v + \frac{j_{8t}}{c^8}\,\sin 5\,v\,, \end{aligned} \tag{5.26}$$

$$\begin{aligned} \frac{2\,\pi}{\Phi}\,(\phi - \phi_0) = v + \left(\frac{f_{4\phi}}{c^4} + \frac{f_{6\phi}}{c^6} + \frac{f_{8\phi}}{c^8}\right)\,\sin 2v + \left(\frac{g_{4\phi}}{c^4} + \frac{g_{6\phi}}{c^6} + \frac{g_{8\phi}}{c^8}\right)\,\sin 3v \\ + \left(\frac{i_{6\phi}}{c^6} + \frac{i_{8\phi}}{c^8}\right)\,\sin 4v + \left(\frac{h_{6\phi}}{c^6} + \frac{h_{8\phi}}{c^8}\right)\,\sin 5v + \frac{k_{8\phi}}{c^8}\,\sin 6\,v + \frac{j_{8\phi}}{c^8}\,\sin 7\,v\,, \end{aligned} \tag{5.27}$$

where $v = 2\arctan[\sqrt{(1+e_\phi)/(1-e_\phi)}\tan(u/2)]$. The 4PN order expressions for the orbital elements a_r, n, Φ, and the post-Newtonian orbital functions that appear at 2PN, 3PN and 4PN orders in terms of the conserved quantities:

$$\begin{aligned} a_r \;=\; & \frac{1}{(-2\,E)}\Bigg\{1 + \frac{(-2\,E)}{4\,c^2}\,(-7+\eta) + \frac{(-2\,E)^2}{16c^4}\left[(1 + 10\,\eta + \eta^2)\right. \\ & \left. + \frac{1}{(-2\,E\,h^2)}(-68 + 44\,\eta)\right] + \frac{(-2\,E)^3}{192\,c^6}\left[3 - 9\,\eta - 6\,\eta^2\right. \\ & \left. + 3\,\eta^3 + \frac{1}{(-2\,E\,h^2)}\left(864 + \left(-3\,\pi^2 - 2212\right)\,\eta + 432\,\eta^2\right)\right. \\ & \left. + \frac{1}{(-2\,E\,h^2)^2}\left(-6432 + \left(13488 - 240\,\pi^2\right)\,\eta - 768\,\eta^2\right)\right] \\ & + \frac{(-2\,E)^4}{3686400\,c^8}\left[14400 - 57600\,\eta + 28800\,\eta^2 - 158400\,\eta^3 + 14400\,\eta^4\right. \\ & + \frac{1}{(-2\,E\,h^2)}\left(-4147200 + (-38071488 + 1280250\pi^2)\,\eta\right. \\ & \left. + \left(19038208 + 4030875\,\pi^2\right)\,\eta^2 + 4262400\,\eta^3\right) \\ & + \frac{1}{(-2\,E\,h^2)^2}\left(316800000 + \left(-661398528 + 21132000\pi^2\right)\,\eta\right. \end{aligned}$$

$$
\begin{aligned}
&+\left(363371776-26908200\pi^2\right)\,\eta^2-20160000\,\eta^3\Big)\\
&+\frac{1}{(-2\,E\,h^2)^3}\left(-1228492800+\left(2644664832-59785200\,\pi^2\right)\,\eta\right.\\
&\left.+\left(-826707456+34613400\,\pi^2\right)\,\eta^2+13824000\,\eta^3\right)\Big]\Big\}\,, \qquad (5.28a)\\
n &= (-2\,E)^{3/2}\Big\{1+\frac{(-2\,E)}{8\,c^2}\,(-15+\eta)+\frac{(-2\,E)^2}{128c^4}\Big[555+30\,\eta\\
&+11\,\eta^2+\frac{192}{\sqrt{(-2\,E\,h^2)}}\,(-5+2\,\eta)\Big]+\frac{(-2\,E)^3}{3072\,c^6}\Big[-29385\\
&-4995\,\eta-315\,\eta^2+135\,\eta^3-\frac{16}{(-2\,E\,h^2)^{3/2}}\Big(10080+123\,\eta\,\pi^2\\
&-13952\,\eta+1440\,\eta^2\Big)+\frac{5760}{\sqrt{(-2\,E\,h^2)}}\left(17-9\,\eta+2\,\eta^2\right)\Big]\\
&+\frac{(-2\,E)^4}{1474560\,c^8}\Big[\frac{3317760\,(-5+2\,\eta)^2}{-2\,E\,h^2}+\frac{138240}{\sqrt{(-2\,E\,h^2)}}\\
&\times\left(-1125+550\,\eta-175\,\eta^2+38\,\eta^3\right)+135\Big(232881\\
&+65300\,\eta+4070\,\eta^2-460\,\eta^3+241\,\eta^4\Big)\\
&-\frac{80}{(-2\,E\,h^2)^{3/2}}\left(-5443200+\left(10467328-150987\pi^2\right)\,\eta\right.\\
&\left.+\left(-3959808+32472\pi^2\right)\,\eta^2+311040\,\eta^3\right)\\
&+\frac{48}{(-2\,E\,h^2)^{5/2}}\Big(-17297280+\left(37556864-771585\,\pi^2\right)\,\eta\\
&+\left(-13464960+236160\,\pi^2\right)\,\eta^2+403200\,\eta^3\Big)\Big]\Big\}\,, \qquad (5.28b)\\
g_{4\,t} &= \frac{3\,(-2\,E)^2}{2}\left\{\frac{5-2\,\eta}{\sqrt{(-2\,E\,h^2)}}\right\}\,, \qquad (5.28c)\\
g_{6\,t} &= \frac{(-2\,E)^3}{192}\Big\{\frac{1}{(-2\,E\,h^2)^{3/2}}\Big(10080+123\,\eta\,\pi^2-13952\,\eta\\
&+1440\,\eta^2\Big)+\frac{1}{\sqrt{(-2\,E\,h^2)}}\left(-3420+1980\,\eta-648\,\eta^2\right)\Big\}\,, \qquad (5.28d)\\
g_{8\,t} &= -\frac{(-2\,E)^4}{92160}\Big\{\frac{3}{(-2\,E\,h^2)^{5/2}}\Big(-17297280+(37556864\\
&-771585\pi^2)\eta+1920\left(-7013+123\,\pi^2\right)\eta^2+403200\eta^3\Big)
\end{aligned}
$$

$$
\begin{aligned}
&-\frac{5}{(-2\,E\,h^2)^{3/2}}\left(-3628800+\left(7835008-128847\pi^2\right)\eta\right.\\
&+36\left(-98144+861\pi^2\right)\eta^2+293760\eta^3\Big)+\frac{207360}{(-2\,E\,h^2)}\,(5-2\,\eta)^2\\
&\left.+\frac{1080}{\sqrt{(-2\,E\,h^2)}}\,(-3375+1600\eta-755\eta^2+246\eta^3)\right\}, \qquad (5.28e)\\
f_{4t} &= -\frac{1}{8}\,\frac{(-2\,E)^2}{\sqrt{(-2\,E\,h^2)}}\left\{(4+\eta)\,\eta\,\sqrt{(1+2\,E\,h^2)}\right\}, \qquad (5.28f)\\
f_{6t} &= \frac{(-2\,E)^3}{192}\left\{\frac{1}{(-2\,E\,h^2)^{3/2}}\,\frac{1}{\sqrt{1+2\,E\,h^2}}\left(1728-4148\,\eta+3\,\eta\,\pi^2\right.\right.\\
&+600\,\eta^2+33\,\eta^3\Big)+3\,\frac{\sqrt{(-2\,E\,h^2)}}{\sqrt{(1+2\,E\,h^2)}}\eta\,\left(-64-4\,\eta+23\,\eta^2\right)\\
&+\frac{1}{\sqrt{(-2\,E\,h^2)\,(1+2\,E\,h^2)}}\left(-1728+4232\,\eta-3\,\eta\,\pi^2\right.\\
&\left.\left.-627\,\eta^2-105\,\eta^3\right)\right\}, \qquad (5.28g)\\
f_{8t} &= -\frac{(-2\,E)^4}{14745600}\,\frac{(-2\,E\,h^2)^{3/2}}{(1+2\,E\,h^2)^{3/2}}\left\{7200\,\eta\,\left(4672+912\,\eta\right.\right.\\
&\left.-303\,\eta^2+902\,\eta^3\right)+\frac{2764800}{\sqrt{(-2\,E\,h^2)}}\,\eta\,(4+\eta)\,(-5+2\eta)\\
&+\frac{1}{(-2\,E\,h^2)}\left(331776000+1350\left(-919776+2377\pi^2\right)\eta\right.\\
&\left.+\left(568404992+2468925\pi^2\right)\eta^2-94248000\eta^3-16128000\eta^4\right)\\
&-\frac{5529600}{(-2\,E\,h^2)^{3/2}}\,\eta\,(4+\eta)\,(-5+2\eta)\\
&+\frac{1}{(-2\,E\,h^2)^2}\left(-2226585600+\left(10348301504-252478050\pi^2\right)\eta\right.\\
&\left.+9\left(-614377024+9064225\pi^2\right)\eta^2+383328000\eta^3+10411200\eta^4\right)\\
&+\frac{2764800}{(-2\,E\,h^2)^{5/2}}\,\eta\,\left(-20+3\eta+2\eta^2\right)\\
&+\frac{1}{(-2\,E\,h^2)^3}\left(3607142400+2\left(-8729633504+247794225\,\pi^2\right)\eta\right.\\
&\left.+\left(9340505856-170534025\,\pi^2\right)\,\eta^2-471441600\,\eta^3+1152000\,\eta^4\right)\\
&+\frac{1}{(-2\,E\,h^2)^4}\left(-1712332800+\left(8314359104-246319350\pi^2\right)\eta\right.
\end{aligned}
$$

$$+\left(-4388287232+86487075\pi^2\right)\eta^2+184226400\eta^3-1944000\eta^4\Big)\Big\}, \quad (5.28h)$$

$$h_{6t} = \frac{(-2\,E)^3}{32}\,\eta\Big\{\frac{(1+2\,E\,h^2)}{(-2\,E\,h^2)^{3/2}}\left(23+12\,\eta+6\,\eta^2\right)\Big\}, \quad (5.28i)$$

$$\begin{aligned} h_{8t} = {} & \frac{(-2\,E)^4}{921600}\Big\{-\frac{300}{\sqrt{-2\,E\,h^2}}\,\eta\left(-8904+12207\eta+2356\eta^2+864\eta^3\right) \\ & +\frac{1}{(-2\,E\,h^2)^{3/2}}\Big(-1857600+\left(10986256-1072425\pi^2\right)\eta \\ & +\left(-38708632+3152775\pi^2\right)\eta^2+4891200\eta^3+176400\eta^4\Big) \\ & +\frac{1}{(-2\,E\,h^2)^{5/2}}\Big(1857600+\left(-12167056+1072425\pi^2\right)\eta \\ & +\left(43313932-3152775\pi^2\right)\eta^2-3709200\eta^3+126000\eta^4\Big)\Big\}, \end{aligned} \quad (5.28j)$$

$$i_{6t} = \frac{13\,(-2\,E)^3}{192}\eta^3\left(\frac{1+2\,E\,h^2}{-2\,E\,h^2}\right)^{3/2}, \quad (5.28k)$$

$$\begin{aligned} i_{8t} = {} & \frac{(-2\,E)^4}{14745600}\left(\frac{1+2\,E\,h^2}{-2\,E\,h^2}\right)^{1/2}\eta\,\Big\{-3600\,\eta^2\,(-839+526\,\eta) \\ & +\frac{1}{(-2\,E\,h^2)}\Big(6\,\left(-9586592+405075\,\pi^2\right) \\ & +5\,\left(-21746432+2673315\,\pi^2\right)\,\eta+23416800\,\eta^2+1368000\,\eta^3\Big) \\ & +\frac{1}{(-2\,E\,h^2)^2}\Big(57519552-2430450\,\pi^2 \\ & +\left(108732160-13366575\,\pi^2\right)\,\eta-23067600\,\eta^2+900000\,\eta^3\Big)\Big\}, \end{aligned} \quad (5.28l)$$

$$k_{8t} = -\frac{(-2\,E)^{3/2}\,\eta\,(150\eta^3+2444\eta^2-3303\eta+516)(1+2\,E\,h^2)^2}{6144h^5}, \quad (5.28m)$$

$$j_{8t} = -\frac{(-2\,E)^{3/2}\eta^3(66\eta-25)\,\left(1+2\,E\,h^2\right)^{5/2}}{4096h^5}, \quad (5.28n)$$

$$\begin{aligned} \Phi = {} & 2\,\pi\Big\{1+\frac{3}{c^2h^2}+\frac{(-2\,E)^2}{4\,c^4}\Big[\frac{3}{(-2\,E\,h^2)}\,(-5+2\,\eta) \\ & +\frac{15}{(-2\,E\,h^2)^2}\,(7-2\,\eta)\Big]+\frac{(-2\,E)^3}{128\,c^6}\Big[\frac{24}{(-2\,E\,h^2)}(5-5\eta \\ & +4\eta^2)-\frac{1}{(-2\,E\,h^2)^2}\Big(10080-13952\,\eta+123\,\eta\,\pi^2+1440\,\eta^2\Big) \\ & +\frac{5}{(-2\,E\,h^2)^3}\Big(7392-8000\,\eta+123\,\eta\,\pi^2+336\,\eta^2\Big)\Big] \end{aligned}$$

$$
\begin{aligned}
&-\frac{(-2\,E)^4}{73728\,c^8}\,\frac{1}{(-2\,E\,h^2)}\Bigg[-6912\,\eta^2\,(-5+4\eta)\\
&+\frac{3}{(-2\,E\,h^2)}\Bigg(-1814400+\left(5202688-106707\pi^2\right)\eta\\
&+240\left(-12944+123\pi^2\right)\eta^2+276480\eta^3\Bigg)\\
&-\frac{6}{(-2\,E\,h^2)^2}\Bigg(-17297280+\left(37556864-771585\pi^2\right)\eta\\
&+1920\left(-7013+123\pi^2\right)\eta^2+403200\eta^3\Bigg)\Bigg]\\
&+\frac{7}{(-2\,E\,h^2)^3}\Bigg(-37065600+\left(63502592-1275315\pi^2\right)\eta\\
&+2400\left(-6056+123\pi^2\right)\eta^2+207360\eta^3\Bigg)\Bigg]\Bigg\}, \qquad (5.28o)
\end{aligned}
$$

$$
f_{4\,\phi} = \frac{(-2\,E)^2}{8}\,\frac{(1+2\,E\,h^2)}{(-2\,E\,h^2)^2}\,\eta\,(1-3\,\eta)\,, \qquad (5.28p)
$$

$$
\begin{aligned}
f_{6\,\phi} = \frac{(-2\,E)^3}{256}\Bigg\{&\frac{4\,\eta}{(-2\,E\,h^2)}\left(-11-40\,\eta+24\,\eta^2\right)\\
&+\frac{1}{(-2\,E\,h^2)^2}\left(-256+1192\,\eta-49\,\eta\,\pi^2+336\,\eta^2-80\,\eta^3\right)\\
&+\frac{1}{(-2\,E\,h^2)^3}\left(256+49\,\eta\,\pi^2-1076\,\eta-384\,\eta^2-40\,\eta^3\right)\Bigg\}, \qquad (5.28q)
\end{aligned}
$$

$$
\begin{aligned}
f_{8\,\phi} = \frac{(-2\,E)^4}{7372800}\Bigg\{&\frac{900\,\eta}{(-2\,E\,h^2)}\left(6844-13989\eta-1530\eta^2+1888\eta^3\right)\\
&+\frac{1}{(-2\,E\,h^2)^2}\Bigg(9273600+2\left(-303923464+7907025\pi^2\right)\eta\\
&+\left(567130588+8219475\pi^2\right)\eta^2-26411400\eta^3+1180800\eta^4\Bigg)\\
&-\frac{2}{(-2\,E\,h^2)^3}\Bigg(84844800+10\left(-149381636+4263405\pi^2\right)\eta\\
&-19\left(-67975466+173325\pi^2\right)\eta^2-54814500\eta^3+2980800\eta^4\Bigg)\\
&\frac{1}{(-2\,E\,h^2)^4}\Bigg(177004800+\left(-2446310192+72629250\pi^2\right)\eta\\
&-15\left(-132716108+963535\pi^2\right)\eta^2-86679000\eta^3+1929600\eta^4\Bigg)\Bigg\}, \qquad (5.28r)
\end{aligned}
$$

$$
g_{4\,\phi} = -\frac{3(-2\,E)^2}{32}\,\frac{\eta^2}{(-2\,E\,h^2)^2}(1+2\,E\,h^2)^{3/2}\,, \qquad (5.28s)
$$

$$
\begin{aligned}
g_{6\,\phi} &= \frac{(-2\,E)^3}{768}\,\sqrt{(1+2\,E\,h^2)}\left\{-\frac{3}{(-2\,E\,h^2)}\,\eta^2\;(9-26\,\eta)\right.\\
&\quad -\frac{1}{(-2\,E\,h^2)^2}\,\eta\left(220+3\,\pi^2+312\,\eta+150\,\eta^2\right)\\
&\quad \left.+\frac{1}{(-2\,E\,h^2)^3}\,\eta\left(220+3\,\pi^2+96\,\eta+45\,\eta^2\right)\right\}, \qquad (5.28t)\\
g_{8\,\phi} &= \frac{(-2\,E)^4}{176947200}\,\frac{1}{\sqrt{(1+2\,E\,h^2)}}\left\{-10800\eta^2\left(36-95\eta+1226\eta^2\right)\right.\\
&\quad +\frac{3\,\eta}{(-2\,E\,h^2)}\left(-404533824+5453550\pi^2\right.\\
&\quad \left.+\left(731023360+381825\,\pi^2\right)\eta-115070400\,\eta^2-9129600\,\eta^3\right)\\
&\quad +\frac{1}{(-2\,E\,h^2)^2}\left(44236800+2\left(-6842155424+127907475\pi^2\right)\eta\right.\\
&\quad -87\left(-253902848+3210525\,\pi^2\right)\,\eta^2\\
&\quad \left.-2262477600\,\eta^3+39096000\,\eta^4\right)\\
&\quad +\frac{1}{(-2\,E\,h^2)^3}\left(-88473600+\left(23556745280-464880750\,\pi^2\right)\eta\right.\\
&\quad +\left(-37649997312+561808575\,\pi^2\right)\eta^2\\
&\quad \left.+3436488000\eta^3-103766400\,\eta^4\right)\\
&\quad +\frac{1}{(-2\,E\,h^2)^4}\left(44236800+\left(-11086035904+225426450\pi^2\right)\eta\right.\\
&\quad +\left(17722415616-281347425\pi^2\right)\eta^2\\
&\quad \left.\left.-1527246000\eta^3+50133600\eta^4\right)\right\}, \qquad (5.28u)\\
i_{6\,\phi} &= \frac{(-2\,E)^3}{128}\,\frac{(1+2\,E\,h^2)^2}{(-2\,E\,h^2)^3}\,\eta\left(5+28\,\eta+10\,\eta^2\right), \qquad (5.28v)\\
i_{8\,\phi} &= \frac{(-2\,E)^4}{14745600}\,\frac{\sqrt{(1+2\,E\,h^2)}}{(-2\,E\,h^2)^2}\left\{-7200\left(440-1330\eta+700\eta^2+173\eta^3\right)\right.\\
&\quad +\frac{1}{(-2\,E\,h^2)}\left(175308224+1767300\pi^2\right.\\
&\quad \left.+\left(-407514720-9062175\pi^2\right)\eta+70257600\eta^2-1713600\eta^3\right)\\
&\quad +\frac{1}{(-2\,E\,h^2)^2}\left(-169548224+1767300\pi^2\right.
\end{aligned}
$$

$$+\left(412741920-9062175\pi^2\right)\eta-58420800\eta^2+3535200\eta^3\Big)\Big\}\,, \tag{5.28w}$$

$$h_{6\,\phi} = \frac{5\,(-2\,E)^3}{256}\,\frac{\eta^3}{(-2\,E\,h^2)^3}\,(1+2\,E\,h^2)^{5/2}\,, \tag{5.28x}$$

$$\begin{aligned} h_{8\,\phi} = {} & \frac{(-2\,E)^4}{6553600}\,\frac{\eta}{(-2\,E\,h^2)^2}\,(1+2\,E\,h^2)^{3/2}\,\Big\{78000\eta^2 \\ & -172000\eta^3+\frac{1}{(-2\,E\,h^2)}\,\Big(8273856+11250\pi^2 \\ & +\left(-24254464-579825\pi^2\right)\eta+7604000\eta^2-238400\eta^3\Big) \\ & +\frac{1}{(-2\,E\,h^2)^2}\,\Big(-8273856+11250\pi^2 \\ & +\left(24254464-579825\pi^2\right)\,\eta-6962000\,\eta^2+490400\,\eta^3\Big)\Big\}\,, \end{aligned} \tag{5.28y}$$

$$k_{8\,\phi} = -\frac{\eta\,\left(150\eta^3+4154\eta^2-5755\eta+1476\right)\,\left(1+2\,E\,h^2\right)^3}{24576\,h^8}\,, \tag{5.28z}$$

$$j_{8\,\phi} = -\frac{35(2\eta-1)\,\eta^3\,\left(1+2\,E\,h^2\right)^{7/2}}{16384\,h^8}\,. \tag{5.29a}$$

Appendix C of Ref. [112] provides the explicit expressions for e_t and 4PN-order relations that connect e_r and e_ϕ to e_t. This is influenced by the GW phasing approach that usually employs the time eccentricity to characterize PN-accurate eccentric orbits. Borrowing from Ref. [101], we refer to as 'phasing', the task of specifying the time dependencies $r(t), \dot{r}(t), \phi(t)$ and $\dot{\phi}(t)$.

Clearly, it is important to go through a consistency check in order to ensure the correctness of these lengthy expressions for the 4PN order orbital elements and functions. The plan is to adapt two consistency checks, detailed in Ref. [79]. This requires us to express PN-accurate expressions for $\dot{r}^2$ and $\dot{\phi}^2$, derived using the Hamiltonian equations of motion and given by Eqs. (5.8), in terms of E, h, η and $(1-e_r\,\cos u)$ while using the fact that $r = a_r\,(1-e_r\,\cos u)$. Note that the expressions for a_r and e_r^2 were obtained from the PN accurate roots s_- and s_+, and therefore, do not involve any of our complicated integrals. In the first part of our check, we compare such an expression

with the one that explicitly employed our parametric solution, namely $\dot{r}^2 = (dr/du \times du/dt)^2$. This expression for $\dot{r}^2$ is found to be in full agreement with our earlier $\dot{r}^2$ expression up to 4PN order after some elaborate simplifications. Thereafter, we performed a similar check on the angular part by computing $\dot{\phi}^2 = (d\phi/dv \times dv/du \times du/dt)^2$ in terms of E, h, η and $(1 - e_r \cos u)$. We have verified that such an expression is identical to our Hamiltonian equations of motion based $\dot{\phi}^2$ expression to 4PN order. Additionally, we have also performed the above two checks using $\tilde{v}$ variable based parametric solution. These computations provided us with two powerful checks on our 4PN order generalized quasi-Keplerian parametrization.

5.2.3 Incorporating non-local in time 4PN Hamiltonian

Having dealt with the local-in-time component of the 4PN Hamiltonian in the previous subsection, we turn our attention to the non-local one. Our strategy will be to treat the 4PN tail effect as a perturbation to the basic Newtonian Kepler problem within the framework of the action-angle formalism. We will employ canonical (or classical) perturbation theory, a perturbation technique that is tailor-made for the action-angle framework [113], following the application this technique as was done in Ref. [104].

5.2.3.1 Action-angles of the Newtonian system

We start with a small review of the action-angle (Delaunay) picture of the Newtonian system Ref. [104, 113–115]. We will consider the planar (two actions, two angles) version of the picture because the system is confined to a plane. The action-angle pairs $\{(\mathcal{L}, l), (\mathcal{G}, g)\}$ written in terms of more familiar quantities become [104]

$$\mathcal{L} = a^{1/2},\ \mathcal{G} = (a(1 - e^2))^{1/2}, \tag{5.30}$$

$$l = u - e \sin u,\ g = \text{arugment of periastron}, \tag{5.31}$$

where a and e are Newtonian versions of a_r and e_r; u is as usual the eccentric anomaly. The Hamiltonian is a function of only one of the actions

$$\mathcal{H}_N = -\frac{1}{2\mathcal{L}^2} \tag{5.32}$$

The rate of change of the first angle variable is

$$\frac{dl}{dt} = \frac{\partial \mathcal{H}_N}{\partial \mathcal{L}} = \frac{1}{\mathcal{L}^3} \equiv \Omega(\mathcal{L}), \tag{5.33}$$

whereas g does not change with time since $\partial \mathcal{H}_N / \partial \mathcal{G} = 0$.

5.2.3.2 The nonlocal-in-time 4PN tail Hamiltonian

To incorporate the effect of the nonlocal-in-time Hamiltonian $\mathcal{H}^{\rm nonlocal}_{\rm 4PN}$ on the BBH dynamics, it suffices to consider it as a perturbation on the Newtonian dynamics. Then the reduced Hamiltonian of interest is [87]

$$\mathcal{H} = \frac{\hat{\mathbf{p}}^2}{2} - \frac{1}{r} + \mathcal{H}^{\rm nonlocal}_{\rm 4PN}, \tag{5.34}$$

where

$$\mathcal{H}^{\rm nonlocal}_{\rm 4PN} = -\frac{G^2}{5\eta c^8} I^{(3)}_{ij}(t') \, {\rm Pf}_{2R/c} \int_{-\infty}^{+\infty} \frac{{\rm d}w}{|w|} I^{(3)}_{ij}(t'+w). \tag{5.35}$$

In the above expression, $I^{(3)}_{ij}$ denotes the third derivative with respect to the coordinate time t' of the center-of-mass Newtonian quadrupole moment I_{ij} of the system (with r^i denoting the components of $\mathbf{r}$)

$$I_{ij} \equiv (GM)^2 \mu \left(r^i r^j - \frac{1}{3} r^2 \delta^{ij} \right), \tag{5.36}$$

and $R \equiv |\mathbf{R}|$. Pf_T stands for the Hadamard partie finie which is defined as [87]

$$\mathrm{Pf}_T \int_0^{+\infty} \frac{\mathrm{d}w}{w} g(w) \equiv \int_0^T \frac{\mathrm{d}w}{w} (g(w) - g(0)) + \int_T^{+\infty} \frac{\mathrm{d}w}{w} g(w), \tag{5.37}$$

a quick application of which gives

$$\mathrm{Pf}_T \int_0^{+\infty} \frac{\mathrm{d}w}{w} \cos(\omega w) = -\left(\gamma_{\mathrm{E}} + \ln(\omega T)\right), \tag{5.38}$$

with $\gamma_E = 0.577...$ being the Euler-Mascheroni constant. The two-sided integral in Eq. (5.35) needs to be converted into one-sided ones so as to make it amenable to the above definition of Pf_T.

Now focusing our attention on $\mathcal{H}^{\mathrm{nonlocal}}_{\mathrm{4PN}}$, to manipulate the integral in Eq. (5.35) we change the variable of differentiation from t' to l and decompose I_{ij} into Fourier components. We get (with $w' \equiv w/(GM)$)

$$\mathcal{H}^{\mathrm{nonlocal}}_{\mathrm{4PN}} = -\frac{G^2}{5\eta c^8}\left(\frac{\Omega}{GM}\right)^6 \sum_{p=-\infty}^{\infty} \frac{d^3(\mathcal{I}_{ij}(p)e^{ipl})}{dl^3} \mathrm{Pf}_{2r/c} \int_{-\infty}^{+\infty} \frac{\mathrm{d}w'}{|w'|} \sum_{q=-\infty}^{\infty} \frac{d^3(\mathcal{I}_{ij}(q)e^{iq(l+\Omega w')})}{dl^3}, \tag{5.39}$$

$$= \frac{G^2}{5\eta c^8}\left(\frac{\Omega}{GM}\right)^6 \sum_{p=-\infty}^{\infty} p^3 \mathcal{I}_{ij}(p)e^{ipl} \mathrm{Pf}_{2r/c} \int_{-\infty}^{+\infty} \frac{\mathrm{d}w'}{|w'|} \sum_{q=-\infty, q\neq 0}^{\infty} q^3 \mathcal{I}_{ij}(q)e^{iq(l+\Omega w')}, \tag{5.40}$$

$$= \frac{G^2}{5\eta c^8}\left(\frac{\Omega}{GM}\right)^6 \sum_{p,q=-\infty, q\neq 0}^{\infty} p^3 q^3 \mathcal{I}_{ij}(p)\mathcal{I}_{ij}(q)e^{i(p+q)l} \mathrm{Pf}_{2r/c} \int_{-\infty}^{+\infty} \frac{\mathrm{d}w'}{|w'|} e^{iq\Omega w'}, \tag{5.41}$$

$$= -\frac{2G^2}{5\eta c^8}\left(\frac{\Omega}{GM}\right)^6 \sum_{p,q=-\infty, q\neq 0}^{\infty} p^3 q^3 \mathcal{I}_{ij}(p)\mathcal{I}_{ij}(q)e^{i(p+q)l}(\gamma_E + \ln(|q|\Omega \times 2r/c)), \tag{5.42}$$

$$= -\frac{2G^2}{5\eta c^8}\left(\frac{\Omega}{GM}\right)^6 \Bigg[\sum_{p,q=-\infty, q\neq 0}^{\infty} p^3 q^3 \mathcal{I}_{ij}(p)\mathcal{I}_{ij}(q)e^{i(p+q)l}(\gamma_E + \ln(|q|\Omega)) - \left(\frac{d^3 I_{ij}}{dl^3}\right)^2 \ln(2r/c)\Bigg]. \tag{5.43}$$

A few comments are needed to clarify the manipulations in the above lines. $\mathcal{I}_{ij}$'s are defined

as per the following Fourier decomposition

$$I_{ij}(t') = \sum_{p=-\infty}^{\infty} \mathcal{I}_{ij}(p) e^{ipl}, \tag{5.44}$$

$$\mathcal{I}_{ij}(p) = \frac{1}{2\pi} \int_0^{2\pi} I_{ij}(t') e^{-\mathrm{i}pl} dl. \tag{5.45}$$

These Fourier coefficients of the Newtonian multipole moments are available in terms of Bessel functions in the appendix of Ref. [1] in dimensionless form. In the above lines and the material below, the summation is over all integers from $-\infty$ to $+\infty$ except where it is explicitly mentioned that $q = 0$ be omitted. We have omitted $q = 0$ from the above summations because $\ln(0)$ is undefined. Also, with the variable of integration having changed from $w \to w'$, we also had to change the time-scale of the Pf operation from $2R/c \to 2r/c$. One may also notice another issue of the arguments inside the two ln's in Eq. (5.43) not being dimensionless, due to breaking the ln in Eq. (5.42) into two ln's in the following line. This is no reason to worry since the final result in Eq. (5.52) combines back the two ln's into one with an argument which is indeed dimensionless. And finally, in Eq. (5.42), use has been made of the result in Eq. (5.38), and a similar result for sine being inside the integrand instead of cosine to evaluate the integral in terms of the logarithm.

Due to the definite integral having been performed above and the application of order-reduction (eliminating the derivatives of variables in the Hamiltonian with the equations of motion of a lower order [104]), we now have to deal only with the local dynamics[2]. The 4PN tail Hamiltonian has been decomposed in this particular way of Eq. (5.43) to render it amenable to the averaging procedure, to be carried out below.

[2]See Refs. [116–118] for a background on order-reduction. The procedure of order-reducing the Hamiltonian leads to shifts in canonical coordinates. Apart from the tail part [104], the instantaneous Hamiltonian of Eq. (5.6) is also order-reduced [118]. Since these shifts lead to amplitude and zero-average oscillatory phase corrections (rather than secular phase corrections), we ignore such shifts, as our IMR waveform is meant to be only leading order accurate in amplitude.

5.2.3.3 4PN tail effect as a perturbation to the Newtonian system

To deal with the 4PN tail Hamiltonian of Eq. (5.43), we employ the so called "Delaunay technique" of averaging the perturbation Hamiltonian which is discussed in Appendix 5.5. The method dictates the following: take the perturbation part $\epsilon H_1(\phi_0, J_0)$ of the full Hamiltonian $H = H_0(J_0) + \epsilon H_1(\phi_0, J_0)$ and average it over ϕ_0, thus yielding $\overline{H}_1(J_0)$. Then there exists a generating function $S(\phi_0, J)$ such that it gives new action-angles (J, ϕ) which are connected to the old ones via Eqs. (5.84) and (5.85), and the total Hamiltonian depends only on the new action J as $E(J) = E_0(J) + \epsilon E_1(J)$, where the functional dependence of E_0 and E_1 on J is the same as that of H_0 and $\overline{H}_1$ on J_0. For our system in consideration, $H_1 = \mathcal{H}^{\rm nonlocal}_{\rm 4PN}$ and $\phi_0 = l$. We now proceed to average H_1 over l.

The two additive terms in Eq. (5.43) will be averaged using different methods. This is so because they possess different structures and hence their averaging is tractable via different means. To average the first term of Eq. (5.43) (the one involving the summation), we note that the averaged value will be equal to the sum of all the terms in this double summation which correspond to $p + q = 0$. Hence, we substitute $q = -p$, thereby turning the double summation into a single summation over p and we choose to retain all the term with $|p| \lesssim 500$ terms in this summation. This is so because we found by inspection that these many terms are enough for $e \lesssim 0.9$. We then try to come up with a certain Padé-like approximant for this series using a method that we now briefly sketch.

Using the Fourier coefficients of the Newtonian multipole moments as given in the appendix of Ref. [119], it can be shown that the summation in the first term of Eq. (5.43) (without the prefactor and $(\gamma_E + \ln(|q|\Omega))$ with $q = -p$ can be written as

$$\sum_{p,q=-\infty,q\neq 0}^{\infty} p^3 q^3 \mathcal{I}_{ij}(p)\mathcal{I}_{ij}(q) e^{i(p+q)l}\Big|_{q=-p} \tag{5.46}$$
$$= -\sum_{p=-\infty}^{\infty} p^6 |\mathcal{I}_{ij}(p)|^2 = -32\mu^2 (aGM)^4 \frac{1 + \frac{73e^2}{24} + \frac{37e^4}{96}}{(1-e^2)^{7/2}}.$$

We actually factored out $(1-e^2)^{-7/2}$ from the above sum before trying to evaluate it to preserve the formal structure in the limit of large angular momentum [120][3]. Note that the above result appears to be exact in e and coincides with the "$f(e)$" of Peters and Mathews [121]. Obtaining this nice exact in e expression became possible due to factoring out $(1-e)^{-7/2}$ in the beginning and then series expanding the remnant.

Focusing our attention back to the summation in Eq. (5.43), we see that it can further be decomposed as (with $q=-p$)

$$-\sum_{p=-\infty}^{\infty} p^6 |\mathcal{I}_{ij}(p)|^2 \left[(\gamma_E + \ln\Omega) + \ln|p|\right]. \tag{5.47}$$

Since the first additive term in the above expression (in the parenthesis) has already been taken care of in Eq. (5.46), we now show how to deal with the second one (involving $\ln|p|$). Again, after factoring out $(1-e^2)^{-7/2}$, we first find the Padé approximation of this second term such that both the numerator and denominator are expanded up to $O(e^{10})$. Then by hand, we add $p_{12}e^{12}+p_{14}e^{14}$ in the numerator, where p_{12} and p_{14} are to be determined by numerically matching (at high eccentricities like $e=0.85, 0.90$) this new Padé-like ansatz with the evaluated value of the series where terms up to $|p| \lesssim 500$ have been retained. Tentatively, we have

$$\begin{aligned}
&-\sum_{p=-\infty}^{\infty} p^6 \left|\mathcal{I}_{ij}(p)\right|^2 \ln|p| \\
&= -G^4\mathcal{L}^8 M^6\eta^2 \\
&\left[\frac{p_{14}e^{14}+p_{12}e^{12}-\frac{382996272e^{10}}{13601521}+\frac{579332351e^8}{4983158}-\frac{324710645e^6}{8433524}-\frac{758231515e^4}{3359177}+\frac{263415291e^2}{1639996}+\frac{286746937}{12927762}}{\left(1-e^2\right)^{7/2}\left(\frac{4447985e^{10}}{4076572203}+\frac{49804512e^8}{1158420851}-\frac{105413189e^6}{194334558}+\frac{103729937e^4}{57112735}-\frac{56374811e^2}{24380301}+1\right)}\right].
\end{aligned} \tag{5.48}$$

[3]It can be checked that the average (over l) of the first term of the nonlocal Hamiltonian of Eq. (5.43) has the following structure in the $h \to \infty$ limit $\overline{H}_{1(\mathrm{A})} \sim (Eh^2)^2 h^{-7}\sum_{n=0} a_n\alpha^n$, with $\alpha = (Eh^2)^{-1}$. This, along with $e^2 = 1+2Eh^2$, lets us see that $\overline{H}_{1(\mathrm{A})}$ has the form $\overline{H}_{1(\mathrm{A})} \sim F(e)/h^7 = F(e)\left(2E/(e^2-1)\right)^{7/2}$. This motivated us to first factor out $(1-e^2)^{-7/2}$ from the Bessel series whose Padé-like approximant is sought.

We call the resulting approximant "Padé-like", since it is a result of combining the methods of Padé approximation and numerical fitting. Such a procedure, combined with the idea of factoring out $(1-e^2)^{-7/2}$ gives us approximants which are valid up to higher e's than would have been possible with the standard Padé approximants. Interestingly, these approximants capture the eccentricity effects up to $e \lesssim 0.9$, despite the existence of Laplace limit of $e < 0.66...$ beyond which the series solution of Kepler equation in e diverges [96, 122, 123].

Finally, averaging the second term of Eq. (5.43) (involving $\ln 2r/c$) over l in closed-form is possible, although lengthy. Using the order-reduced Newtonian equations

$$x = a(\cos u - e), \tag{5.49a}$$

$$y = a\sqrt{1-e^2}\sin u, \tag{5.49b}$$

$$z = 0 \tag{5.49c}$$

$$l = u - e\sin u, \tag{5.49d}$$

$$r = a(1 - e\cos u), \tag{5.49e}$$

$$I_{ij} = (GM)^2\mu\left(r^i r^j - \frac{1}{3}r^2\delta^{ij}\right), \tag{5.49f}$$

(with x, y, z being the components of $\mathbf{r}$) in the second term of Eq. (5.43), we arrive at

$$\begin{aligned}
&\frac{1}{2\pi\, a^4\, G^4\, M^4\, \mu^2}\int_0^{2\pi}\left(\frac{d^3 I_{ij}}{dl^3}\right)^2 \ln(2r/c)\, dl \\
=&\frac{2}{3\pi}\int_0^{2\pi}\frac{(24-23e^2-e^2\cos 2u)\left(\ln\left[\frac{2a(1-e\cos u)}{c}\right]\right)}{(1-e\cos u)^5}du \qquad (5.50)\\
=&\frac{12\left(37e^4+292e^2+96\right)\ln\left[\frac{4a\left(1-e^2\right)\left(1-\sqrt{1-e^2}\right)}{c\,e^2}\right]-\left(255e^4+3792e^2+2408\right)}{36\left(1-e^2\right)^{7/2}}+\frac{\left(673e^2+602\right)}{9\left(1-e^2\right)^3}. \qquad (5.51)
\end{aligned}$$

Finally, Eqs. (5.46), (5.48) and (5.50) culminate in the expression of order-reduced averaged 4PN

tail Hamiltonian

$$\overline{\mathcal{H}}^{\rm nonlocal}_{\rm 4PN} = \frac{2\,\eta}{5\,c^8\,\mathcal{L}^{10}}\left[\frac{12\left(37e^4+292e^2+96\right)\ln\left[\frac{4\left(1-e^2\right)\left(1-\sqrt{1-e^2}\right)\exp(\gamma_E)}{\mathcal{L}c\,e^2}\right]-\left(255e^4+3792e^2+2408\right)}{36\left(1-e^2\right)^{7/2}} + \frac{\left(673e^2+602\right)}{9\left(1-e^2\right)^3}+\mathcal{H}_{\rm Padé}\right], \tag{5.52}$$

where

$$\mathcal{H}_{\rm Padé} = \frac{1}{\left(1-e^2\right)^{7/2}\left(\frac{4447985e^{10}}{4076572203}+\frac{49804512e^8}{1158420851}-\frac{105413189e^6}{194334558}+\frac{103729937e^4}{57112735}-\frac{56374811e^2}{24380301}+1\right)}\times \left(\frac{14262437e^{14}}{328008227}-\frac{6775509e^{12}}{248174614}-\frac{382996272e^{10}}{13601521}+\frac{579332351e^8}{4983158}-\frac{324710645e^6}{8433524} -\frac{758231515e^4}{3359177}+\frac{263415291e^2}{1639996}+\frac{286746937}{12927762}\right), \tag{5.53}$$

is the Padé-like approximant that we constructed above. Eliminating e using $e=\sqrt{1-\mathcal{G}^2/\mathcal{L}^2}$ expresses this averaged Hamiltonian in terms of only the actions.

Now, in the action-angles formalism, one can compute the "frequencies" corresponding to all the angle variables by partially differentiating the Hamiltonian with respect to the corresponding action variables. Application of this to our system in consideration yields the 4PN tail correction to the frequencies n and kn (where n denotes the mean motion and k is the periastron advance parameter) [94]. After partially differentiating with respect to $\mathcal{L}$ and $\mathcal{G}$, we write the results in terms of $\mathcal{L}$ and e. For illustration, we give their small e expanded expressions

$$n_{\rm tail} \equiv \frac{\partial\overline{\mathcal{H}}^{\rm nonlocal}_{\rm 4PN}(\mathcal{G},\mathcal{L})}{\partial\mathcal{L}} = \frac{19289894530752349825264\,\eta}{323061509079949009095\,\mathcal{L}^{11}\,c^8}+\frac{592\eta\left(\ln\left(\frac{1}{\mathcal{L}c}\right)+\gamma_E+\ln(2)\right)}{15\,\mathcal{L}^{11}\,c^8} \tag{5.54}$$

$$+\frac{e^2\,\eta\,\left(-184\ln\left(\frac{1}{\mathcal{L}c}\right)-184\gamma_E+\frac{1767641571176972328643511253275859554005100 29}{6044357148405572674088439201054411639506 10}-184\ln(2)\right)}{5\mathcal{L}^{11}\,c^8}$$

$$+O\left(e^4\right), \tag{5.55}$$

$$(k\,n)_{\rm tail}\equiv\frac{\partial\overline{\mathcal{H}}^{\rm nonlocal}_{\rm 4PN}(\mathcal{G},\mathcal{L})}{\partial\mathcal{G}}, \tag{5.56}$$

$$\begin{aligned} k_{\rm tail} &= -\frac{74831546379478710201598\,\eta}{3230615090799490090 95\mathcal{L}^8\,c^8}+\frac{352\,\eta}{5\mathcal{L}^8\,c^8}-\frac{2512\eta\left(\ln\left(\frac{1}{\mathcal{L}c}\right)+\gamma_E+\ln(2)\right)}{15\mathcal{L}^8\,c^8} \\ &+\frac{1}{15\mathcal{L}^8\,c^8}\times \\ &\left(e^2\eta\left(-\frac{5164100568419311748345089878114388585281349219}{2014785716135190891362813067018137213168 70}-13264\ln\left(\frac{1}{\mathcal{L}c}\right)\right.\right. \\ &\left.\left.-13264\gamma_E+10196-13264\ln(2)\right)\right)+O\left(e^4\right). \end{aligned} \tag{5.57}$$

Note that $k=\Delta\Phi/2\pi$, where $\Delta\Phi$ is the angle of periastron advance in the radial period (periastron to periastron) P, which means that $k=\Phi/(2\pi)-1$. This means that among the earlier presented set of equations for the 4PN local-in-time quasi-Keplerian parameterization (QKP), it is Eqs. (5.28b) and (5.28o) which should include the effects encoded in Eqs. (5.54) and (5.56), but they do not since Eqs. (5.28b) and (5.28o) are meant to include only the local-in-time contributions only. We have checked that Eqs. (5.54) and (5.56) agree with the results of Ref. [88] in the circular limit.

Also, note that the argument of ln in Eqs. (5.50) and (5.52) becomes undefined at $e=0$ although its $e\to 0$ limit is well defined. Therefore, in our MATHEMATICA package, we chose to replace this argument of ln by its Taylor expansion so that it is valid in the range $0\leq e\lesssim 0.85$.

To bring all the pieces together, let us have a bird's eye view of the situation. We are trying to include the effect of 4PN tail Hamiltonian as a perturbation to the Newtonian one in the action-angles framework. The effect entails

1. the action-angles being perturbed as per Eqs. (5.83), (5.84) and (5.85).

2. the functional dependence of the Hamiltonian on the actions being perturbed as per Eqs. (5.86),

(5.88) and Eq. (5.52).

At this point, we invoke the "semi-perturbation" scheme detailed in Appendix 5.6, whereby we don't use the information contained in Eqs. (5.83), (5.84) and (5.85), but rather only make use of the information in Eqs. (5.86), (5.88). This way we don't need the oscillatory corrections to the action-angles and the generating function. All one needs to do is to average the perturbation Hamiltonian and find the perturbed frequencies, as has already been done in Eqs. (5.54) and (5.56) above.

Now we discuss how to merge the results of Eqs. (5.54) and (5.56) into the QKP Eqs. (5.28) if one wants to. Since we have chosen not to perturb the actions, there won't be any corrections to the eccentricity and semi-major axis due to the tail effects (see Eqs. (5.30)). This means that in the RHSs of Eqs. (5.54) and (5.56), after evaluating the partial derivatives, we can replace $\mathcal{L}$ and $\mathcal{G}$ with a and e using Eqs. (5.30) and then make the substitutions $(e, a) \to ((1 + 2Eh^2)^{1/2}, -1/(2E))$ to write $n_{\rm tail}$ and $k_{\rm tail}$ in terms of E and h. Then with the earlier derived equation $k = \Phi/(2\pi) - 1$, $n_{\rm tail}$ and $k_{\rm tail}$ can both be incorporated as the 4PN tail effects into the quasi-Keplerian solution (specifically Eqs. (5.28b) and (5.28o)) for the 4PN local Hamiltonian presented in the previous subsection. We do not take it because we have reserved Eqs. (5.28) for local-in-time effects only. Note that in accordance with our decision to adopt the semi-perturbation scheme, the 4PN tail corrections do not enter in the expressions for any other quantity except n and Φ (or k), as far as the 4PN conservative quasi-Keplerian solution is concerned.

Strictly speaking, we have not worked out the full 4PN dynamics since we have ignored the corrections to the action-angles (linear in ϵ terms on the RHSs of Eqs. (5.84) and (5.85)) due to the tail effects. Adopting the semi-perturbation scheme rather than full perturbation scheme simplifies the calculations and the ignored 4PN zero-average, oscillatory corrections to action-angles (due to tail effects) are less important than the 4PN secular tail effects for GW data analysis purposes. An alert reader may be able to point out that we have included the oscillatory terms in the Keplerian type solution for the 4PN local Hamiltonian (the ones with sinusoidal functions of integer multiples of v in Eq. (5.26)), despite dropping the oscillatory correction terms to action-angles (as per the

semi-perturbation scheme) resulting from the 4PN tail effect. One may insist that all the oscillatory terms should be discarded. One could do so. We decided to include these oscillatory terms for the local Hamiltonian in Eq. (5.26) just to be in line with the tradition of including all the terms, be it oscillatory or secular, while giving the QKP solution of a BBH for various PN accurate local conservative Hamiltonians as has been done in Refs. [78, 79, 93].

We finally mention beforehand that both Eqs. (5.54) and (5.56) have a bearing on Eq. (5.71b) which gives the mean motion n, so that when it comes to the IMR waveform construction, of all the equations in Sec. 5.3, only Eq. (5.71b) incorporates the 4PN tail effect as per our choice of adopting the semi-perturbation strategy to include the tail effects. The accompanying MATHEMATICA notebook contains the relevant expressions for n (both local and nonlocal). We now move on to apply the above parametric solution to construct a time-domain eccentric IMR waveform, influenced by Ref. [2].

5.3 An improved time-domain eccentric IMR waveform

The present section details our effort to incorporate 4PN order Keplerian type parametric solution into a MATHEMATICA package, namely `EccentricIMR`, available as an open source software [90], in an accurate and efficient manner. This package implements an eccentric IMR model, detailed in Ref. [2], where an eccentric PN-accurate inspiral model was combined with a quasi-circular merger waveform. Detailed interpolation using several non-eccentric and non-spinning NR waveforms in the neighborhood of their merger phase ensured that the analytic quasi-circular merger waveform of Ref. [2] is accurate for non-spinning BH binaries with mass ratio $q \equiv m_1/m_2$ between 1 and 4 and for arbitrary ϕ_0 (the initial phase of the waveform). The IMR model of Ref. [2] combines the post-Newtonian inspiral waveform, adapted from Ref. [124], and their above described quasi-circular merger model (CMM) to obtain a time-domain eccentric IMR waveform. This involves 'blending' of the above two models in a transition region where neither PN approximation is valid nor the binary can be assumed to have circularized.

It was noted in Ref. [2] that incorporating higher order PN corrections should improve the

performance of the early inspiral phase. In fact, Ref. [2] invoked 3PN order conservative and 2PN order reactive contributions to the BBH dynamics for describing the inspiral part of their IMR $h(t)$. The present effort improves the treatment of the conservative part in the `EccentricIMR` package with the help of our 4PN order Keplerian type parametric solution while adapting PN-accurate results from Refs. [1, 125] to incorporate effects of 3PN-accurate GW emission. Moreover, we provide computationally efficient version of the x-model [124], employed in `EccentricIMR`, by adapting the GW phasing approach of Refs. [101, 102] during the modeling of the eccentric inspiral phase. These changes are incorporated into the MATHEMATICA package accompanying Ref. [2] and we treat their circular merger model as a black box [90]. The resulting package is available at Ref. [91, 92]. In what follows, we present our approach to improve various aspects of the x-model. In this section we will employ t to denote the ADM coordinate time for the sake of convenience (unlike the previous section). A derivative with respect to the ADM time will be represented by an overdot.

5.3.1 4PN conservative and 3PN radiative phasing

We begin by listing the usual expression for the quadrupolar order (or restricted) complex gravitational waveform for compact binaries in non-circular orbits [84, 101, 124, 126]

$$h_{\rm sig} = h_+ - i h_\times \tag{5.58a}$$

$$h_+ = -\frac{GM\eta}{c^4 D}\left\{\left(\cos^2\theta+1\right)\left[\left(\frac{GM}{R}-\dot{R}^2+R^2\dot{\phi}^2\right)\cos 2\phi' + 2R\dot{\phi}\dot{R}\sin 2\phi'\right] + \left(\frac{GM}{R}-\dot{R}^2-R^2\dot{\phi}^2\right)\sin^2\theta\right\}, \tag{5.58b}$$

$$h_\times = -\frac{2GM\eta}{c^4 D}\cos\theta\left\{\left(\frac{GM}{R}-\dot{R}^2+R^2\dot{\phi}^2\right)\sin 2\phi' - 2R\dot{\phi}\dot{R}\cos 2\phi'\right\}, \tag{5.58c}$$

where $\phi' \equiv \phi - \varphi$ and θ and φ are the spherical polar angles that specify the observer in a frame centered around the source which is a distance D away from the detector. Recall that R and ϕ serve to specify the relative separation vector $\mathbf{R}$ between the two BHs whereas $r \equiv R/(GM)$. Also, we have $\dot{r} \equiv dr/dt$ and $\dot{\phi} \equiv d\phi/dt$. The NR relevant spin-weight -2, $\ell = 2, m = 2$ spherical harmonic

mode of $h(t)$ reads

$$\begin{aligned} h^{22} &= \int {}_{-2}Y_2^{2^*}(\theta,\varphi) h_{\rm sig}(\theta,\varphi) d\Omega \\ &= -\frac{4GM\eta e^{-2i\phi}}{c^4 D}\sqrt{\frac{\pi}{5}}\left(\frac{GM}{R} + (\dot{\phi}R + i\dot{R})^2\right), \end{aligned} \tag{5.59}$$

where the spherical harmonic ${}_{-2}Y_2^2(\theta,\varphi) = \frac{1}{2}e^{2i\varphi}\sqrt{5/\pi}\cos^4(\theta/2)$. In what follows, we describe our improved x-model to obtain $h^{22}(t)$ for non-spinning BH binaries inspiralling along relativistic eccentric orbits in a computationally accurate and efficient manner.

We adapt, as mentioned earlier, the GW phasing approach of Refs. [101, 102] to model eccentric inspiral of BH binaries to describe the temporal evolution of dynamical variables that appear in the above $h^{22}(R(t), \dot{R}(t), \phi(t), \dot{\phi}(t))$ expression. This approach imposes numerically the effects of GW emission on the conservative dynamics of eccentric binaries by incorporating changes in orbital configurations that occur at the orbital, periapsis advance and gravitational radiation reaction time scales. In the GW phasing approach, the conservative BBH dynamics is described using our Keplerian type parametric solution and we first focus on describing parametrically the temporal evolution of $r, \dot{r}$ and $\dot{\phi}$, whereas ϕ will be dealt with later. We begin by expressing the 4PN-accurate expressions for these variables as

$$r(-2\,E, h, u) = a_r(-2\,E, h) \times \Big(1 - e_r(-2\,E, h) \times \cos u\Big), \tag{5.60}$$

$$\dot{r}(-2\,E, h, u) = \frac{dr}{du} \times \frac{du}{dt}, \tag{5.61}$$

$$\dot{\phi}(-2\,E, h, u) = \frac{d\phi}{dv} \times \frac{dv}{du} \times \frac{du}{dt}. \tag{5.62}$$

where

$$\frac{du}{dt} = \frac{du}{dl}\frac{dl}{dt} = \frac{du}{dl}\frac{n}{GM}. \tag{5.63}$$

Recall that t in this section stands for the ADM time, whereas it stood for the scaled ADM time in

Sec. 5.2. Employing the 4PN solution given in Eqs. (5.25)-(5.27), we can see that the resulting 4PN order expressions of r, $\dot{r}$ and $\dot{\phi}$ will be functions of $(-2\,E)$, h, e_r, e_t, e_ϕ, u and η. Conventionally in the x-model, we rather write these expressions in terms of ω, e_t and u. This is achieved with the help of the following steps.

In the first step, we define a 4PN order ω from our 4PN order expressions for n and $k = \Delta\Phi/2\,\pi$ as $\omega \equiv n \times (1 + k)$. It is now possible to invert 4PN order ω expression in a PN-accurate manner to express $(-2\,E)$ in terms of ω and h. In the next step, we invert 4PN order e_t expression (given by the first of Eqs. (C1) of Ref. [47]) to get an intermediate 4PN order expression for h in terms of e_t and $(-2\,E)$. Then use the above obtained expression of $(-2E)$ (in terms of ω and h) to express h in terms of e_t and ω up to 4PN order in a post-Newtonian perturbative way. Using this expression of $h(e_t, \omega)$ in the above expression of $(-2E)$ finally gives us $(-2E)$ in terms of e_t and ω. The resulting relations for $(-2\,E)$ and h (in terms of e_t and ω) allow us to express e_r and e_ϕ in terms of ω, e_t to 4PN order with the help of Eqs. (C1) of Ref. [47]. All these relations in conjunction with Eqs. (5.60)-(5.62) lead to 4PN order parametric expressions for $r, \dot{r}$ and $\dot{\phi}$ in terms of ω, e_t, u. We provide the expressions of E and h in terms of $x \equiv (GM\omega/c^3)^{2/3}$ and e_t in Appendix D of Ref. [112].

An additional requirement of the GW phasing approach is to split the orbital phase into two parts such that (with $\lambda(t_0) = 0$)

$$\phi(t) = \lambda(t) + W(u(l), (-2\,E), h), \tag{5.64a}$$

$$\lambda(t) = (1 + k)n(t - t_0) \equiv \omega(t - t_0)\,, \tag{5.64b}$$

as done in Ref. [101]. Note that Eqs. (5.64) are for conservative dynamics only and need to be modified by the application of the method of variation of arbitrary constants (as done in Ref. [101]) to include the radiation reaction effects[4]. This will be done later in Eqs. (5.71). The above equations ensure that the secular evolution of the orbital phase depends linearly on time which makes it easier

[4]See Box. 3.3 of Ref. [127] for a pedagogical treatment of the method of variation of arbitrary constants.

to track the evolution of the argument of periapsis while the W part provides the periodic variations, present in the ϕ evolution due to its dependence on l. Additionally, we need to express the above 4PN order expression for W in terms of ω, e_t and u which we write symbolically as

$$W = (v-u) + e_t \sin u + W^{1\mathrm{PN}} x + W^{2\mathrm{PN}} x^2 + W^{3\mathrm{PN}} x^3 + W^{4\mathrm{PN}} x^4. \tag{5.65}$$

For the ease of implementation, it is helpful to use the following 4PN order expression of Ref. [102]

$$v - u = 2 \arctan\left(\frac{\beta_\phi \sin u}{1 - \beta_\phi \cos u}\right). \tag{5.66}$$

Our parametric solution allows us to obtain the following 4PN order expression for β_ϕ in terms of e_t, x, u as

$$\beta_\phi = \frac{1-\sqrt{1-e_t^2}}{e_t} + \beta_\phi^{1\mathrm{PN}} x + \beta_\phi^{2\mathrm{PN}} x^2 + \beta_\phi^{3\mathrm{PN}} x^3 + \beta_\phi^{4\mathrm{PN}} x^4. \tag{5.67}$$

The explicit and lengthy expressions for these 4PN order quantities are listed in the accompanying MATHEMATICA notebook [91, 92].

We now collect relevant expressions that describe the temporal evolution of a precessing eccentric orbit whose conservative (without radiation reaction) orbital dynamics is specified by the 4PN order Hamiltonian, given by Eq. (8.41) of Ref. [86]. These equations may be symbolically written as

$$\begin{aligned}
\frac{\dot{R}}{c} &= \frac{\sqrt{x} e_t \sin u}{1 - e_t \cos u} \left\{1 + \dot{R}^{1\mathrm{PN}}(\eta, e_t)\, x + \dot{R}^{2\mathrm{PN}}(\eta, e_t, u)\, x^2 + + \dot{R}^{3\mathrm{PN}}(\eta, e_t, u)\, x^3 \right. \\
&\quad \left. + \dot{R}^{4\mathrm{PN}}(\eta, e_t, u)\, x^4 \right\}, \qquad (5.68a) \\
\dot{\phi} &= \frac{x^{3/2} c^3 \sqrt{1-e_t^2}}{GM(1 - e_t \cos u)^2} \left\{1 + \dot{\phi}^{1\mathrm{PN}}(\eta, e_t, u)\, x + \dot{\phi}^{2\mathrm{PN}}(\eta, e_t, u)\, x^2 + \dot{\phi}^{3\mathrm{PN}}(\eta, e_t, u)\, x^3 \right.
\end{aligned}$$

$$+\dot{\phi}^{\rm 4PN}\left(\eta, e_t, u\right) x^4\Big\}\,, \tag{5.68b}$$

$$R = \frac{GM(1-e_t\cos u)}{c^2 x}\left\{1 + R^{\rm 1PN}\left(\eta, e_t, u\right) x + R^{\rm 2PN}\left(\eta, e_t, u\right) x^2 + R^{\rm 3PN}\left(\eta, e_t, u\right) x^3 \right.$$
$$\left. + R^{\rm 4PN}\left(\eta, e_t, u\right) x^4\right\}\,, \tag{5.68c}$$

$$\phi = \lambda + W\,, \tag{5.68d}$$

$$\lambda(t) = \omega(t - t_0)\,, \tag{5.68e}$$

$$W = (v-u) + e_t \sin u + W^{\rm 1PN}\left(\eta, e_t, u\right) x + W^{\rm 2PN}\left(\eta, e_t, u\right) x^2 + W^{\rm 3PN}\left(\eta, e_t, u\right) x^3$$
$$+ W^{\rm 4PN}\left(\eta, e_t, u\right) x^4\,, \tag{5.68f}$$

where we employ the 4PN-accurate expression for $(v-u)$ given symbolically by Eq. (5.66). It should be noted that the above equations provide analytically 4PN order conservative dynamics of BH binaries in terms of u and we require to numerically solve our 4PN order Kepler equation after re-writing it in terms of x and e_t to obtain $u(l(t))$. Our full system however, is not conservative and as we will soon see that inclusion of the radiation reaction effects will modify some of the above equations. For the purpose of illustration, we list the 1PN contributions that appear in Eqs. (5.68) as

$$\dot{R}^{\rm 1PN}\left(\eta, e_t\right) = \frac{-7\eta + e_t^2(-6+7\eta)}{6\left(1-e_t^2\right)}, \tag{5.69a}$$

$$\dot{\phi}^{\rm 1PN}\left(\eta, e_t, u\right) = \frac{\left(-1+\chi+e_t^2\right)(-4+\eta)}{\chi\left(1-e_t^2\right)}, \tag{5.69b}$$

$$R^{\rm 1PN}\left(\eta, e_t, u\right) = \frac{1}{6\chi\left(1-e_t^2\right)}\left(-24 + 9\eta + \chi(18-7\eta) + e_t^2[24 - 9\eta + \chi(-6+7\eta)]\right), \tag{5.69c}$$

$$W^{\rm 1PN}\left(\eta, e_t, u\right) = 3\frac{e_t\sin u + (v-u)_{\rm 1PN}}{1-e_t^2},$$

$$\beta_\phi^{\rm 1PN}\left(\eta, e_t\right) = \frac{-4 + \eta + e_t^2(8-2\eta) + (4-\eta)\sqrt{1-e_t^2}}{e_t\sqrt{1-e_t^2}}\,, \tag{5.69d}$$

where χ stands for $1 - e_t\cos u$.

We now impose the effects of GW emission and explain how we provide the full temporal

evolution for a BBH, characterized by m_1 and m_2 and specified by initial values of (x, e_t, λ, l). Clearly, we require to specify how these variables vary in time and Ref. [101] demonstrated that ω (or x) and e_t evolve due to gravitational radiation reaction effects. It turns out that the secular variations of ω and e_t arise by employing the orbital (binding) energy and angular momentum balance arguments [128]. This requires PN accurate expressions of ω and e_t in terms of $(-2E)$ and h and PN-accurate expressions for the orbit-averaged far-zone energy and angular momentum fluxes associated with non-spinning compact binaries in PN-accurate eccentric orbits [84, 129]. We employ the following 3PN-accurate expressions for $\dot{x}$ and $\dot{e}_t$, extractable from Ref. [1], and displayed symbolically as

$$\dot{x} = \frac{c^3 x^5 \eta}{GM}\Bigg[\frac{192 + 584 e_t^2 + 74 e_t^4}{15\left(1-e_t^2\right)^{7/2}} + \dot{x}^{\rm 1PN}\left(\eta, e_t\right) x + \dot{x}^{\rm 1.5PN}\left(\eta, e_t\right) x^{3/2} + \dot{x}^{\rm 2PN}\left(\eta, e_t\right) x^2 + \dot{x}^{\rm 2.5PN}\left(\eta, e_t\right) x^{2.5} + \dot{x}^{\rm 3PN}\left(\eta, e_t\right) x^3\Bigg], \tag{5.70a}$$

$$\dot{e}_t = -\frac{c^3 x^4 \eta\, e_t}{GM}\Bigg[\frac{304 + 121 e_t^2}{15\left(1-e_t^2\right)^{5/2}} + \dot{e}_t^{\rm 1PN}\left(\eta, e_t\right) x + \dot{e}_t^{\rm 1.5PN}\left(\eta, e_t\right) x^{3/2} + \dot{e}_t^{\rm 2PN}\left(\eta, e_t\right) x^2 + \dot{e}_t^{\rm 2.5PN}\left(\eta, e_t\right) x^{2.5} + \dot{e}_t^{\rm 3PN}\left(\eta, e_t\right) x^3\Bigg]. \tag{5.70b}$$

The explicit expressions for various PN contributions are available in Refs. [1, 125]. We would like to point out that the contributions appearing at the 1.5PN, 2.5PN and 3PN orders contain certain hereditary contributions while the Newtonian, 1PN and 2PN terms are purely instantaneous. Additionally, the 1.5PN and 2.5PN contributions in the above equations are purely hereditary and the relative 3PN terms contain both instantaneous and hereditary parts. The hereditary parts are expressed in terms of certain 'eccentricity enhancement functions' (such as the ones given in Eqs. (6.22) of [1]). We employed accurate Padé approximants for these enhancement functions and ensured that they are consistent with analytic fits to these functions up to at least $e_t = 0.85$, as detailed in Ref. [125].

We now provide a prescription for the secular evolution λ and l as we specify the orbital configuration of our eccentric BH binary by specifying the initial values of (x, e_t, λ, l). Eqs. (5.26)

and (5.68e) which imply constant time derivatives of l and λ, are valid only when the radiation reaction is ignored. Under the radiation reaction, the differential equations that specify the secular evolution of λ and l can be considered to be extensions of our 4PN order Keplerian type parametric solution and are given by

$$\frac{d\lambda}{dt} = \omega \equiv \frac{x^{3/2}c^3}{GM}, \tag{5.71a}$$

$$\frac{dl}{dt} = n = \frac{x^{3/2}c^3}{GM}\left\{1 + i^{\rm 1PN}\left(e_t\right)x + i^{\rm 2PN}\left(\eta, e_t\right)x^2 + i^{\rm 3PN}\left(\eta, e_t\right)x^3 + i^{\rm 4PN}\left(\eta, e_t, \ln x\right)x^4\right\} \tag{5.71b}$$

Promoting Eqs. (5.64) to Eqs. (5.71) to incorporate radiation-reaction effects is basically an application of the method of variation of arbitrary constants [101, 127]. Both the 4PN local and nonlocal-in-time contributions can be found in the accompanying MATHEMATICA notebook [91, 92]. Note that Eq. (5.71b) arises from our 4PN order expression for n, given by Eq. (5.28b), and requires 4PN order expressions for $(-2\,E)$ and 3PN order expression for h in terms of ω and e_t. Plus, as per our choice of ignoring the oscillatory 4PN tail corrections to action-angles (as per the semi-perturbation scheme) as detailed in 5.2.3.3, Eq. (5.71b) is the only equation in this Sec. 5.3 which incorporates the 4PN tail effects via Eqs. (5.54) and (5.56), as far as the IMR waveform construction is concerned. Also, we are only imposing secular variations to the four variables whose initial values we employ to specify the BBH configurations. It is fairly straightforward to include quasi-periodic variations to these variables that occur at 2.5PN and 3.5PN orders, detailed in Ref. [102]. We now give the 1PN contributions to Eqs. (5.70) and (5.71) for illustration

$$\dot{x}^{\rm 1PN}\left(\eta, e_t\right) = \frac{-11888 - 14784\eta + e_t^2(87720 - 159600\eta) + e_t^4(171038 - 141708\eta) + e_t^6(11717 - 8288\eta)}{420\left(1 - e_t^2\right)^{9/2}}, \tag{5.72}$$

$$\dot{e}_t^{\rm 1PN}\left(\eta, e_t\right) = -\frac{67608 + 228704\eta + e_t^2(-718008 + 651252\eta) + e_t^4(-125361 + 93184\eta)}{2520\left(1 - e_t^2\right)^{7/2}}, \tag{5.73}$$

$$l^{\rm 1PN}\left(e_t\right) = -\frac{3}{1-e_t^2}. \tag{5.74}$$

The last ingredient, required to obtain temporal evolution for the dynamical variables $(r, \dot{r}, \dot{\phi}, \phi = \lambda + W)$, is an accurate and efficient way of solving our 4PN order Kepler equation, given by Eq. (5.24), which we symbolically write as $l = \mathscr{L}(u, x, e_t)$. We employ Mikkola's method [130] to numerically solve the 4PN order Kepler equation. Since Mikkola's method was originally built and optimized to handle the classical Kepler equation (with no PN corrections), the process of solving the 4PN order Kepler equation using this method requires the numerical inversion to be done in a PN iterative manner as detailed in Ref. [3]. The need to bypass this numerical iteration procedure led us to introduce a new 'auxiliary eccentric anomaly' $\hat{u}$ such that our 4PN order Kepler equation takes the same form as the Newtonian one when written in terms of $\hat{u}$

$$\mathscr{L}(u, x, e_t) = \hat{u} - e_t \, \sin \hat{u}, \tag{5.75}$$

and therefore we can obtain $\hat{u}$ values essentially by employing Mikkola's method just once on Eq. (5.75). Thereafter, we evaluate u from the PN accurate relation $u = u(\hat{u}, x, e_t)$ by demanding that the following equality holds

$$l = \hat{u} - e_t \cos \hat{u} = u - e_t \cos u + \mathcal{O}(x^2)\,, \tag{5.76}$$

where the RHS of the last equality includes corrections all the way up to 4PN as in Eq. (5.24). The straightforward way to do so would be to start with an ansatz $u = \sum C_i(\hat{u}) x^i$ and plug it into the RHS of the second equality of Eq. (5.76) and evaluate the undetermined $C_i(\hat{u})$ as functions of $\hat{u}$. For illustration, we present u in terms of $\hat{u}$ up to 2PN order as

$$u = \hat{u} + x^2 \left\{ \frac{e_t \, \eta \, (4+\eta) \, \sin \hat{u}}{8 \, (1 - e_t \, \cos \hat{u})^2} + \frac{3 \, (5 - 2\,\eta)}{\sqrt{1-e_t^2}\,(1 - e_t \cos \hat{u})} \arctan\left(\frac{\left(\sqrt{1-e_t^2} - 1\right) \sin \hat{u}}{\left(\sqrt{1-e_t^2} - 1\right) \cos \hat{u} + e_t} \right) \right\}$$

$$+ O(x^3), \tag{5.77}$$

whereas the 4PN-accurate version of the above equation is provided in the accompanying MATHEMATICA notebook `Lengthy_Expressions.nb` [91, 92]. We have verified that the relative difference between numerical values of u and $\hat{u}$ around late inspiral for a handful of cases is $\sim 0.0001\%-0.01\%$ with the lower and upper bounds corresponding to cases with $q \sim 1$ and 3 respectively.

We now sketch our procedure to generate temporally evolving eccentric inspiral $h^{22}(t)$ in a computationally efficient way. The following steps are required

1. Specify an eccentric BH binary configuration by providing values for $\{x, e_t, \lambda, l\}$ at an initial epoch t_0 along with values of fixed parameters like m_1, m_2 and D.

2. With the help of our numerical solution to 4PN order Kepler equation via Eq. (5.75) and Eqs. (5.68) for $R, \dot{R}, \phi$ and $\dot{\phi}$, we evaluate Eq. (5.59) and obtain the value of h^{22} at t_0.

3. Thereafter, solve the coupled differential equations for x, e_t, λ and l to obtain their values at $t_0 + \Delta t$. Find $R, \dot{R}, \phi, \dot{\phi}$ and h^{22} at $t_0 + \Delta t$ using the same steps as before and so on.

This gives the quadrupolar order waveform h^{22} associated with our eccentric and non-spinning BH binary that inspirals due to the effect of 3PN-accurate GW emission along 4PN order orbits.

A few comments are required to contrast our approach with the x-model of Ref. [2]. A close inspection reveals that our differential equations for x, e_t, λ and l do not contain any orbital time scale variations. However, the numerical treatment of $\dot{\phi}$ equation in the x-model of Ref. [2] ensures that the secular and periodic variations are intertwined in their approach, especially while dealing with the orbital phase evolution. The reason behind this contrast is that we have closed-form solutions for the orbital time-scale dynamics (in the form of 4PN generalized quasi-Keplerian parameterization) and hence numerical integration can happen on radiation-reaction time scale. Additionally, we use Mikkola method to solve our PN Kepler equation without needing to iterate as in Ref. [3] because of writing the PN Kepler equation in terms of a new variable $\hat{u}(u)$. These features make our computation routine efficient, apart from being accurate (3PN and 4PN accurate in reactive

and conservative dynamics, respectively). It should be noted that we have not incorporated the GW emission induced orbital time scale variations to x, e_t, λ and l, as detailed in Refs. [101, 102], although this is fairly straightforward to do so using our prescription. However, it will be rather difficult to include such periodic contributions in the x-model of Ref. [2] due to their use of PN-accurate $\dot{\phi}(x, e_t, u)$ expression. In what follows, we explain briefly how we attach our eccentric inspiral h^{22} to the circular merger h^{22} model of Ref. [2] while treating their approach as a black box.

5.3.2 Stitching the circular merger-ringdown waveform to the eccentric inspiral waveform

As mentioned earlier, we exclusively follow Ref. [2] as a black box when it comes to stitching the merger-ringdown waveform to our inspiral waveform and it involves the following steps. First, we mark four special time instants: $t_{\rm ref}$, $t_{\rm blend}$, $t_{\rm circ}$ and $t_{\rm peak}$ such that $t_{\rm ref} < t_{\rm blend} < t_{\rm circ} < t_{\rm peak}$. The first two instants correspond to epochs when $x = 0.11$ and 0.12, respectively. Further, the instant $t_{\rm circ}$ is the time after which the binary can be treated as circular and $t_{\rm peak}$ is the time at which the dominant $\ell = 2, m = 2$ mode of the GW strain h_{22} reaches the maximum value in magnitude.

Importantly, Ref. [2] demonstrated the circularization of BBHs with $q < 3$ and initial eccentricity $e_t \lesssim 0.2$ (measured when $x \sim 0.07$) for $t > t_{\rm peak} - 30M$. This implies that $t_{\rm circ} = t_{\rm peak} - 30M$. It allowed Ref. [2] to propose the use of their circular merger model (CMM) for $t > t_{\rm circ}$. For its construction, three circular, non-spinning BBH waveforms from the Simulating eXtreme Spacetimes catalog [131] with $q = 1, 2$ and 4 were used and an interpolating function for the amplitude and frequency was constructed for all q values in the range $1 < q < 4$.

We employ our earlier described PN-accurate eccentric waveform in the interval $t < t_{\rm blend}$ by specifying the eccentric BBH with its PN parameters (x, e_t, ϕ, l)[5] at a certain initial epoch. We employ the CMM for $t > t_{\rm circ}$. This leaves only the 'blending region' to deal with, which is the interval $t_{\rm blend} < t < t_{\rm circ}$. Using 23 NR simulations, a fitting function for $\Delta t \equiv t_{\rm peak} - t_{\rm ref}$ was arrived at (see Eq. (9) of Ref. [2]) with $q, e_t(x = 0.11)$ and $l(x = 0.11)$ as its arguments. This Δt

[5]Switching from (x, e_t, λ, l) to (x, e_t, ϕ, l) is easy since $\phi = \lambda + W(u(l))$

fit is crucial to model the waveform in the blending region as we soon see below in Eqs. (5.78).

Let us mention that there was a certain "NR-PN" fitting done in Ref. [124] which made it possible to assign PN parameters (x and e) to the 23 NR simulations in Table I of Ref. [2]; the top row of the table displays those PN parameters. Assignment of these parameters was crucial to performing the above mentioned Δt fit and by extension, constructing the IMR waveform of Ref. [2]. As expected, this NR-PN fitting is sensitive to the PN model used and becomes less so if the fit is performed earlier during the inspiral phase, as is evident in Figs. 4 and 5 of Ref. [124]. This is so because the PN parameter is smaller during earlier stages of inspiral. Since Ref. [124] explicitly mentions that the authors chose the earliest possible fitting interval to extract "a unique set of PN parameters", we don't feel the need to redo these NR-PN fits and thereby the Δt fit. Hence we don't perform them and stick with Eq. (9) of Ref. [2] for our IMR waveform.

Now we discuss how to deal with the blending region. The waveform is written as $h_{\rm sig} = Ae^{i\phi_w}$ with $\omega_w \equiv \dot{\phi_w}$. The subscript '$w$' stand for 'wave' and serves to distinguish ϕ_w and ω_w from the orbital phase ϕ and frequency ω. The IMR waveform in the blending region is then given by Eqs. (10)-(17) of Ref. [2] which we reproduce almost exactly below (with the superscripts 'PN' and 'circ' standing for the PN waveform model and the CMM)[6]

$$t_{\rm peak} = t_{\rm ref} + \Delta t, \tag{5.78a}$$

$$t_{\rm circ} = t_{\rm peak} - 30M, \tag{5.78b}$$

$$\alpha(t) = \mathcal{T}(t; t_{\rm blend}, t_{\rm circ}), \tag{5.78c}$$

$$h_{\rm sig}(t) = A(t)e^{i\phi_w(t)}, \tag{5.78d}$$

$$A(t) = (1-\alpha(t))A^{\rm PN} + \alpha(t)A^{\rm circ}(t - t_{\rm peak}), \tag{5.78e}$$

$$\omega_w(t) = (1-\alpha(t))\omega_w^{\rm PN} + \alpha(t)\omega_w^{\rm circ}(t - t_{\rm peak}), \tag{5.78f}$$

$$\phi_w(t) = \int^t \omega_w(t')dt'. \tag{5.78g}$$

[6]Eqs. (5.78e) and (5.78f) are different from Eqs. (14) and (15) of Ref. [2] because there are typos in the latter set of equations.

$$\mathcal{T}(t,t_1,t_2) = \begin{cases} 0 & t \leq t_1, \\ \left[\exp\left(\frac{t_2-t_1}{t-t_1}+\frac{t_2-t_1}{t-t_2}\right)+1\right]^{-1} & t_1 < t < t_2, \\ 1 & t \geq t_2. \end{cases} \tag{5.79}$$

A few remarks in regard to the above equations are in order. $A^{\rm PN}, \omega_w^{\rm PN}, A^{\rm circ}$ and $\omega_w^{\rm circ}$ refer to the values of the amplitude and frequency (time derivative of the phase) of the PN and the CMM waveforms, respectively. The function $\mathcal{T}(t,t_1,t_2)$ is a smooth function which goes from 0 to 1 between t_1 to t_2 and essentially does the job of 'blending' the PN waveform with the CMM waveform. The argument of $A^{\rm circ}$ and $\omega_w^{\rm circ}$ in the above equations is $(t - t_{\rm peak})$ because the CMM is time-shifted such that the peak occurs at $t = 0$.

We are now in a position to plot the waveforms got from our extension of the eccentric IMR family of Ref. [2] which we term as the 4-3PN (4PN conservative, 3PN reactive) IMR waveform in contrast to the 3-2PN (3PN conservative, 2PN reactive) family of Ref. [2]. In Fig. 5.1, we provide a visual contrast between these two IMR families for two mass ratios, namely $q = 1$ and 3. Clearly, some dephasing is evident near the late inspiral and it may be attributed to the use of 3PN-accurate effects of GW emission in our approach. Let us mention that we have added some missing terms in the expression of $\dot{x}$ in the MATHEMATICA package accompanying Ref. [2] prior to plotting. Further, we have gauge-transformed the eccentricity parameter before making the above comparison because the work of Ref. [2] was done in the harmonic gauge. We now move on to explore preliminary data analysis implications of our time-domain IMR waveforms.

5.3.3 Preliminary data analysis implications

It will be interesting to explore the de-phasing and possible data analysis implications of our updated eccentric IMR waveform family in comparison with what is available in the literature. A cursory look of the Fig. 5.1 reveals that the effect of neglecting 3PN contributions to the GW emission can be substantial and we infer that this is mainly due to the late inspiral stage de-phasing of 4-3PN IMR waveform in contrast to the 3-2PN family. Therefore, we here restrict our attention

to explore the implications of our 4PN order contributions to the conservative dynamics while keeping the radiation reactions effects fixed at the 3PN order. Further, we restrict our attention to the inspiral domain only. The plots in Fig. 5.2 provide visual comparisons between the members of the eccentric 4-3PN and 3-3PN inspiral waveform families and the associated orbital phase differences for 3 different initial values of orbital eccentricity. The plotted waveforms on the left panels of the first two rows are visually indistinguishable and their differences in the accumulated orbital phases are less than a fraction of a radian. However, the plots in the bottom row suggests that the effects of 4PN contributions to the conservative dynamics can shift the location of periastron passages in the moderately high initial eccentricity scenario as is evident from the differences in the peaks of these two waveform families. Additionally, the accumulated orbital phase difference can be roughly a radian for such eccentric binaries. Therefore, it is reasonable to expect that 4PN order contributions to the conservative orbital dynamics should be relevant for high eccentric black hole binaries.

We now move on to probe a preliminary GW data analysis implications of our 4PN order corrections to the orbital dynamics by computing certain "faithfulness" estimates between the members of the above two inspiral families. The faithfulness between two GW signals $h_1(t)$ and $h_2(t)$ is defined as the following integral, maximized over the time and phase of coalescence t_c and ϕ_c such that [2, 132, 133]

$$F(h_1, h_2) \equiv \max_{t_c, \phi_c} \frac{(h_1(t_c, \phi_c), h_2)}{\sqrt{(h_1, h_1)(h_2, h_2)}}\,, \tag{5.80}$$

and the above inner product between two waveforms (h_1, h_2) being defined as

$$(h_1, h_2) \equiv 4\,\Re \int_{f_{\rm min}}^{f_{\rm max}} \frac{\tilde{h}_1^*(f)\,\tilde{h}_2(f)}{S_{\rm h}(f)} df\,, \tag{5.81}$$

where $\tilde{h}_i(f)$ stands for the Fourier transform of $h_i(t)$ and $S_h(f)$ is the noise power spectral density of the aLIGO detector. For the present analysis, we employed the zero-detuned, high-power noise configuration of aLIGO [134]. The faithfulness plots of Fig. 5.3 are for non-spinning compact

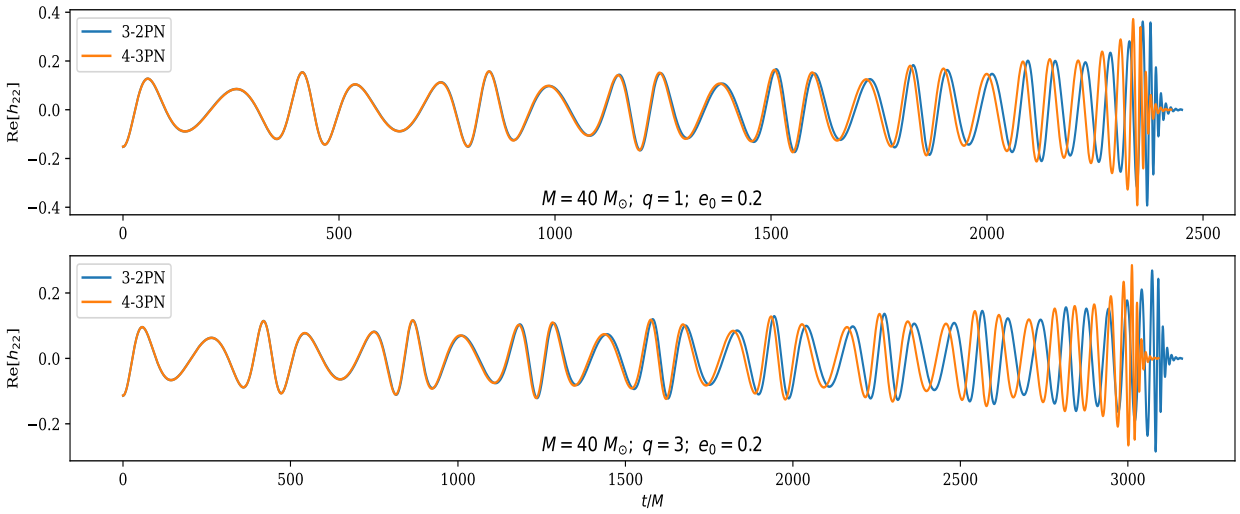

Figure 5.1: Plots of GW strains that originate from (4PN-3PN) waveform against the 3PN-2PN IMR waveform.

binaries of different mass ratios. The faithfulness values are above the traditional 0.97 value for equal mass binaries which suggest that 3-3PN inspiral templates are 'faithful' to the expected 4-3PN inspiral GW signals [133]. Additionally, the above commonly accepted lower bound ensures the recovery of 90% of the hidden signals in the noisy data [135, 136]. However, the 3-3PN inspiral templates need not be 'faithful' to their 4-3PN counterparts for moderately eccentric and unequal mass compact binaries as evident from the plots in the right panel of Fig. 5.3. Therefore, it should be interesting to pursue computations to incorporate the effects of 4PN hereditary contributions to the conservative dynamics and model the resulting inspiral templates.

A true measure of validity of our 4-3PN IMR waveform can be had from comparisons with the corresponding NR simulations which we do not perform here. However it's reasonable to expect our IMR waveform to be valid across a slightly larger parameter range than that for the waveform of Ref. [2] although we have not checked it. As far as the Ref. [2] is concerned, the faithfulness F (defined in Eq. (5.80)) between their IMR waveform and the NR counterparts > 0.97 for systems with $M \leq 85 M_\odot,\ e_{t(7)} \leq 0.08,\ q \leq 3$ and $M \geq 70 M_\odot,\ e_{t(7)} \lesssim 0.05,\ q \leq 3$ with $e_{t(7)}$ here standing for the eccentricity at ~ 7 cycles before the merger. This faithfulness was computed in Ref. [2] with the detector configuration of the first observing run (O1) of advanced LIGO with

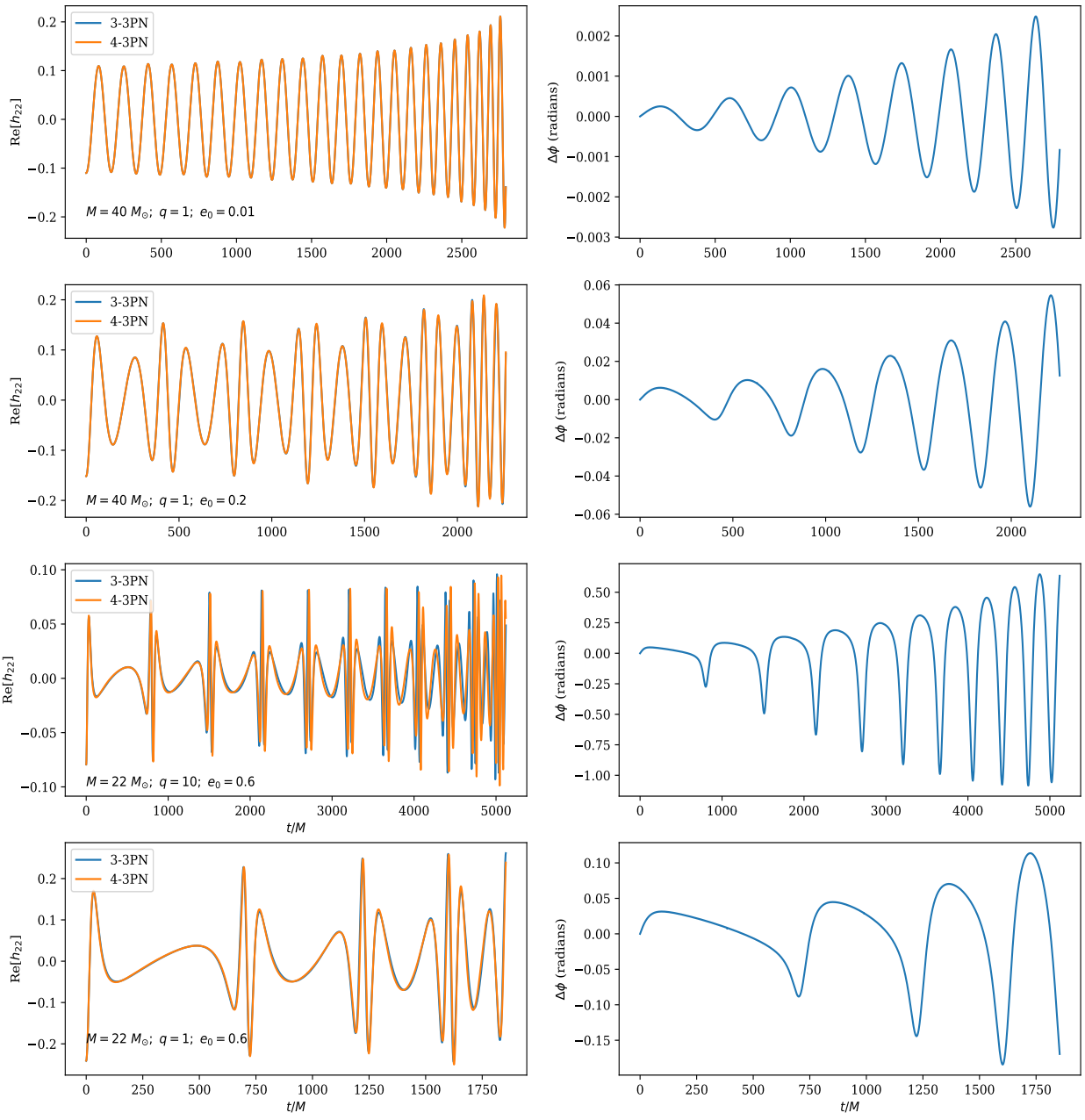

Figure 5.2: Inspiral GW strains associated with the (4PN-3PN) and (3PN-3PN) inspiral waveforms and the dephasing.

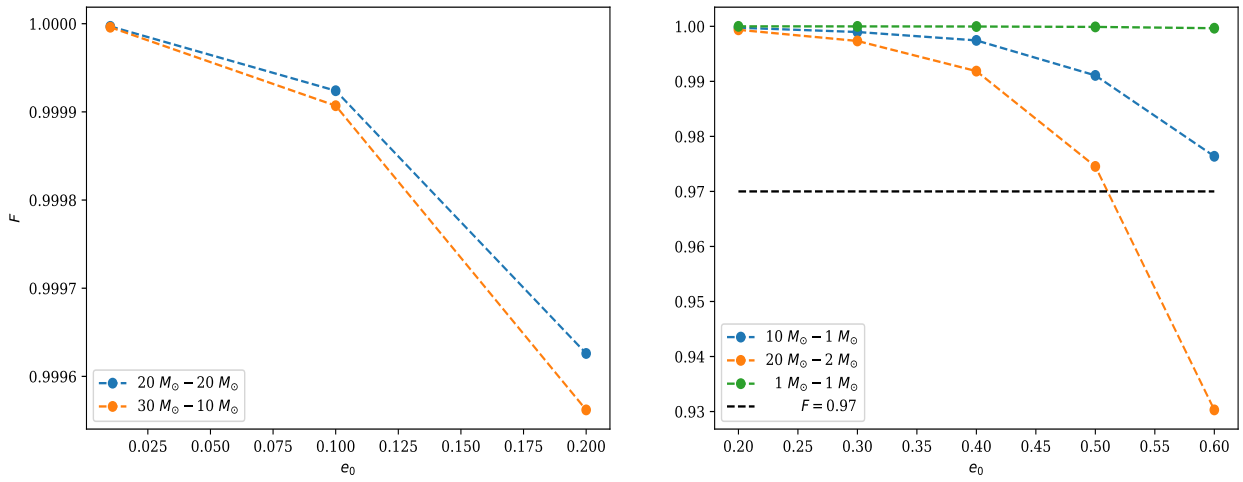

Figure 5.3: Faithfulness plots between 4PN-3PN and 3PN-3PN IMR waveforms (left panel) and the associated inspiral only waveforms (right panel) .

$f_{\rm min}$ (lower frequency limit in Eq. (5.80)) being 30 Hz.

It should be obvious that the validity range in eccentricity of our inspiral prescription (based on PN equations) should be much larger than that for the entire IMR waveform. This is so because stitching the inspiral part with the CMM part severely restricts the validity range of the IMR waveform in eccentricity as the CMM assumes that the BBH has circularized towards the merger. We therefore also present a derived package which outputs the waveform by only using the PN equations of motion [91, 92] and is valid for much higher e_t's. Recall that most of our PN equations are exact in e_t, except for the Padé approximants, all of which do reasonably well up to $e_t \lesssim 0.85$. Of course, this PN package can be trusted for the inspiral part only.

5.4 Summary and Next Steps

We incorporated the dynamics entailed by the 4PN-accurate Hamiltonian for non-spinning compact binaries, available in Ref. [86]. This was done using Keplerian type solution for the local part of the Hamiltonian and canonical perturbation theory for the non-local part. We ignored certain zero-average, oscillatory terms from our solution arising due to 4PN tail effects. Additionally, we provided consistency checks with existing results and detailed checks on the correctness of our lengthy results. Thereafter, we employed our results to obtain an eccentric IMR family by adapting

what is done in Ref. [2]. This included providing an accurate and efficient implementation of GW phasing approach of Ref. [101] to model the inspiral part of eccentric IMR family. A preliminary and quick study revealed that the conservative 4PN order contributions should be relevant for BH binaries with high mass ratios and moderately high initial eccentricities.

We modify the publicly available MATHEMATICA package [90] of Ref. [2] to obtain our updated eccentric IMR family using our 4PN-order parametric solution [91, 92]. We also present a derived package which makes use of only the PN equations of motion to produce the waveforms and hence can be trusted only for the inspiral part. Since this second package does not use the circular-merger-model, it should be valid for a much higher range of e_t ($e_t \lesssim 0.85$) than our former package.

There are a number of extensions that should be pursued in the near future to provide a ready-to-use time domain eccentric IMR templates. Naturally, such a waveform family should be able to model eccentric mergers that should allow us to model BH binaries with moderately high initial eccentricities of $e_t \sim 0.5$. A very recent effort that developed a method to reconstruct eccentric merger waveforms from its circular counterparts, detailed in Ref. [137], should be helpful for such an effort. It will be interesting to stitch what is done in Ref. [137] to our inspiral approximant and probe its validity with the full NR based eccentric IMR waveforms for various initial eccentricities and mass ratios. It will be also desirable to include the spin effects to our inspiral part as these effects are now fully computed to the next-to-leading order [138, 139]. However, it will be desirable to develop Keplerian type parametric solution associated with these next-to-leading order effects by extending what is pursued in Ref. [125]. Additionally, efforts should be pursued to extend our solution for non-spinning binaries to higher PN orders since the action and Hamiltonian computations of compact binaries have recently been pushed to 6PN [140–142]. Very recent efforts suggest that it should be possible to include 4PN order contributions to the GW emission in the coming years [143, 144]. However, this will require us to provide our improved Keplerian type parametric solution to 4PN order in the modified harmonic gauge with the help of Ref. [111]. We plan to complete 4PN-accurate GW phasing for eccentric binaries with such inputs while

incorporating the currently missing radiation reaction induced periodic terms in orbital elements that appear at 2.5PN, 3.5PN and 4PN orders [101, 102].

5.5 Appendix: canonical perturbation theory

Focusing our attention on an integrable and one degree of freedom[7] system for now, we have the total Hamiltonian (unperturbed plus the perturbation) written as

$$H(\phi_0, J_0) = H_0(J_0) + \epsilon H_1(\phi_0, J_0), \tag{5.82}$$

where (ϕ_0, J_0) are the action-angles of the unperturbed system. If the perturbed system is also integrable in the perturbative sense, then there exists a canonical transformation to the new action-angles $(\phi_0, J_0) \leftrightarrow (\phi, J)$ such that $E(J)$ is the total Hamiltonian in terms of the new action J: $E(J) = H(\phi_0, J_0)$. With a type-2 generator $S(\phi_0, J)$ of the form

$$S(\phi_0, J) = \phi_0 J + \epsilon S_1(\phi_0, J) + O(\epsilon^2), \tag{5.83}$$

we have

$$J_0 = \frac{\partial S}{\partial \phi_0} = J + \epsilon \frac{\partial S_1}{\partial \phi_0} + O(\epsilon^2), \tag{5.84}$$

$$\phi = \frac{\partial S}{\partial J} = \phi_0 + \epsilon \frac{\partial S_1}{\partial J} + O(\epsilon^2). \tag{5.85}$$

One of the main results of the canonical perturbation theory is that the leading and the linear in ϵ order contributions to $E(J) = E_0(J) + \epsilon E_1(J) + O(\epsilon^2)$ read

$$E_0(J) = H_0(J) \tag{5.86}$$

$$E_1(J) = H_1(\phi_0, J) + \frac{\partial H_0}{\partial J} \frac{\partial S_1}{\partial \phi_0}. \tag{5.87}$$

[7] One degree of freedom implies one position and one conjugate momentum variable. Integrability is equivalent to the existence of action-angle variables [113].

It is implied here that $H_0(J)$ and $H_1(\phi_0, J)$ have the same functional dependence on J as $H_0(J_0)$ and $H_1(\phi_0, J_0)$ have on J_0. We have borrowed the above concept and presentation largely from Sec. 6.3 of Ref. [113] ; the reader is referred to it for more details, including how to obtain S_1. Evaluation of S_1 is required to get the perturbed action-angles from the unperturbed ones.

As explained in Ref. [104], it is easy to see from Eq. (5.87) that a term of the form $A(J)\cos n\phi_0$ in H_1 (with n being a non-zero integer) can be eliminated by a term $-A(J)\sin n\phi_0/(n\Omega)$ in S_1 where $\Omega(J) \equiv \partial H_0(J)/\partial J$. And since all the sine terms in H_1 can also be eliminated similarly, all there is left to deal with is the non-oscillatory part of H_1 possessing a non-zero average over ϕ_0. Hence, we can write

$$E_1(J) = \overline{H}_1, \tag{5.88}$$

where $\overline{H}_1$ denotes the average of $H_1(\phi_0, J)$ over ϕ_0.

Actually, this technique of averaging the perturbation is basically the von Zeipel-Brouwer technique applied to the Kepler problem (also known as the Delaunay technique). The von Zeipel-Brouwer technique is one of the many *degenerate* perturbation techniques [115], which differs from the non-degenerate one [113] in one crucial aspect that the averaging is not performed over all the angles (as in non-degenerate perturbation theory) but rather only a subset of them. This variation of the non-degenerate method can cure the problem of vanishing denominators which occurs when one tries to apply non-degenerate perturbation method to a degenerate system, such as the Newtonian Kepler system.

5.6 Appendix: the "semi-perturbation" scheme: neglecting oscillatory corrections to action-angles

The main results of canonical perturbation theory are mainly contained in Eqs. (5.84), (5.85), (5.86), (5.87), and (5.88), along with an equation for S_1, which we don't present. But often it is not necessary to retain all the information contained in these equations. We will elucidate this

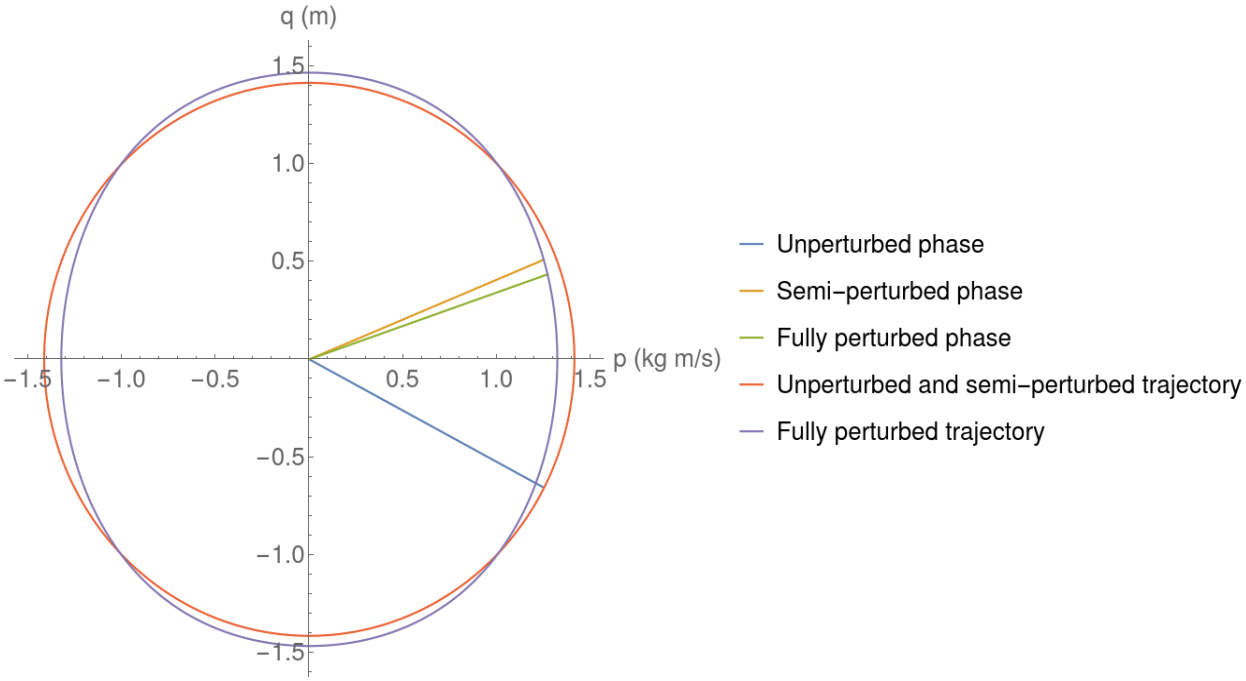

Figure 5.4: The unperturbed, semi-perturbed and fully perturbed trajectories of an SHO with a quartic (in q) perturbation.

with a 1 DOF example of a simple harmonic oscillator (SHO).

With (q, p) being the pair of canonical variables (q in this appendix does not stand for the mass ratio), the full Hamiltonian of the perturbed SHO is

$$H = \frac{p^2}{2m} + \frac{1}{2}m\omega_0^2 q^2 + \frac{1}{4}\epsilon m q^4 \equiv H_0 + \epsilon H_1, \tag{5.89}$$

where $\omega_0 = \sqrt{k/m}$ with k and m being the spring constant and the mass of the oscillator respectively. ϵ is a small perturbation parameter. This is the subject of Worked Example 6.5 of Ref. [113]. We will simply use the results obtained there without showing the entire derivation. (q, p) as a function of unperturbed action-angles (J_0, ϕ_0) is

$$\begin{aligned} q &= \sqrt{\frac{2J_0}{m\omega_0}}\sin\phi_0, \\ p &= \sqrt{2J_0 m\omega_0}\cos\phi_0, \end{aligned} \tag{5.90}$$

whereas Eqs. (5.84) and (5.85) connect the unperturbed action-angles with the perturbed ones as (with $\mu = 1/m\omega_0^2$)

$$\begin{aligned} J_0 &= J + \epsilon \frac{\mu J^2}{8\omega_0} \left(4\cos 2\phi - \cos 4\phi\right) + O(\epsilon^2), \\ \phi_0 &= \phi - \epsilon \frac{\mu J}{4\omega_0} \left(2\sin^2\phi + 3\right) \sin\phi\cos\phi + O(\epsilon^2). \end{aligned} \tag{5.91}$$

Note that Eqs. (5.91) look a little different than the ones in the Worked Example 6.5 of Ref. [113] because we have swapped $\phi \leftrightarrow \phi_0$ in linear in ϵ term. This is justified since it makes a difference at the $O(\epsilon^2)$ absolute order. Finally, Eqs. (5.86) and (5.87) give the perturbed Hamiltonian and the perturbed frequency as

$$\begin{aligned} E(J) &= \omega_0 J + \epsilon \frac{3\mu}{8} J^2 + O(\epsilon^2), \\ \omega &= \frac{\partial E}{\partial J} = \omega_0 + \epsilon \frac{3\mu}{4} J + O(\epsilon^2). \end{aligned} \tag{5.92}$$

We now try to describe this system at three varying levels of complication: (i) unperturbed (least accurate) (ii) fully perturbed (most accurate) (iii) semi-perturbed (slightly less accurate than the "fully perturbed" scheme).

1. Unperturbed: The equations of motion (EOMs) are Eqs. (5.90) with $\phi_0 = \omega_0 t$ and a given fixed value of J_0. The unperturbed action J_0 stays constant during evolution.

2. Fully perturbed: The EOMs are Eqs. (5.90), (5.91) and (5.92) with $\phi = \omega t$ with J (rather than J_0) staying constant.

3. Semi-perturbed: The EOMs are

$$\begin{aligned} q &= q(J_0, \phi_0)|_{(J_0,\phi_0)\to(J,\phi)} = \sqrt{\frac{2J}{m\omega_0}} \sin\phi, \\ p &= p(J_0, \phi_0)|_{(J_0,\phi_0)\to(J,\phi)} = \sqrt{2Jm\omega_0} \cos\phi, \end{aligned} \tag{5.93}$$

again with $\phi = \omega t$. In other words, in the semi-perturbed scheme, (q, p) are taken to have the same dependence on (J, ϕ) as they have on (J_0, ϕ_0). Along with this, we also have Eqs. (5.92). Thus, in the semi-perturbed scheme, the oscillatory corrections to action-angles and the generating function S (Eqs. (5.84), (5.85) and (5.83)) don't need to be computed and hence can be ignored. This leads to significant simplifications when compared to the fully perturbed case without much loss of information, as we will see below. An example of these zero-average oscillatory corrections are the sinusoidal terms in Eqs. (5.91).

To see what concrete effects the three above schemes bring about, we plot the respective trajectories in the phase space for all the three cases in Fig. 5.4, for the following numerical values: $k = 1$ N/m, $m = 1$ kg, $J = J_0 = 1$ kg m^2/s, $\epsilon = 0.2$. The closed contours denote the trajectories and the three rays denote the phase swept ($\arctan(m\omega_0 q/p)$) for all the above three cases from $t = 0$ to $t = 5.8$ s (an arbitrarily chosen numerical value). Since $\phi_0(t = 0) = \phi(t = 0) = 0$, at $t = 0$ we start from the points where the closed trajectories of Fig. 5.4 intersect the positive p-axis for all the above three cases. At the final time $t = 5.8$ s, in the fully perturbed and semi-perturbed cases, we have swept a little over a full revolution whereas in the unperturbed case, we have a significant phase lag compared with the other two. The full effect of the perturbation ϵH_1 (corresponding to the "fully perturbed" case above) is that the perturbed trajectory starts to deform around the unperturbed one and there is a dephasing which increases with time. The dephasing is due to the frequency correction term (linear in ϵ) in Eq. (5.92). In addition, note that the unperturbed trajectory (labeled by $J_0 = J_N$) is the "averaged version" of the fully perturbed trajectory (labeled by $J = J_N$), with J_N standing for some numerical value of the action.

Now let's come to the semi-perturbed case. The semi-perturbed approximation gives us

the same trajectory as the unperturbed one (see Fig. 5.4), but with a phase (yellow ray) that differs from the fully perturbed phase (green ray) in an oscillatory fashion, rather than secular. This means that we get the averaged version of the fully perturbed trajectory and a small amount of oscillatory dephasing with respect to the fully perturbed one, which does not grow in time and whose time-average is zero. The upshot is that instead of capturing the full perturbation effect, we can settle with the semi-perturbed case which has got no secular differences (either in phase or amplitude) with respect to the fully perturbed case. This way we don't need to compute S. Similar approaches have been adopted in some textbooks (Sec. 12.3 and 12.4 of Ref. [114]). Even from the GW data analysis point of view, it is the secular effects that matter much more than the oscillatory ones because the method of matched filter employed in the analysis builds up signal-to-noise ratio by following the phase of the two waveforms to be matched in a coherent manner [145–147].

It is important to note that to model the system using the semi-perturbed scheme, one needs to be given the numerical values of (J, ϕ) at some initial time; initial values of (q, p) or (J_0, ϕ_0) won't do. On the other hand, initial numerical values of (q, p) or (J_0, ϕ_0) are required to model the system as per the unperturbed and the fully-perturbed schemes. All this is not a cause for concern because the 4-3PN IMR MATHEMATICA package [91, 92] provided with this thesis requires the user to input the PN parameter x and eccentricity which are ultimately related to the perturbed actions of the BBH system.

CHAPTER 6

CONVERGENCE OF FOURIER-DOMAIN TEMPLATES FOR INSPIRALING ECCENTRIC COMPACT BINARIES

The contents of this chapter can be found at Ref. [148].

6.1 Introduction

This chapter is motivated by the possibility of identifying the formation channels of binary black holes (BBHs) using a combination of Earth- and space-based GW detectors [149–152], and in particular by the prospect of using eccentricity measurements to distinguish between two of the main proposed formation channels [153–155]: field and dynamical formation. Most BBHs are expected to circularize by the time they enter the most sensitive band of ground based detectors, so we must rely on measurements of masses, spins, redshifts and kicks to distinguish between different formation scenarios [156–165]. However, typical BBH eccentricities are larger for binaries formed dynamically than for binaries formed in the field (see e.g. Fig. 1 of [155]), at the typical frequencies $\sim 10^{-2}$ Hz targeted by the planned Laser Interferometer Space Antenna (LISA) [166]. Therefore LISA has the potential to measure BBH eccentricities and to shed light on their formation channel in a way that is complementary to ground based detectors [153–155, 167–173].

There is a large body of work extending the pioneering study of GWs from eccentric compact binaries by Peters and Mathews [121], where the binary dynamics was treated at Newtonian order, to higher post-Newtonian (PN) orders. The first analytic Fourier-domain templates were calculated within the stationary-phase approximation for arbitrary initial eccentricity, including the effect of periastron advance, in [174]. Analytical expressions for the decay of the orbital parameters under radiation reaction using hypergeometric functions were derived in [175–177] at Newtonian order,

and in [177] at 1PN order. A Kepler-like parametrization was introduced and extended up to 3PN order in [79, 93, 94], and the decay of the orbital parameters under radiation reaction was computed in [178–181]. Now the evolution of the orbital parameters under radiation reaction is known up to 3.5 PN order [182, 183]. A time-domain template for compact binaries where the orbital elements were evolved via numerical integration was introduced in Ref. [3], and it can be regarded as the eccentric extension of the popular `TaylorT4` approximant for quasicircular binaries.

In the analysis of quasicircular binary inspirals it is common to use analytic Fourier-domain templates computed within the stationary-phase approximation (SPA), such as the `TaylorF2` template. Reference [184] generalized these Fourier-domain templates to eccentric binaries, computing templates which are valid at Newtonian order and up to order e_0^8 in a small-eccentricity expansion of the phase (here e_0 is defined to be the eccentricity at some reference orbital frequency $f_{\rm orb} = f_{\rm orb,\,0}$).

This work was extended to 2PN-e_0^6 in Ref. [3], which will be the starting point of our study. Moore et al. [185] extended Ref. [3] to 3PN order, but only at leading order in e_0. All of the templates above are valid at Newtonian order in amplitude and do not include the effect of periastron advance in the phase. Reference [186] constructed analytic templates which are valid for arbitrary initial eccentricity e_0 within the SPA using a truncated sum of harmonics and hypergeometric functions. This work was recently extended to 3PN accuracy [187], and efforts are underway to extend Ref. [184] up to 3PN-e_0^6 order in phase and 1PN order in amplitude, incorporating periastron advance effects [188].

With so many parallel efforts on analytic Fourier-domain eccentric templates underway, it is crucial to investigate the convergence of these proposed GW templates. This is the main goal of our work. We study the convergence properties of the 2PN-e_0^6 accurate template proposed in Ref. [3]. This "*fiducial template*" is a sum over harmonics (labeled by j), where each harmonic has a phase which itself is a bivariate series in the initial eccentricity e_0 and in the PN parameter

$$x \equiv \left(\frac{2\pi G m_z f_{\rm orb}}{c^3}\right)^{2/3}\,, \tag{6.1}$$

where $f_{\rm orb}$ is the orbital frequency for a circular binary, and $m_z = (1+z)m$ is the redshifted total mass of the binary. A preliminary, more limited investigation of the convergence of this bivariate series in the context of parameter estimation can be found in [189]. Our work should be helpful in guiding future efforts to extend the above templates to higher orders, and it can readily be generalized as soon as more accurate templates become available.

We focus on the convergence of the expansion of the phasing (rather than the amplitude) because the phasing is known to have greater impact on detectability and parameter estimation. We first drop some terms from the fiducial template to get (presumably) less accurate "reduced" templates, then we perform calculations of the so-called "unfaithfulness" between these reduced templates and the fiducial 2PN-e_0^6 accurate template to assess the importance of the dropped term(s). We also investigate the conditions under which systematic errors due to dropping high-order terms from the fiducial template exceed the statistical errors. This is useful because whenever systematic errors are negligible with respect to statistical errors, one can choose a truncated template to improve computational efficiency in parameter estimation. Finally we study the convergence of statistical errors.

The chapter is organized as follows. Section 6.2 describes the waveform model and gives details on our calculation of matches and Fisher matrices. Section 6.3 is an overview of data analysis concepts that are relevant for our study. Our results on unfaithfulness are presented in Sec. 6.4.1, the comparison of systematic and statistical errors is shown in Sec. 6.4.2, and the convergence of statistical errors is studied in Sec. 6.4.3. In Sec. 6.5 we summarize our main results and outline directions for future work. To improve readability, some technical details are relegated to the Appendices. Appendix 6.6 illustrates why certain cross terms in the Fisher matrix integrands can be neglected due to their oscillatory nature, and Appendix 6.7 defines beam pattern functions and other quantities appearing in the calculation of the GW strain. The code used in our analysis is publicly available online [190].

6.2 Waveforms, match and Fisher matrix calculations

In this section we describe our waveform model, and then we give details of our unfaithfulness and Fisher matrix calculations.

Our analytic frequency-domain GW template for compact binaries inspiraling in eccentric orbits uses Newtonian amplitudes, the first six harmonics ($j = 1, \ldots, 6$), and a 2PN-e_0^6 accurate phase. Here e_0 is the eccentricity at which the orbital frequency of the binary is $f_0/2$, and we (somewhat arbitrarily) set $f_0 = 10$ mHz. In other words, when the binary has eccentricity e_0, the second harmonic (which dominates the signal for small eccentricities) has frequency f_0. From Appendix 6.7 and Eq. (3.11) of [184] it follows that if we include six harmonics, the expression of e used in the amplitude should be accurate up to $O(e_0^3)$. Below we list the relevant expressions only at Newtonian order for illustration, but in the actual calculations we retained all terms up to 2PN-e_0^6 order; these can be found in Appendix A of [3]. The waveform in the stationary phase approximation has the form

$$\tilde{h}(f) = \frac{\sqrt{3}}{2}\tilde{\mathcal{A}}\left(\frac{G m_z \pi f}{c^3}\right)^{-7/6} \sum_{j=1}^{6} \xi(f,j)\left(\frac{j}{2}\right)^{2/3} e^{-i(\pi/4+\Psi(f,j)-\phi_D(f,j))}\,, \tag{6.2}$$

where the symmetric mass ratio $\eta = m_1 m_2/m^2$,

$$\tilde{\mathcal{A}} = -\left(\frac{5\eta\pi}{384}\right)^{1/2}\frac{G^2 m_z^2}{c^5 D_L}, \tag{6.3a}$$

$$\xi(f,j) = \frac{\left(1-e(f,j)^2\right)^{7/4}}{\left(1+\frac{73}{24}e(f,j)^2+\frac{37}{96}e(f,j)^4\right)^{1/2}}\left(\Gamma(f,j)+i\,\Sigma(f,j)\right)\,, \tag{6.3b}$$

the quantity D_L is the luminosity distance to the source, and

$$\Gamma(f,j) = F_+(f,j)C_+^j(f) + F_\times(f,j)C_\times^j(f)\,, \tag{6.4}$$

$$\Sigma(f,j) = F_+(f,j)S_+^j(f) + F_\times(f,j)S_\times^j(f)\,. \tag{6.5}$$

The definitions of $F_+, F_\times, C_+^j, C_\times^j, S_+^j, S_\times^j$ are given in Appendix 6.7. The Fourier phase $\Psi(f,j)$ and $e(f,j)$, up to the leading PN order and sixth order in e_0, are given by

$$\Psi(f,j) = j\phi_c - 2\pi f t_c - \frac{3}{128\eta}\left(\frac{Gm_z\pi f}{c^3}\right)^{-5/3}\left(\frac{j}{2}\right)^{8/3} C(f,j), \tag{6.6}$$

$$\begin{aligned} e(f,j) = e_0\chi(f,j)^{-19/18} + \frac{3323}{1824}e_0^3\left(\chi(f,j)^{-19/18} - \chi(f,j)^{-19/6}\right) + \left(\frac{15994231}{6653952}\chi(f,j)^{-19/18}\right. \\ \left. -\frac{11042329}{1108992}\chi(f,j)^{-19/6} + \frac{50259743}{6653952}\chi(f,j)^{-95/18}\right)e_0^5, \end{aligned} \tag{6.7}$$

with $\chi(f,j) = 2f/(jf_0)$ and

$$\begin{aligned} C(f,j) = 1 - \frac{2355}{1462}e_0^2\,\chi(f,j)^{-19/9} + \left(-\frac{2608555}{444448}\chi(f,j)^{-19/9} + \frac{5222765}{998944}\chi(f,j)^{-38/9}\right)e_0^4 \\ + \left(-\frac{1326481225}{10134144}\chi(f,j)^{-19/9} + \frac{173355248095}{455518464}\chi(f,j)^{-38/9} - \frac{75356125}{3326976}\chi(f,j)^{-19/3}\right)e_0^6. \end{aligned} \tag{6.8}$$

We also introduced the Doppler phase

$$\phi_D(f,j) = 2\pi R f \sin\bar{\theta}_S \cos\left(\bar{\phi}(f,j) - \bar{\phi}_S\right), \tag{6.9}$$

where $R = 1AU$ and the orbital phase $\bar{\phi}(f,j)$ of LISA's barycenter around the Sun is

$$\begin{aligned} &\mathrm{T}_0\bar{\phi}(f,j) = 2\pi t(f,j) \\ &= 2\pi t_c + \frac{Gm_z}{\eta c^3}\left(\frac{2Gm_z\pi f}{jc^3}\right)^{-8/3}\left(-\frac{5}{256} + \frac{785e_0^2}{11008}\chi(f,j)^{-19/9} + e_0^4\left(-\frac{5222765}{14475264}\chi(f,j)^{-38/9}\right.\right. \\ &\left. + \frac{2608555}{10039296}\chi(f,j)^{-19/9}\right) + e_0^6\left(\frac{75356125}{35487744}\chi(f,j)^{-19/3} + \frac{17355248095}{6600720384}\chi(f,j)^{-38/9}\right. \\ &\left.\left. + \frac{1326481225}{2288959488}\chi(f,j)^{19/9}\right)\right). \end{aligned} \tag{6.10}$$

Here $T_0 = 1$ yr, the angles $(\bar{\theta}_S, \bar{\phi}_S)$ define the direction of the source in the Solar barycenter frame, and t_c and ϕ_c denote the time and phase at coalescence, respectively [191, 192]. The amplitudes

$C^j_+, C^j_\times, S^j_+, S^j_\times$ are computed by keeping the first two terms in the expansion of Eq. (6.7): cf. Appendix 6.7. This is consistent with retaining a Newtonian amplitude and six harmonics. The beam pattern functions F_+ and $F_\times$ depend on f and j through $\bar{\phi}(f, j)$. The equations listed above are of order x^0 in a PN expansion, hence they do not depend on x.

2PN (x^2)	A	B	C	D
1.5PN ($x^{3/2}$)				E
1PN (x^1)				F
Newtonian (x^0)				G
	e_0^0	e_0^2	e_0^4	e_0^6

Table 6.1: Template naming conventions. According to the alphabetical naming convention, the template obtained by dropping terms corresponding to the letters B, C and D from the phase is called "template B", and so on (see text). In the curly bracket convention, the $\{e_0^2\}$ template is obtained by retaining terms of order up to e_0^2 (i.e., the two leftmost columns). Additionally, "template H" corresponds to dropping cells C, D and E from the fiducial template.

The above template is slightly modified with respect to Ref. [3]: the amplitude has an extra factor of $\sqrt{3}/2$ to account for the 60° opening angle of the LISA arms [193], and the Fourier phase has been changed from Ψ to $(\Psi - \phi_D)$ to account for the Doppler phase due to the motion of the detector around the Sun [189, 192].

6.2.1 Fiducial template and truncated templates

We will now introduce the structure of the templates used in our calculations. We refer to the 2PN-e_0^6 order accurate template of [3] as the "*fiducial template*". To assess convergence, we also consider various "truncated templates," i.e., templates derived from the fiducial one by dropping certain terms in the phase. The amplitude of all templates is accurate at Newtonian order and $O(e^4)$, because the phase plays a more important role than the amplitude for detection and parameter estimation (see e.g. [3, 182–184]).

Table 6.1 illustrates the difference between the various templates. Each cell in the table represents a term of a certain order in the PN frequency parameter x (rows) and in the initial eccentricity e_0 (columns). We will use two different notations to distinguish between templates.

A "letter-based" template means that we drop all terms of order greater than or equal to the corresponding cell in the table. For example, "waveform A" is obtained by neglecting cells A, B, C and D, i.e., all of the 2PN corrections to the waveform; "waveform B" is obtained by neglecting cells B, C and D, i.e., all 2PN corrections of order e_0^2 and higher in the initial eccentricity; and "waveform C" is obtained by neglecting cells C and D. Similarly, "waveform G" is obtained by neglecting cells G, F, E and D; "waveform F" is obtained by neglecting cells F, E and D; and "waveform E" is obtained by neglecting cells E and D. "Waveform D" corresponds to neglecting only the 2PN, e_0^6 term.

We will also use a curly bracket notation $\{y^n\}$, meaning that the phase is y^n accurate in the parameter y, where y stands either for e_0 or for x in the bivariate series for the Fourier phase of Eq. (6.6). For example, the $\left\{e_0^2\right\}$ template is accurate up to order e_0^2 (and 2PN) in phase, i.e., we retain the first two columns from the left in Table 6.1. Likewise, for the $\left\{x^1\right\}$ template we retain terms up to 1PN (and order e_0^6) in phase, i.e., the two bottom rows in Table 6.1.

The fiducial template of Eq. (6.2) is a series of harmonics labeled by the integer j, where the phase $\Psi(f, j)$ of each harmonic is itself a bivariate series in x and e_0: cf. Eqs. (6.6) and (6.8). Here we focus on the convergence of $\Psi(f, j)$ as a bivariate series because, as already mentioned, the phase of a GW template is more important than the amplitude (as long as e_0 is small, so that a small-e_0 expansion is valid). [1] In this work we have retained only the first six harmonics ($j = 1, \ldots, 6$) in all of our templates. The convergence of the harmonic expansion is an interesting topic for future work.

[1] At Newtonian order, the radiation reaction timescale $T_{\rm rr} = \omega/\dot{\omega}$ (where $\omega = 2\pi f_{\rm orb}$ is the angular frequency) is

$$T_{\rm rr} = \frac{5GM}{96c^3}\left(\frac{GM\omega}{c^3}\right)^{-8/3}\left[\frac{\left(1-e^2\right)^{7/2}}{1+\frac{73}{24}e^2+\frac{37}{96}e^4}\right].$$

The quantity in square brackets – say, $Z(e)$ – must be expanded for small e to finally arrive at the expression of the Fourier phase Ψ which occurs in Eq. (6.2) [184]. Any Taylor series has a radius of convergence equal at most to the distance from the expansion point (here $e = 0$) and the nearest singularity in the complex plane [194], which here is located at $e \sim \pm\, 0.58\, i$. Therefore none of our templates should be trusted beyond $e_0 \sim 0.58$ (although they may become unfaithful for much smaller values of e_0).

6.2.2 Match calculations

Our convergence analysis of PN, small-eccentricity waveforms is based on some data analysis concepts that we introduce below. First of all, we define the "faithfulness" M between two GW signals $h_1(t)$ and $h_2(t)$ as the following integral, maximized over the time and phase of coalescence t_c and ϕ_c:

$$M = \max_{t_c,\phi_c} \frac{(h_1, h_2)}{\sqrt{(h_1, h_1)(h_2, h_2)}}, \tag{6.11}$$

and the "unfaithfulness" as $(1 - M)$. The inner product between two waveforms (h_1, h_2) is defined as

$$(h_1, h_2) = 4\,\Re \int_{f_{\rm min}}^{f_{\rm max}} \frac{\tilde{h}_1^*(f)\,\tilde{h}_2(f)}{S_{\rm h}(f)} df\,, \tag{6.12}$$

where $\tilde{h}_i(f)$ stands for the Fourier transform of $h_i(t)$ and $S_h(f)$ is the noise power spectral density of the LISA detector [195]. The signal-to-noise ratio (SNR) ρ of template h in the detector can be estimated by

$$\rho^2(h) = (h|h). \tag{6.13}$$

Unlike [195], we do not use a sky-averaged response, and thus we should not include the corresponding factor of 5 in the noise curve. We also treat the two channels separately (so our noise curve differs by an extra factor of 2) and we include the geometrical factor $\sqrt{3}/2$ in the waveform definition (6.2), yielding an extra factor of 3/4. For these reasons, we use the noise curve of [195] *without* the overall factor 10/3, i.e.,

$$S_h(f) = \frac{1}{L^2}\left[P_{\rm OMS}(f) + \frac{4P_{\rm acc}(f)}{(2\pi f)^4}\right]\left[1 + \frac{6}{10}\left(\frac{f}{f_*}\right)^2\right] + S_c(f), \tag{6.14}$$

where $L = 2.5$ Gm and $f_* = 19.09$ mHz. Furthermore $P_{\rm OMS}(f)$, $P_{\rm acc}$ and the confusion noise

$S_c(f)$ are given by

$$P_{\rm OMS} = (1.5\times10^{-11}{\rm m})^2\left[1+\left(\frac{2{\rm mHz}}{f}\right)^4\right]{\rm Hz}^{-1}, \tag{6.15}$$

$$P_{\rm acc} = (3\times10^{-15}{\rm m\ s^{-2}})^2\left[1+\left(\frac{0.4\ {\rm mHz}}{f}\right)^2\right]\left[1+\left(\frac{f}{8\ {\rm mHz}}\right)^4\right]{\rm Hz}^{-1}, \tag{6.16}$$

$$S_c(f) = A\left(\frac{f}{\rm Hz}\right)^{-7/3} e^{-f\alpha+\beta f\sin(\kappa f)}\left[1+\tanh(\gamma(f_k-f))\right]{\rm Hz}^{-1}, \tag{6.17}$$

where $A = 9\times10^{-45}$ and all parameters have been chosen corresponding to an observation time of 2 years: $\alpha = 0.165\ {\rm Hz}^{-1}$, $\beta = 299\ {\rm Hz}^{-1}$, $\kappa = 611\ {\rm Hz}^{-1}$, $\gamma = 1340\ {\rm Hz}^{-1}$ and $f_k = 0.00173$ Hz.

6.2.3 Fisher matrix and cross terms

Our eccentric GW templates depend on 11 parameters: $\ln\mathcal{M}_z, \ln\eta, t_c, \phi_c, \ln D_L, e_0, \bar{\theta}_S, \bar{\phi}_S, \bar{\theta}_L, \bar{\phi}_L$ and β. Here $\mathcal{M}_z = \eta^{3/5}m_z$ is the redshifted chirp mass, $\eta = m_1m_2/m^2$ is the symmetric mass ratio, t_c and ϕ_c are the coalescence time and orbital phase, D_L is the luminosity distance and e_0 is the initial eccentricity, defined as the eccentricity corresponding to an orbital frequency $f_{\rm orb} = 5$ mHz (so that the second harmonic of the radiation is at 10 mHz). The angles $(\bar{\theta}_S, \bar{\phi}_S)$ and the angles $(\bar{\theta}_L, \bar{\phi}_L)$ define the direction of the source and of the binary's orbital angular momentum in the Solar barycenter frame. Finally, β represents the position of the pericenter in the binary's orbital frame [184, 196].

Let $\mathbf{p} = \{p_A\}$ be a vector whose components are any of these eleven parameters. The Fisher matrix is defined as the matrix with elements

$$\tau_{AB} = 4\Re\int_0^\infty \left[\frac{\partial\tilde{h}(f)}{\partial p_A}^*\frac{\partial\tilde{h}(f)}{\partial p_B}\right]\frac{1}{S_h(f)}df. \tag{6.18}$$

In the high SNR regime, the statistical errors associated with estimating the parameters can be approximated by the square root of the diagonal elements of the inverse Fisher matrix [197].

Each of our templates $\tilde{h}(f)$ is obtained by summing over the first six harmonics, i.e., $\tilde{h}(f) = \sum_{j=1}^{6}\tilde{h}_j$. Therefore the integrand above contains 36 terms: 6 "diagonal terms" where

both harmonics are the same, and 30 "cross terms" involving different harmonics. Examples of a diagonal term and of a cross term are

$$4\Re\int_0^\infty \left[\frac{\partial\tilde{h}_1(f)}{\partial p_A}^* \frac{\partial\tilde{h}_1(f)}{\partial p_B}\right]\frac{1}{S_h(f)}df, \tag{6.19}$$

and

$$4\Re\int_0^\infty \left[\frac{\partial\tilde{h}_2(f)}{\partial p_A}^* \frac{\partial\tilde{h}_3(f)}{\partial p_B}\right]\frac{1}{S_h(f)}df, \tag{6.20}$$

respectively.

Numerical calculations show that the cross terms oscillate rapidly and that they do not significantly contribute to the integral, so they can be dropped. An analytical justification for this approximation can be found in Appendix 6.6.

6.2.4 Binary catalog and cosmology

To investigate the statistical properties of our waveforms we use a catalog of 1000 systems. The individual source-frame masses of the binary components are uniformly distributed between $5M_\odot$ and $45M_\odot$. The angles $\bar{\theta}_S, \bar{\phi}_S, \bar{\theta}_L, \bar{\phi}_L$ are uniformly distributed over the sphere, and the angle β is uniformly distributed between $[0, 2\pi]$. We set t_c and ϕ_c equal to 0. We truncate the Fisher matrix integrals of Eq. (6.18) at $f_{\rm max} = 1$ Hz, and we choose $f_{\rm min}$ so that the observation time is 2 years. We assume a ΛCDM cosmology and a spatially flat universe with $H_0 = 67.36$ km/s/Mpc, $\Omega_M = 0.3153$ and $\Omega_\Lambda = 0.6847$ and we fix $z = 0.1$ (corresponding to $D_L = 447.8$ Mpc) for all binaries.

6.3 Some data analysis background and motivation

There are two kinds of parameter estimation errors: systematic and statistical. Systematic errors are due (e.g.) to mismodeling of GW signals, and statistical errors are due to the noise in "ideal" detectors (real detectors usually contribute to systematic errors as well) [146]. If the

systematic errors associated with neglecting some terms in the waveform template are smaller than statistical errors, we can safely neglect those terms and increase the computational efficiency of parameter recovery without compromising its accuracy. Here we follow Appendix G of [198] and we introduce a criterion to decide whether systematic errors are smaller than statistical errors.

Consider a detection scenario where systematic errors are negligible, so all parameter estimation errors are statistical and due to noise. Assume also that the SNR for this detection is large enough that the posterior probability distribution is sharply peaked close to the true parameter values $\mathbf{p}_0$ [146]. For a parameter vector $\mathbf{p}$ close to $\mathbf{p}_0$, the unfaithfulness is $1 - M_{\rm sta}$, and the mean value of the unfaithfulness over the posterior probability is [198]

$$1 - E(M_{\rm sta}) = \frac{(D-1)}{2\,\mathrm{SNR}^2}, \tag{6.21}$$

where E denotes the expectation value, $D = 11$ is the dimension of our parameter space, and the subscript "sta" stands for "statistical."

Let us now include systematic errors. If we demand systematic errors to be negligible with respect to statistical errors, then the unfaithfulness $(1 - M)$ due to GW mismodeling should be negligible with respect to the expected value of the unfaithfulness in Eq. (6.21), i.e.,

$$1 - M \ll \frac{(D-1)}{2\,\mathrm{SNR}^2}. \tag{6.22}$$

We also need a measure of the overall statistical uncertainty. Following e.g. Lyons [199], we can associate an n-dimensional error ellipsoid (about the maximum of the posterior distribution) with a Gaussian posterior in an n-dimensional parameter space. This ellipsoid is the region of 1 σ confidence interval, within which the parameter vector can be found with probability ~ 0.68. The square roots of the diagonal elements of the inverse Fisher matrix are the projections of this error ellipse on the parameter axes. Define ϵ as the product of Fisher errors on all parameters, and ϵ_0 as the volume of the error ellipsoid. It can be shown that ϵ_0 is given by the square root of the determinant of the inverse Fisher matrix and that $\epsilon \geq \epsilon_0$, where the equality is realized when

the parameters are uncorrelated with each other, while having $\epsilon/\epsilon_0 > 1$ means that there is some correlation between the parameters. The parameter ϵ_0 can be considered an overall measure of statistical errors and it is unaffected by a linear transformation of the parameters (or equivalently, by a rotation of the parameter axes): in fact, ϵ_0 measures the volume of the error ellipsoid, which should be independent of the orientation of the parameter axes. The ratio ϵ/ϵ_0 ("correlation factor") quantifies the degree of correlation among the parameters, or the misalignment of the error ellipsoid with the parameter axes.

6.4 Results

In this section we present our results on the convergence properties of the 2PN-${e_0}^6$ accurate bivariate template (the fiducial template) proposed in Ref. [3], as measured in terms of the unfaithfulness and Fisher matrix errors. In subsection 6.4.1 we compute the unfaithfulness due to truncating the fiducial template in various ways (described below), to get an idea of the relative importance of various terms. Subsection 6.4.2 identifies criteria under which systematic errors due to neglecting certain terms in the phase are smaller than statistical errors. Finally, subsection 6.4.3 discusses the convergence properties of the statistical errors.

6.4.1 Unfaithfulness of truncated templates

We compute unfaithfulness distributions for the 1000 binaries in our catalog. We compare the eight truncated templates A-H defined in Sec. 6.2.1 (cf. Table 6.1) against the fiducial template for three selected initial eccentricities ($e_0 = 0.04, 0.07, 0.1$). A large value of the unfaithfulness indicates that the dropped term(s) are significant.

Our results are shown in Fig. 6.1. The histograms in the top panel show the effect of dropping terms of various orders in the initial eccentricity e_0 at 2PN order (i.e., we move "horizontally" along the top row Table 6.1). As expected, the unfaithfulness decreases as we move from template A to template D: template D is the closest to the fiducial template. Similarly, the middle panel shows the effect of dropping terms of various PN orders at order e_0^6 in the initial eccentricity

(i.e., we move vertically along the right column of Table 6.1). Again, as we move from template G to template D (thereby dropping all terms higher than the Newtonian, 1PN, 1.5PN and 2PN order terms, respectively) the unfaithfulness decreases. Finally, the bottom panel corresponds to moving diagonally inwards along Table 6.1, starting from the top-right corner. In each panel, the unfaithfulness gets larger as we increase e_0: this is expected, since all of these waveforms are small-eccentricity expansions.

An interesting exception is template A. In this case we are dropping a *circular* term of order 2PN and e_0^0, so the unfaithfulness is largely independent of e_0 (as it should be). The small faithfulness ($M \sim 0.65$) of template A means that the 2PN-e_0^0 term is very important, and it is suggestive of the necessity to include higher PN orders for circular (e_0^0 order) templates. This is well known in the GW data analysis community, and it is indeed implemented in the 3.5PN accurate circular template `TaylorF2` [146].

2PN (x^2)	–	0.16	0.21	0.30
1.5PN ($x^{3/2}$)	–	0.03	0.12	0.24
1PN (x^1)	–	0.008	0.06	0.18
Newtonian (x^0)	–	0.0007	0.015	0.05
	e_0^0	e_0^2	e_0^4	e_0^6

Table 6.2: Maximum e_0 such that detections with $\rho < 25$ have systematic errors smaller than statistical errors, when terms corresponding to the respective cells in the table are dropped. A dash means that the mismatch is so low that systematic errors are larger than statistical errors for all e_0 in the range we consider.

6.4.2 Systematic errors vs. statistical errors

In Fig. 6.2 we study the conditions under which systematic errors are smaller than statistical errors for selected truncated templates. Each panel shows the unfaithfulness (left y-axis) and the SNR obtained when we replace the inequality in (6.22) by an equality (right y-axis) of selected truncated templates as a function of e_0. Solid lines correspond to the median unfaithfulness (or SNR) over our sample of 1000 binaries. Shaded areas correspond to the 25th and 75th percentiles,

so they give an idea of the spread in the data.

Consider, for example, a detection with SNR $\rho = 20$ and initial eccentricity $e_0 = 0.02$. If the corresponding point in one of these plots lies *below* the unfaithfulness-SNR curve of the corresponding template, then systematic errors are negligible with respect to statistical errors. The faithfulness by itself is not sufficient to decide whether systematic errors are negligible: we also need Eq. (6.22) to determine the maximum SNR beyond which systematic errors dominate. Note also that it would be incorrect to use these plots for low SNRs, since large SNRs were assumed to derive Eq. (6.22).

Another way to read these plots is as follows. Suppose that we want to compute the posterior distribution for a detection with maximum likelihood corresponding to $e_0 = 2 \times 10^{-2}$, $\rho \sim 20$. If we want systematic errors to be negligible with respect to statistical errors when we construct the posterior distribution, we can choose a template whose unfaithfulness-SNR curve at $e_0 \sim 2 \times 10^{-2}$ (as shown in Fig. 6.2) gives $\rho > 20$. For example, templates B, C and D satisfy this criterion, whereas template A does not. Let us remark once again that Fig. 6.2 should not be trusted for low SNRs, therefore (for example) the unfaithfulness-SNR curve for template A cannot be trusted in this example.

Curves corresponding to low unfaithfulness (or high ρ) mean that the GW template will have negligible systematic errors (recall that a point must lie below the unfaithfulness-SNR curve for systematic errors to be negligible). Figure 6.2 implies that systematic errors become negligible as we move from templates A to D, G to D and H to D, i.e., as we move towards templates which are closer to the fiducial template, and our mismodeling errors become smaller. Furthermore, the ratio of systematic to statistical errors becomes smaller as e_0 decreases (ρ gets higher as e_0 decreases). An exception is template A, for which the dominant dropped term is independent of e_0.

When are systematic errors negligible with respect to statistical errors? Focus, for example, on template H in the bottom-left panel of Fig. 6.2 and on the two templates in the bottom-right panel. For template H, systematic errors are negligible in the whole range $0 < e_0 < 0.1$ when $\rho < 10^3$. For the $\{e_0^4\}$ template, the bottom-right panels shows that systematic errors become

negligible in the range $e_0 < 6 \times 10^{-2}$ for SNRs below the blue curve. The corresponding range is smaller for the $\{e_0^2\}$ template. In these regions the truncated template can be used for parameter estimation to save computational time and the dominant errors are statistical. The convergence of statistical errors will be the topic of the next subsection. Similarly, Table 6.2 shows the maximum e_0 such that detections with $\rho < 25$ have systematic errors smaller than statistical errors when terms corresponding to the respective cells in the table are dropped.

6.4.3 Convergence of statistical errors

Unfaithfulness-SNR plots can be used to identify templates for which systematic errors are smaller than statistical errors. Given such a template, statistical errors can be computed (in the high-SNR limit) as the square root of the diagonal elements of the inverse Fisher matrix. We computed statistical errors for the 1000 binaries in our catalog using the $\{e_0^0\}$, $\{e_0^2\}$, $\{e_0^4\}$ and $\{e_0^6\}$ templates (where the last one is the fiducial template).[2] In Fig. 6.3 we plot median statistical errors for these four templates.

Statistical errors change going from template $\{e_0^0\}$ to template $\{e_0^2\}$, but then they plateau. This convergence of statistical errors was not observed in [189], where errors were computed only for the circular and $O(e_0^2)$-accurate templates.

The error on the eccentricity Δe_0 decreases when we go from a circular template $\{e_0^0\}$ to the $\{e_0^2\}$ template, but it is roughly constant as we increase the order of the e_0 expansion. This is because the phase of the circular template $\{e_0^0\}$ is independent of e_0, so all information comes from the amplitude alone, leading to large errors. The errors Δt_c, $\Delta\Omega_S$, and $\Delta \ln D_L$ decrease mildly (within a factor of two) as e_0 increases for all four templates: these are all extrinsic parameters for which measurement information comes largely from the motion of the detector, which is not significantly affected by the template we use. The mass errors $\Delta\mathcal{M}/\mathcal{M}$ and $\Delta\eta/\eta$ are underestimated by a factor of 5-10 when we use the circular template $\{e_0^0\}$, and they are largely the same for all eccentric templates $\{e_0^n\}$ with $n = 2, 4, 6$; in other words, the simplest eccentric template $\{e_0^2\}$

[2] Similar calculations were performed in [189] for two templates: a circular template and a template at leading order in e_0 with different amplitudes.

already contains enough information to estimate mass measurement errors. Note also that most errors (with the exception of Δe_0) vary by at most factor of 2 as functions of e_0.

The bottom row of Fig. 6.3 addresses the question: how do statistical errors change as we increase the order of the e_0 expansion in the phase? The bottom central panel shows that $|\tau|^{-1/2}$ (the volume of the error ellipsoid, as given by the square root of the determinant of the inverse Fisher matrix) decreases going from the $\{e_0^0\}$ to the $\{e_0^2\}$ template: the 11-dimensional error ellipsoid shrinks (i.e., statistical errors decrease) with more accurate templates. This is in apparent contradiction with previous plots, showing that many errors on individual parameters increase. The solution to this apparent paradox (as shown in the bottom-right panel) has to do with correlations between parameters, as measured by ϵ/ϵ_0 – see the discussion below Eq. (6.22): this quantity[3] increases by a factor of $10^2 - 10^3$ going from the $\{e_0^0\}$ template to the $\{e_0^2\}$ template, and then remains roughly constant. Recall that all plots refer to a fixed redshift $z = 0.1$ ($D_L = 447.8$ Mpc), but errors scale linearly with D_L in the large-SNR limit.

In Fig. 6.4 we plot histograms of the statistical errors for all 1000 binaries using our fiducial template. These histograms essentially confirm the conclusions of [189]. We can measure the initial eccentricity as long as $\Delta e_0 < e_0$: this is true for most binaries when $e_0 > 0.1$. If $e_0 = 0.01$, $\Delta e_0 < e_0$ for about 90% of the binaries in our sample.

Before closing this section, we would like to mention that setting $\beta = 0$ (as was done in [189], thereby reducing the number of parameters from 11 to 10) results in a decrease of $\Delta\Omega_S$ by a factor of ~ 10. This suggests that the parameter β is correlated with sky location parameters, and that setting it to zero can lead to an underestimation of those errors.

6.5 Conclusions

We studied the convergence of the frequency domain 2PN-e_0^6 order accurate "fiducial" GW templates for compact eccentric binaries of [3]. We built truncated templates by dropping certain

[3]We slightly modify the definition of the correlation factor to stand for the product of $\Delta\mathcal{M}/\mathcal{M}$, $\Delta\eta/\eta$, $\Delta t_c, \Delta\phi_c$, $\Delta\mathcal{D}_L/\mathcal{D}_L$, $\Delta\Omega_S$, $\Delta\Omega_L$, $\Delta\beta$ and $|\tau|^{1/2}$. Note that $|\tau|$ is equal to the reciprocal of the parameter ϵ_0 introduced in Sec. 6.3, thus quantifying an overall measure of the statistical errors.

terms, and assessed the importance of those terms by computing the unfaithfulness (Fig. 6.1). Dropping most terms leads to unfaithfulness < 0.02 for $e_0 < 0.1$. The terms that produce the largest unfaithfulness when dropped are the 2PN$-e_0^0$ and 0PN$-e_0^6$ terms; extensions at 0PN$-e_0^n$ with $n > 6$ [184] and mPN$-e_0^0$ with $m > 2$ [200] (e.g., the `TaylorF2` approximant) are already available in the literature.

We then investigated the conditions under which truncated templates produce systematic errors which are smaller than statistical errors (Fig. 6.2). This helps us to identify "fast templates" that can be used for parameter estimation considering only statistical errors.

In Fig. 6.3 we studied the convergence of statistical errors. Statistical errors converge very quickly, and they do not change much as long as we include terms of order e_0^2 in the phasing. More accurate templates yield larger statistical errors than the $\{e_0^0\}$ template for most parameters, with the exception of the error Δe_0 on the initial eccentricity. However the error ellipsoid shrinks as we increase the order of the e_0 expansion: indeed, statistical errors for most of the individual parameters increase because of the larger correlations between parameters. Figure 6.4 shows statistical errors for the fiducial template, and it confirms the main conclusions of Ref. [189] (which used slightly different templates).

Several extensions of this work are possible and necessary. An important limitation of our study is that we kept only the three leading-order harmonics in our templates; future work should further explore the convergence of $\tilde{h}(f)$ [Eq. (6.2)] as the number of harmonics changes. Our analysis is specific to stellar-origin BH binaries observed with LISA, but similar work should be done for second- and third-generation Earth-based detectors and using other templates (see e.g. [182, 183]). There are ongoing efforts to extend our "fiducial templates" [3] to 1PN order in amplitude and 3PN order in phase, including the effects of periastron advance [188]. As soon as these templates are available, an extension of our analysis can be used to assess the relative significance of PN amplitude corrections with respect to phase corrections. It will also be important and useful to extend our study to Fourier-domain templates accurate at 3PN and valid for large eccentricities, which are currently under development [186, 201].

6.6 Appendix: Oscillatory cross-terms in the Fisher matrix

As discussed in Sec. 6.2, the cross terms in the integrand of Eq. (6.18) are highly oscillatory, and thus can be neglected. This can be understood analytically as follows. Let us first truncate the templates of [3] at leading order in both the PN parameter x and the initial eccentricity e_0 (i.e., we consider circular templates). We first decompose the template into its first six harmonics:

$$\tilde{h}(f) = \tilde{h}_1(f) + \tilde{h}_2(f) + \tilde{h}_3(f) + \tilde{h}_4(f) + \tilde{h}_5(f) + \tilde{h}_6(f), \tag{6.23}$$

and then we decompose each harmonic into an amplitude and a phase to get

$$\tilde{h}_j(f) = \sum_j A_j(f) e^{i\Psi_j(f)}, \tag{6.24}$$

$$\Psi_j(f) = 2\pi f t_c - j\phi_c + \frac{3}{128\eta}\left(\frac{Gm_z\pi f}{c^3}\right)^{-5/3}\left(\frac{j}{2}\right)^{8/3} - \frac{\pi}{4}. \tag{6.25}$$

By Eq. (6.18), the Fisher matrix elements involve derivatives of the template with respect to the parameters:

$$\frac{\partial\tilde{h}_j(f)}{\partial p_A} = \left[\frac{\partial A_j}{\partial p_A} + iA_j\frac{\partial\Psi_j}{\partial p_A}\right]e^{i\Psi_j}. \tag{6.26}$$

and they can be broken down into a sum of integrals of the form

$$\begin{aligned}&\Re\int_{f_{\rm min}}^{f_{\rm max}}\frac{1}{S_n(f)}\frac{\partial\tilde{h}_{j_1}(f)}{\partial p_A}\frac{\partial\tilde{h}_{j_2}(f)^*}{\partial p_B}df\\ =&\Re\int_{f_{\rm min}}^{f_{\rm max}}\frac{1}{S_n(f)}\left[\frac{\partial A_{j_1}}{\partial p_A} + iA_{j_1}\frac{\partial\Psi_{j_1}}{\partial p_A}\right]\left[\frac{\partial A_{j_2}}{\partial p_B} - iA_{j_2}\frac{\partial\Psi_{j_2}}{\partial p_B}\right]e^{i(\Psi_{j_1}-\Psi_{j_2})}df,\end{aligned} \tag{6.27}$$

as a result of the coupling of different harmonics $(j_1,\ j_2)$ and different parameters $(p_A,\ p_B)$. The phase term in the exponential reads

$$\Psi_{j_1} - \Psi_{j_2} = (j_2 - j_1)\phi_c + \frac{3}{128\eta}\left(\frac{Gm_z\pi f}{c^3}\right)^{-5/3}\left[\left(\frac{j_1}{2}\right)^{8/3} - \left(\frac{j_2}{2}\right)^{8/3}\right]. \tag{6.28}$$

Therefore the integrand has a rapidly oscillatory phase $\Delta\Psi \propto f^{-5/3}$ whenever $j_1 \neq j_2$. For diagonal elements of the Fisher matrix ($p_A = p_B$) terms with $j_1 = j_2$ always exist, and those integrals dominate. For certain off-diagonal terms (e.g. the $\ln D_L$-ϕ_c term), the integrals with $j_1 = j_2$ exactly vanish. However, the natural scale for these terms is set by the corresponding diagonal elements of the Fisher matrix, and the integrals with $j_1 \neq j_2$ can still be neglected.

6.7 Appendix: Beam pattern functions and other quantities appearing in the templates

In this appendix, for completeness, we define certain quantities appearing in the GW strain via [Eqs. (6.2), (6.3), (6.4) and (6.5)]. It is well known that certain combinations of trigonometric functions of the eccentric anomaly u of a binary with eccentricity e can be written as Fourier-Bessel series [145, 184]:

$$\frac{\sin u}{1 - e\cos u} = 2\sum_{k=1}^{\infty} J'_k(ke)\sin kl, \tag{6.29}$$

$$\frac{\cos u}{1 - e\cos u} = \frac{2}{e}\sum_{k=1}^{\infty} J_k(ke)\cos kl, \tag{6.30}$$

where J_k denotes Bessel functions of the first kind

$$J_k(x) = \sum_{n=0}^{\infty} \frac{(-1)^m}{n!\,\Gamma(n+k+1)}\left(\frac{x}{2}\right)^{2n+k}, \tag{6.31}$$

and Γ is the Gamma function. When combined with the well-known relations involving the orbital phase ϕ of a Keplerian orbit

$$\cos\phi = \frac{\cos u - e}{1 - e\cos u}, \tag{6.32}$$

$$\sin\phi = (1 - e^2)^{1/2}\frac{\sin u}{1 - e\cos u}, \tag{6.33}$$

the equations above yield

$$\cos\phi = -e + \frac{2}{e}(1-e^2)\sum_{k=1}^{\infty} J_k(ke)\cos kl \tag{6.34}$$

$$\sin\phi = (1-e^2)^{1/2}\sum_{k=1}^{\infty}(J_{k-1}(ke) - J_{k+1}(ke))\sin kl. \tag{6.35}$$

Following [184], the plus and cross polarizations can be written as

$$\begin{aligned} h_+ = -\frac{G^2\mu}{c^4 p D_L}\Bigg[&\left(2\cos(2\phi-2\beta) + \frac{5e}{2}\cos(\phi-2\beta)\right.\\ &\left. + \frac{e}{2}\cos(3\phi-2\beta) + e^2\cos(2\beta)\right)(1+\cos^2\iota)\\ &+ (e\cos\phi + e^2)\sin^2\iota\Bigg], \end{aligned} \tag{6.36}$$

$$\begin{aligned} h_\times = -\frac{G^2\mu}{c^4 p D_L}\Big[&4\sin(2\phi-2\beta) + 5e\sin(\phi-2\beta)\\ &+ e\sin(3\phi-2\beta) - 2e^2\sin(2\beta)\Big]\cos\iota, \end{aligned} \tag{6.37}$$

where $\mu = m_1 m_2/(m_1+m_2)$ and p (the semilatus rectum of the orbit) is related to the orbital angular frequency ω via

$$\omega = (m_1+m_2)^{1/2}\left(\frac{p}{1-e^2}\right)^{-3/2}. \tag{6.38}$$

where the inclination angle ι is defined by $\cos\iota = \hat{L}\cdot\hat{N}$ [192, 196], where $\hat{L}$ and $\hat{N}$ are unit vectors in the direction of the orbital angular momentum and in the direction of the source, respectively. By plugging Eqs. (6.34) and (6.35) into the expressions for h_+ and $h_\times$ above, we get

$$h_{+,\times} = -\frac{G^2\mathcal{M}}{c^4 D_L}(\mathcal{M}\omega)^{2/3}\sum_{j=1}^{\infty}\left[C^j_{+,\times}\cos(jl) + S^j_{+,\times}\sin(jl)\right]. \tag{6.39}$$

The quantities $C^j_{+,\times}$ and $S^j_{+,\times}$ read [184]

$$C^1_+ = e\left(-\frac{3c_{2\beta}}{2} - \frac{3}{2}c_{2\beta}c_i^2 + s_i^2\right) + \frac{1}{24}e^3\left(16c_{2\beta} + 16c_{2\beta}c_i^2 - 3s_i^2\right), \tag{6.40}$$

$$S^1_+ = -\frac{3}{2}e\left(c_i^2+1\right)s_{2\beta} + \frac{23}{24}e^3\left(c_i^2+1\right)s_{2\beta}, \tag{6.41}$$

$$C^1_\times = 3\ e\ c_i s_{2\beta} - \frac{4}{3}e^3 c_i s_{2\beta}, \tag{6.42}$$

$$S^1_\times = -3\ e\ c_{2\beta}c_i + \frac{23}{12}e^3 c_{2\beta}c_i, \tag{6.43}$$

$$C^2_+ = 2\left(c_{2\beta} + c_{2\beta}c_i^2\right) + e^2\left(-5c_{2\beta} - 5c_{2\beta}c_i^2 + s_i^2\right) + \frac{1}{12}e^4\left(33c_{2\beta} + 33c_{2\beta}c_i^2 - 4s_i^2\right), \tag{6.44}$$

$$S^2_+ = 2\left(c_i^2+1\right)s_{2\beta} - 5e^2\left(c_i^2+1\right)s_{2\beta} + 3e^4\left(c_i^2+1\right)s_{2\beta}, \tag{6.45}$$

$$C^2_\times = -4c_i s_{2\beta} + 10e^2 c_i s_{2\beta} - \frac{11}{2}e^4 c_i s_{2\beta}, \tag{6.46}$$

$$S^2_\times = 4c_{2\beta}c_i - 10e^2 c_{2\beta}c_i + 6e^4 c_{2\beta}c_i, \tag{6.47}$$

$$C^3_+ = \frac{9}{2}e\left(c_{2\beta} + c_{2\beta}c_i^2\right) - \frac{9}{16}e^3\left(19c_{2\beta} + 19c_{2\beta}c_i^2 - 2s_i^2\right), \tag{6.48}$$

$$S^3_+ = \frac{9}{2}e\left(c_i^2+1\right)s_{2\beta} - \frac{171}{16}e^3\left(c_i^2+1\right)s_{2\beta}, \tag{6.49}$$

$$C^3_\times = -9e c_i s_{2\beta} + \frac{171}{8}e^3 c_i s_{2\beta}, \tag{6.50}$$

$$S^3_\times = 9e c_{2\beta}c_i - \frac{171}{8}e^3 c_{2\beta}c_i, \tag{6.51}$$

$$C^4_+ = 8e^2\left(c_{2\beta} + c_i^2 c_{2\beta}\right) + e^4\left(-20c_{2\beta} - 20c_i^2 c_{2\beta} + \frac{4s_i^2}{3}\right), \tag{6.52}$$

$$S^4_+ = 8e^2\left(s_{2\beta} + c_i^2 s_{2\beta}\right) - 20e^4\left(s_{2\beta} + c_i^2 s_{2\beta}\right), \tag{6.53}$$

$$C^4_\times = -16e^2 c_i s_{2\beta} + 40e^4 c_i s_{2\beta}, \tag{6.54}$$

$$S^4_\times = 16e^2 c_i c_{2\beta} - 40e^4 c_i c_{2\beta}, \tag{6.55}$$

$$C_+^5 = \frac{625}{48} e^3 \left(c_{2\beta} + c_{2\beta} c_i^2 \right), \tag{6.56}$$

$$S_+^5 = \frac{625}{48} e^3 \left(c_i^2 s_{2\beta} + s_{2\beta} \right), \tag{6.57}$$

$$C_\times^5 = -\frac{625}{24} e^3 c_i s_{2\beta}, \tag{6.58}$$

$$S_\times^5 = \frac{625}{24} e^3 c_{2\beta} c_i, \tag{6.59}$$

$$C_+^6 = \frac{81}{4} e^4 \left(c_{2\beta} + c_{2\beta} c_i^2 \right), \tag{6.60}$$

$$S_+^6 = \frac{81}{4} e^4 \left(c_i^2 s_{2\beta} + s_{2\beta} \right), \tag{6.61}$$

$$C_\times^6 = -\frac{81}{2} e^4 c_i s_{2\beta}, \tag{6.62}$$

$$S_\times^6 = \frac{81}{2} e^4 c_{2\beta} c_i, \tag{6.63}$$

where $c_{2\beta} = \cos 2\beta$, $s_{2\beta} = \sin 2\beta$, $c_i = \cos \iota$ and $s_i = \sin \iota$. The GW strain at the detector is the linear combination $h(t) = F_+ h_+ + F_\times h_\times$, and its Fourier transform is given by Eq. (6.2). The beam pattern functions F_+ and $F_\times$ can be found, e.g., in [191, 192].

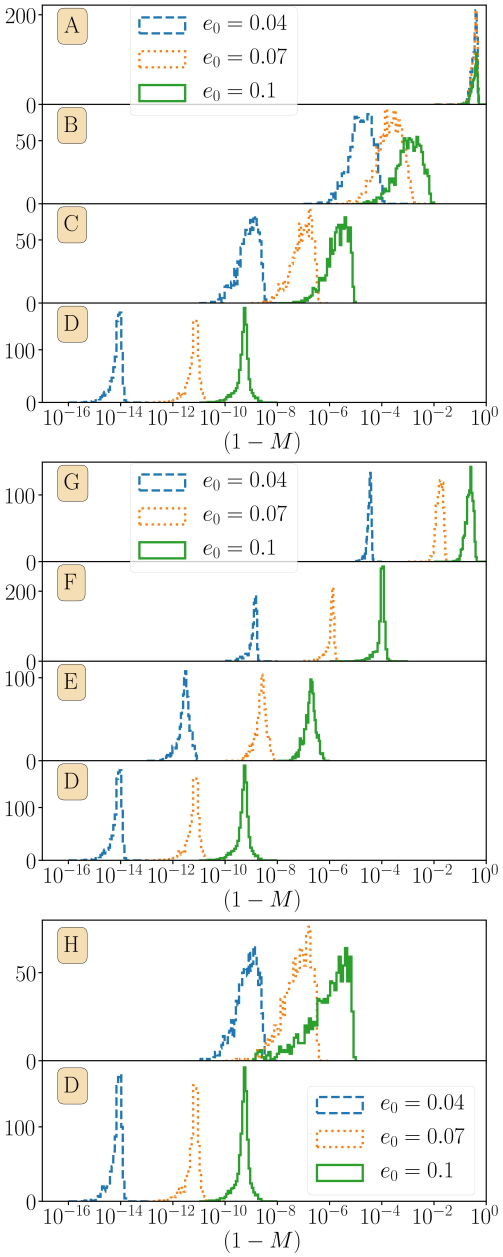

Figure 6.1: Unfaithfulness histograms for templates A-D (top), D-G (middle), D and H (bottom) with respect to the fiducial template.

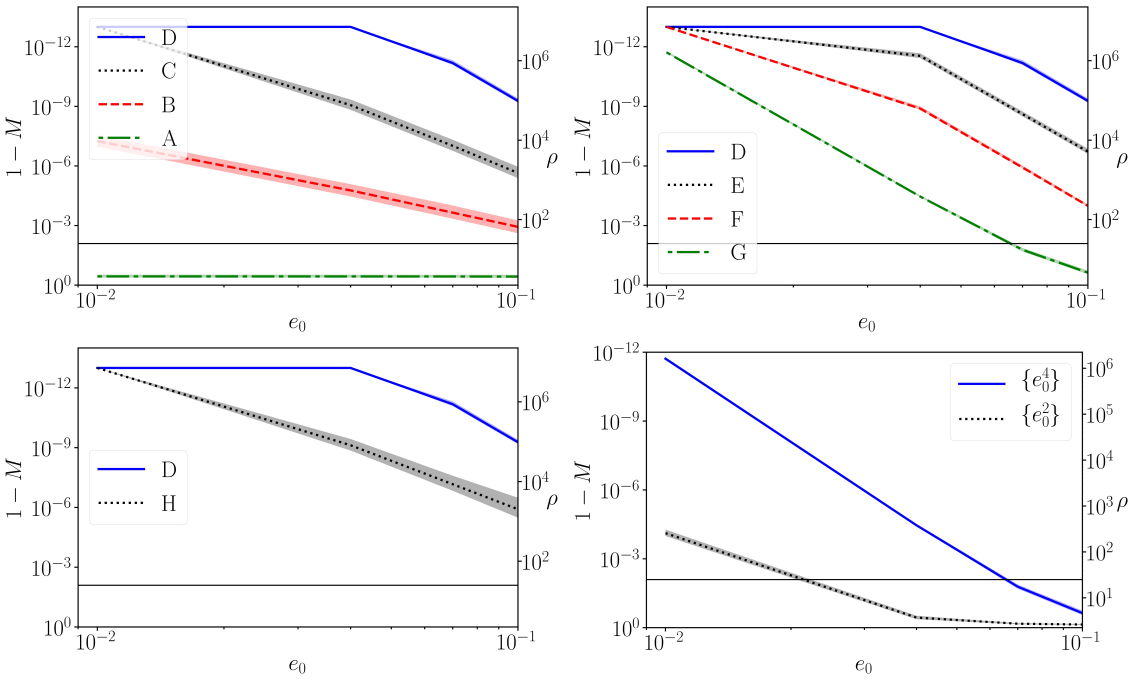

Figure 6.2: Unfaithfulness-SNR plots for various templates with respect to the fiducial template.

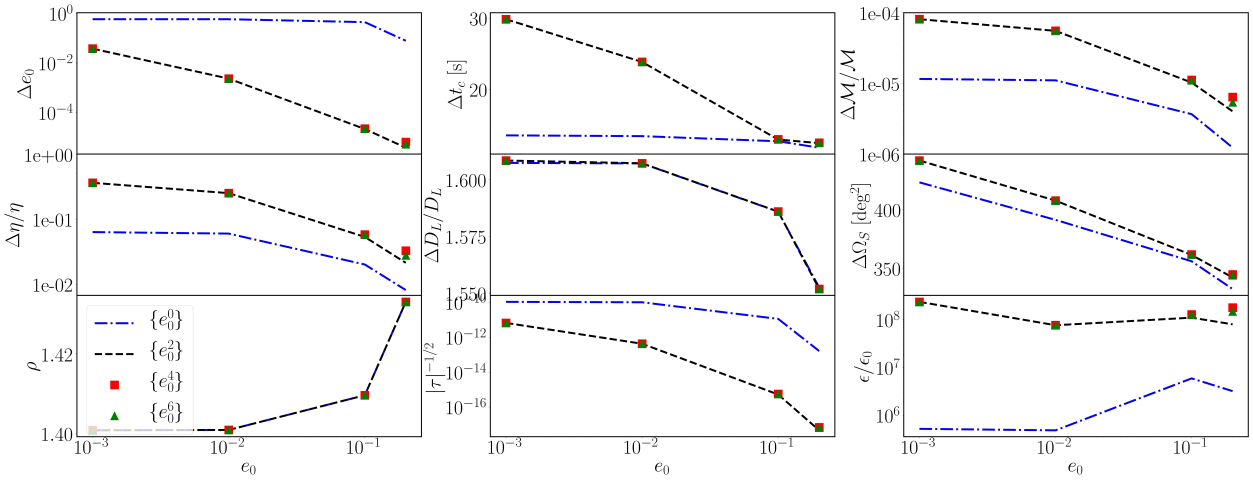

Figure 6.3: Top two rows: statistical errors for the $\{e_0^0\}$, $\{e_0^2\}$, $\{e_0^4\}$ and $\{e_0^6\}$ (fiducial) template. Bottom: SNR (left); volume of the error ellipsoid $|\tau|^{-1/2}$ (center); and correlation between parameters (right).

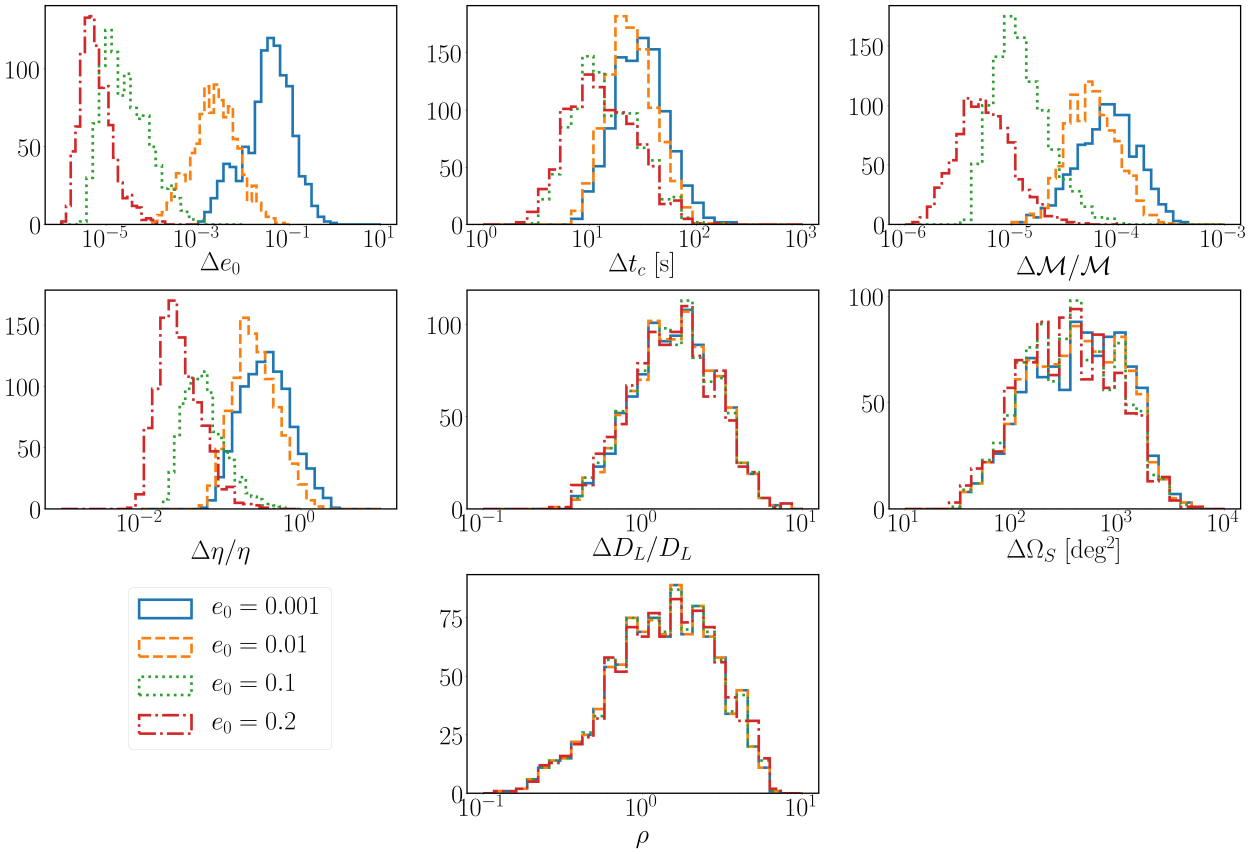

Figure 6.4: Statistical error histograms for the fiducial template and four selected values of e_0.

CHAPTER 7

CONCLUSIONS

In this dissertation, we have made progress towards modeling of stellar-mass BBHs (the primary sources of GWs). As GW detector sensitivities increase in the coming years, we expect more and more detections. Crucial to detections is the accurate modeling of BBH dynamics and the associated GWs. And crucial to fast detections of these GW signals is that the modeling of GWs and BBH dynamics be done analytically, rather numerically.

Overall, this dissertation is an effort in that direction. Chapters 2 and 3 do analytical modeling of spinning, eccentric BBHs. Chapter 4 tried to answer the question if analytical modeling of BBHs at 2PN is feasible or not. Chapter 5 does analytical modeling of the conservative sector of non-spinning, eccentric BBHs. It also constructs the full IMR waveform, which is not fully analytical in nature. Chapter 6 explores the numerical convergence properties of the fully analytical waveform of non-spinning, eccentric BBHs presented in Ref. [3].

GW detections and parameter estimation is marred by two kinds of errors: systematic (due to mismodeling of the GW signal) and statistical (due to detector noise). As GW detectors become more and more sensitive (due to a decrease in detector noise), there will be a need to make our GW models more and more accurate. We will therefore need to push the PN accuracy of our GW models to higher PN orders. Reduction of detector noise enables us to detect fainter and fainter signals, thereby increasing the volume of the universe accessible to the detector which in turn increases the number of anticipated detections. To handle larger and larger number of detections, our GW and BBHs modeling should be as much analytical (rather than numerical) as possible. This has also been the main aim of this dissertation. In the future, we will need to push our results to higher PN order and keeping them analytical if possible.

It also needs to be monitored at what point the analytical expressions used for BBH and GW modeling become so unwieldy that it's faster to use the numerical integration routines. As we keep building our analytical models at higher order accuracies, we anticipate the need for some studies which compare the speed at which GW signals can be generated via analytical and semi-analytical techniques. This will be done to assess the break-even point beyond which more analytical modeling is more of an impediment rather than a boost to the efforts of GW signal modeling.

LIST OF REFERENCES

[1] K.G. Arun, L. Blanchet, B.R. Iyer, and S. Sinha, *Phys. Rev. D* **80**, 124018 (2009), arXiv:0908.3854.

[2] I. Hinder, L.E. Kidder, and H.P. Pfeiffer, *Phys. Rev.* **D98**, 044015 (2018), arXiv:1709.02007.

[3] S. Tanay, M. Haney, and A. Gopakumar, *Phys. Rev. D* **93**, 064031 (2016), arXiv:1602.03081.

[4] **S. Tanay**, L.C. Stein, and J.T. Gálvez Ghersi, *Phys. Rev. D* **103**, 064066 (2021, arXiv: 2012.06586), arXiv:2012.06586.

[5] S. Tanay, G. Cho, and L.C. Stein, (2021), arXiv:2110.15351.

[6] B. Abbott *et al.* (LIGO Scientific, Virgo), *Phys. Rev. X* **9**, 031040 (2019), arXiv:1811.12907.

[7] R. Abbott *et al.* (LIGO Scientific, Virgo), (2020), arXiv:2010.14527.

[8] B.P. Abbott *et al.* (LIGO Scientific, Virgo), *Phys. Rev. Lett.* **119**, 161101 (2017), arXiv:1710.05832.

[9] C. Cutler, *Phys. Rev. D* **57**, 7089 (1998), arXiv:gr-qc/9703068.

[10] P. Amaro-Seoane *et al.* (LISA), (2017), arXiv:1702.00786.

[11] S. Tiwari, A. Gopakumar, M. Haney, and P. Hemantakumar, *Phys. Rev. D* **99**, 124008 (2019), arXiv:1905.07956.

[12] M. Kesden, D. Gerosa, R. O'Shaughnessy, E. Berti, and U. Sperhake, *Phys. Rev. Lett.* **114**, 081103 (2015), arXiv:1411.0674.

[13] D. Gerosa, M. Kesden, U. Sperhake, E. Berti, and R. O'Shaughnessy, *Phys. Rev. D* **92**, 064016 (2015), arXiv:1506.03492.

[14] I. Hinder, L.E. Kidder, and H.P. Pfeiffer, *Phys. Rev. D* **98**, 044015 (2018), arXiv:1709.02007.

[15] K. Chatziioannou, A. Klein, N. Yunes, and N. Cornish, *Phys. Rev. D* **95**, 104004 (2017), arXiv:1703.03967.

[16] A. Klein and P. Jetzer, *Phys. Rev. D* **81**, 124001 (2010), arXiv:1005.2046.

[17] A. Klein, Y. Boetzel, A. Gopakumar, P. Jetzer, and L. de Vittori, *Phys. Rev. D* **98**, 104043 (2018), arXiv:1801.08542.

[18] C. Konigsdorffer and A. Gopakumar, *Phys. Rev. D* **73**, 124012 (2006), arXiv:gr-qc/0603056.

[19] C. Konigsdorffer and A. Gopakumar, *Phys. Rev. D* **71**, 024039 (2005), arXiv:gr-qc/0501011.

[20] G. Cho and H.M. Lee, *Phys. Rev. D* **100**, 044046 (2019), arXiv:1908.02927.

[21] S. Tanay, L.C. Stein, and J.T. Gálvez Ghersi, *Phys. Rev. D* **103**, 064066 (2021), arXiv:2012.06586.

[22] H. Goldstein, C. Poole, and J. Safko, *Classical Mechanics*.

[23] T. Damour and N. Deruelle, *Ann. Inst. Henri Poincaré Phys. Théor* **43**, 107 (1985).

[24] T. Damour and G. Schafer, *Nuovo Cimento B Serie* **101B**, 127 (1988).

[25] T. Damour, *Phys. Rev. D* **64**, 124013 (2001), arXiv:gr-qc/0103018.

[26] G. Cho and H.M. Lee, *Phys. Rev.* **D100**, 044046 (2019), arXiv:1908.02927.

[27] T. Damour and G. Schaefer, *Nuovo Cim. B* **101**, 127 (1988).

[28] T. Damour, *Phys. Rev. D* **64**, 124013 (2001), arXiv:gr-qc/0103018.

[29] E. Racine, *Phys. Rev.* **D78**, 044021 (2008), arXiv:0803.1820.

[30] P. Ajith *et al.*, *Phys. Rev. Lett.* **106**, 241101 (2011), arXiv:0909.2867.

[31] J. José and E. Saletan, *Classical Dynamics: A Contemporary Approach* (Cambridge University Press, 1998).

[32] V. Arnold, K. Vogtmann, and A. Weinstein, *Mathematical Methods of Classical Mechanics*, Graduate Texts in Mathematics.

[33] A. Fasano, S. Marmi, and B. Pelloni, *Analytical Mechanics: An Introduction*, Oxford Graduate Texts.

[34] B.M. Barker, S.N. Gupta, and R.D. Haracz, *Phys. Rev.* **149**, 1027 (1966).

[35] B. Barker and R. O'Connell, *Phys. Rev. D* **12**, 329 (1975).

[36] M.D. Hartl and A. Buonanno, *Phys. Rev. D* **71**, 024027 (2005), arXiv:gr-qc/0407091.

[37] J. Steinhoff, *Annalen Phys.* **523**, 296 (2011), arXiv:1106.4203.

[38] See Supplemental Material at (URL to be determined after submission) for a MATHEMATICA notebook which verifies this calculation.

[39] "xAct: Efficient tensor computer algebra for the Wolfram Language," `http://www.xact.es/`.

[40] L.E. Kidder, *Phys. Rev. D* **52**, 821 (1995), arXiv:gr-qc/9506022.

[41] J.D. Schnittman, *Phys. Rev.* **D70**, 124020 (2004), arXiv:astro-ph/0409174.

[42] M. Kesden, D. Gerosa, R. O'Shaughnessy, E. Berti, and U. Sperhake, *Phys. Rev. Lett.* **114**, 081103 (2015), arXiv:1411.0674.

[43] D. Gerosa, M. Kesden, U. Sperhake, E. Berti, and R. O'Shaughnessy, *Phys. Rev. D* **92**, 064016 (2015), arXiv:1506.03492.

[44] L. Landau, E. Lifshitz, J. Sykes, and J. Bell, *Mechanics: Volume 1*, Course of theoretical physics.

[45] W. Schmidt, *Class. Quant. Grav.* **19**, 2743 (2002), arXiv:gr-qc/0202090.

[46] A. Gopakumar and G. Schafer, *Phys. Rev.* **D84**, 124007 (2011).

[47] G. Cho, S. Tanay, A. Gopakumar, and H.M. Lee, (2021), arXiv:2110.09608.

[48] A. Buonanno and T. Damour, *Phys. Rev. D* **59**, 084006 (1999), arXiv:gr-qc/9811091.

[49] V. Witzany, *Phys. Rev. D* **100**, 104030 (2019), arXiv:1903.03651.

[50] R. Abraham and J. Marsden, *Foundations of Mechanics*, AMS Chelsea publishing.

[51] DLMF, "*NIST Digital Library of Mathematical Functions*," http://dlmf.nist.gov/, Release 1.1.3 of 2021-09-15, f. W. J. Olver, A. B. Olde Daalhuis, D. W. Lozier, B. I. Schneider, R. F. Boisvert, C. W. Clark, B. R. Miller, B. V. Saunders, H. S. Cohl, and M. A. McClain, eds.

[52] D. Gerosa, U. Sperhake, and J. Vošmera, *Class. Quant. Grav.* **34**, 064004 (2017), arXiv:1612.05263.

[53] J.J. Levin, *Phys. Rev. Lett.* **84**, 3515 (2000), arXiv:gr-qc/9910040.

[54] J.J. Levin, *Phys. Rev. D* **67**, 044013 (2003), arXiv:gr-qc/0010100.

[55] S.A. Hughes, *Phys. Rev. Lett.* **85**, 5480 (2000), arXiv:gr-qc/0101024.

[56] J.D. Schnittman and F.A. Rasio, *Phys. Rev. Lett.* **87**, 121101 (2001), arXiv:gr-qc/0107082.

[57] N.J. Cornish and J.J. Levin, *Class. Quant. Grav.* **20**, 1649 (2003), arXiv:gr-qc/0304056.

[58] X. Wu and Y. Xie, *Phys. Rev. D* **81**, 084045 (2010), arXiv:1004.4549.

[59] X. Wu and S.Y. Zhong, *General Relativity and Gravitation* **43**, 2185 (2011).

[60] L. Mei, M. Ju, X. Wu, and S. Liu, *Mon. Not. Roy. Astron. Soc.* **435**, 2246 (2013).

[61] G. Huang, X. Ni, and X. Wu, *Eur. Phys. J. C* **74**, 3012 (2014), arXiv:1403.0378.

[62] X. Wu and G. Huang, *Mon. Not. Roy. Astron. Soc.* **452**, 3167 (2015).

[63] L. Huang and X. Wu, *Eur. Phys. J. C* **76**, 488 (2016), arXiv:1604.05810.

[64] A. Gopakumar and C. Konigsdorffer, *Phys. Rev. D* **72**, 121501 (2005), arXiv:gr-qc/0511009.

[65] C. Bender and S. Orszag, *Advanced Mathematical Methods for Scientists and Engineers I: Asymptotic Methods and Perturbation Theory*, Advanced Mathematical Methods for Scientists and Engineers.

[66] S. Tanay, G. Cho, and L.C. Stein, *arXiv e-prints* , arXiv:2110.15351 (2021), arXiv:2110.15351.

[67] T. Nutma, *Comput. Phys. Commun.* **185**, 1719 (2014), arXiv:1308.3493.

[68] J.M. Martín-García, *Comp. Phys. Commun.* **179**, 597 (2008), arXiv:0803.0862.

[69] S. Khan, K. Chatziioannou, M. Hannam, and F. Ohme, *Phys. Rev. D* **100**, 024059 (2019), arXiv:1809.10113.

[70] G. Pratten *et al.*, (2020), arXiv:2004.06503.

[71] A. Klein and P. Jetzer, *Phys. Rev. D* **81**, 124001 (2010), arXiv:1005.2046.

[72] A. Klein, Y. Boetzel, A. Gopakumar, P. Jetzer, and L. de Vittori, *Phys. Rev. D* **98**, 104043 (2018), arXiv:1801.08542.

[73] C.R. Galley, *Phys. Rev. Lett.* **110**, 174301 (2013), arXiv:1210.2745.

[74] C.R. Galley, D. Tsang, and L.C. Stein, (2014), arXiv:1412.3082.

[75] C.R. Galley and I.Z. Rothstein, *Phys. Rev.* **D95**, 104054 (2017), arXiv:1609.08268.

[76] D. Tsang, C.R. Galley, L.C. Stein, and A. Turner, *Astrophys. J. Lett.* **809**, L9 (2015), arXiv:1506.08443.

[77] G. Cho, **S. Tanay**, A. Gopakumar, and H.M. Lee, *Phys. Rev. D* **105**, 064010 (2022, arXiv: 2110.09608), arXiv:2110.09608.

[78] G. Schäfer and N. Wex, *Physics Letters A* **174**, 196 (1993).

[79] R.M. Memmesheimer, A. Gopakumar, and G. Schäfer, *Phys. Rev. D* **70**, 104011 (2004), gr-qc/0407049.

[80] G. Schäfer and P. Jaranowski, *Living Reviews in Relativity* **21**, 7 (2018), arXiv:1805.07240.

[81] L. Blanchet, *Living Reviews in Relativity* **17**, 2 (2014), arXiv:1310.1528.

[82] E.A. Huerta, C.J. Moore, P. Kumar, D. George, A.J.K. Chua, R. Haas, E. Wessel, D. Johnson, D. Glennon, A. Rebei, A.M. Holgado, J.R. Gair, and H.P. Pfeiffer, *Phys. Rev. D* **97**, 024031 (2018), arXiv:1711.06276.

[83] L. Blanchet and G. Schaefer, *MNRAS* **239**, 845 (1989).

[84] W. Junker and G. Schaefer, *MNRAS* **254**, 146 (1992).

[85] A. Gopakumar and B.R. Iyer, *Phys. Rev. D* **56**, 7708 (1997), arXiv:gr-qc/9710075.

[86] P. Jaranowski and G. Schäfer, *Phys. Rev. D* **92**, 124043 (2015), arXiv:1508.01016.

[87] T. Damour, P. Jaranowski, and G. Schäfer, *Phys. Rev. D* **89**, 064058 (2014), arXiv:1401.4548.

[88] D. Bini, T. Damour, and A. Geralico, *Phys. Rev. D* **102**, 084047 (2020), arXiv:2007.11239.

[89] J. Blümlein, A. Maier, P. Marquard, and G. Schäfer, *Nuclear Physics B* **955**, 115041 (2020), arXiv:2003.01692.

[90] `https://github.com/ianhinder/EccentricIMR` (2017).

[91] `https://github.com/sashwattanay/EccentricIMR` (2021).

[92] See Supplemental Material at [URL will be inserted by publisher] for the MATHEMATICA packages, notebook and pdf files that produce the gravitational waveforms (IMR and inspiral) and contain various lengthy expressions.

[93] T. Damour and N. Deruelle, *Ann. Inst. Henri Poincaré Phys. Théor., Vol. 43, No. 1, p. 107 - 132* **43**, 107 (1985).

[94] T. Damour and G. Schafer, *Nuovo Cimento B Serie* **101**, 127 (1988).

[95] S.A. Klioner, *arXiv e-prints* , arXiv:1609.00915 (2016), arXiv:1609.00915.

[96] P. Colwell, *Solving Kepler's Equation Over Three Centuries*.

[97] Y. Boetzel, A. Susobhanan, A. Gopakumar, A. Klein, and P. Jetzer, *Phys. Rev. D* **96**, 044011 (2017), arXiv:1707.02088.

[98] G. Cho, A. Gopakumar, M. Haney, and H.M. Lee, *Phys. Rev. D* **98**, 024039 (2018), arXiv:1807.02380.

[99] T. Damour and N. Deruelle, *Ann. Inst. Henri Poincaré Phys. Théor* **44**, 263 (1986).

[100] T. Damour and J.H. Taylor, *Phys. Rev. D* **45**, 1840 (1992).

[101] T. Damour, A. Gopakumar, and B.R. Iyer, *Phys. Rev. D* **70**, 064028 (2004), gr-qc/0404128.

[102] C. Königsdörffer and A. Gopakumar, *Phys. Rev. D* **73**, 124012 (2006), gr-qc/0603056.

[103] A. Susobhanan, A. Gopakumar, G. Hobbs, and S.R. Taylor, *Phys. Rev. D* **101**, 043022 (2020), arXiv:2002.03285.

[104] T. Damour, P. Jaranowski, and G. Schäfer, *Phys. Rev. D* **91**, 084024 (2015), arXiv:1502.07245.

[105] C.R. Galley, A.K. Leibovich, R.A. Porto, and A. Ross, *Phys. Rev. D* **93**, 124010 (2016), arXiv:1511.07379.

[106] T. Damour, P. Jaranowski, and G. Schäfer, *Physics Letters B* **513**, 147 (2001), arXiv:gr-qc/0105038.

[107] P. Jaranowski and G. Schäfer, *Phys. Rev. D* **86**, 061503 (2012), arXiv:1207.5448.

[108] P. Jaranowski and G. Schäfer, *Phys. Rev. D* **87**, 081503 (2013), arXiv:1303.3225.

[109] S. Foffa, R.A. Porto, I. Rothstein, and R. Sturani, *Phys. Rev. D* **100**, 024048 (2019), arXiv:1903.05118.

[110] S. Foffa and R. Sturani, *Phys. Rev. D* **100**, 024047 (2019), arXiv:1903.05113.

[111] T. Marchand, L. Bernard, L. Blanchet, and G. Faye, *Phys. Rev. D* **97**, 044023 (2018), arXiv:1707.09289.

[112] G. Cho, S. Tanay, A. Gopakumar, and H.M. Lee, *Phys. Rev. D* **105**, 064010 (2022), arXiv:2110.09608.

[113] J. José and E. Saletan, *Classical Dynamics: A Contemporary Approach*.

[114] H. Goldstein, C. Poole, and J. Safko, *Classical Mechanics*.

[115] S. Ferraz-Mello, *Canonical Perturbation Theories: Degenerate Systems and Resonance*, Astrophysics and Space Science Library.

[116] T. Damour and G. Schaefer, *J. Math. Phys.* **32**, 127 (1991).

[117] T. Damour, P. Jaranowski, and G. Schäfer, *Phys. Rev. D* **93**, 084014 (2016), arXiv:1601.01283.

[118] T. Damour, P. Jaranowski, and G. Schaefer, *Phys. Rev. D* **62**, 044024 (2000), arXiv:gr-qc/9912092.

[119] K.G. Arun, L. Blanchet, B.R. Iyer, and M.S.S. Qusailah, *Phys. Rev. D* **77**, 064034 (2008), arXiv:0711.0250.

[120] C. Dlapa, G. Kälin, Z. Liu, and R.A. Porto, *arXiv e-prints* , arXiv:2106.08276 (2021), arXiv:2106.08276.

[121] P.C. Peters and J. Mathews, *Physical Review* **131**, 435 (1963).

[122] F. Moulton, *An Introduction to Celestial Mechanics*, Dover books in astronomy.

[123] S. Finch and G. Rota, *Mathematical Constants*, Encyclopedia of Mathematics and its Applications.

[124] I. Hinder, F. Herrmann, P. Laguna, and D. Shoemaker, *Phys. Rev. D* **82**, 024033 (2010), arXiv:0806.1037.

[125] A. Klein, Y. Boetzel, A. Gopakumar, P. Jetzer, and L. de Vittori, *Phys. Rev. D* **98**, 104043 (2018), arXiv:1801.08542.

[126] E.A. Huerta *et al.*, *Phys. Rev. D* **95**, 024038 (2017), arXiv:1609.05933.

[127] E. Poisson and C. Will, *Gravity: Newtonian, Post-Newtonian, Relativistic* (Cambridge University Press, 2014).

[128] L. Blanchet and G. Schaefer, *MNRAS* **239**, 845 (1989).

[129] A. Gopakumar and B.R. Iyer, *Phys. Rev. D* **56**, 7708 (1997), gr-qc/9710075.

[130] S. Mikkola, *Celestial Mechanics* **40**, 329 (1987).

[131] A.H. Mroue *et al.*, *Phys. Rev. Lett.* **111**, 241104 (2013), arXiv:1304.6077.

[132] S. Tanay, A. Klein, E. Berti, and A. Nishizawa, *Phys. Rev. D* **100**, 064006 (2019), arXiv:1905.08811.

[133] T. Damour, B.R. Iyer, and B.S. Sathyaprakash, *Phys. Rev. D* **62**, 084036 (2000), arXiv:gr-qc/0001023.

[134] `https://dcc.ligo.org/public/0002/T0900288/003/ZERO_DET_high_P.txt/`.

[135] T.A. Apostolatos, *Phys. Rev. D* **52**, 605 (1995).

[136] B.J. Owen and B.S. Sathyaprakash, *Phys. Rev. D* **60**, 022002 (1999), arXiv:gr-qc/9808076.

[137] Y. Setyawati and F. Ohme, *arXiv e-prints* , arXiv:2101.11033 (2021), arXiv:2101.11033.

[138] L. Blanchet, A. Buonanno, and G. Faye, *Phys. Rev. D* **74**, 104034 (2006), arXiv:gr-qc/0605140.

[139] G. Cho, B. Pardo, and R.A. Porto, *Phys. Rev. D* **104**, 024037 (2021), arXiv:2103.14612.

[140] D. Bini, T. Damour, and A. Geralico, *Phys. Rev. Lett.* **123**, 231104 (2019), arXiv:1909.02375.

[141] D. Bini, T. Damour, and A. Geralico, *Phys. Rev. D* **102**, 024062 (2020), arXiv:2003.11891.

[142] D. Bini, T. Damour, and A. Geralico, *Phys. Rev. D* **102**, 024061 (2020), arXiv:2004.05407.

[143] F. Larrouturou, Q. Henry, L. Blanchet, and G. Faye, *arXiv e-prints* , arXiv:2110.02240 (2021), arXiv:2110.02240.

[144] F. Larrouturou, L. Blanchet, Q. Henry, and G. Faye, *arXiv e-prints* , arXiv:2110.02243 (2021), arXiv:2110.02243.

[145] M. Maggiore, *Gravitational Waves: Volume 1: Theory and Experiments*, Gravitational Waves.

[146] J. Creighton and W. Anderson, *Gravitational-Wave Physics and Astronomy: An Introduction to Theory, Experiment and Data Analysis*, Wiley Series in Cosmology.

[147] B.S. Sathyaprakash and B.F. Schutz, *Living Rev. Rel.* **12**, 2 (2009), arXiv:0903.0338.

[148] **S. Tanay**, A. Klein, E. Berti, and A. Nishizawa, *Phys. Rev. D* **100**, 064006 (2019, arXiv:1905.08811), arXiv:1905.08811.

[149] A. Sesana, *Phys. Rev. Lett.* **116**, 231102 (2016), arXiv:1602.06951.

[150] K.W.K. Wong, E.D. Kovetz, C. Cutler, and E. Berti, *Phys. Rev. Lett.* **121**, 251102 (2018), arXiv:1808.08247.

[151] C. Cutler *et al.*, (2019), arXiv:1903.04069.

[152] D. Gerosa, S. Ma, K.W.K. Wong, E. Berti, R. O'Shaughnessy, Y. Chen, and K. Belczynski, (2019), arXiv:1902.00021.

[153] A. Nishizawa, E. Berti, A. Klein, and A. Sesana, *Phys. Rev.* **D94**, 064020 (2016), arXiv:1605.01341.

[154] K. Breivik, C.L. Rodriguez, S.L. Larson, V. Kalogera, and F.A. Rasio, *Astrophys. J.* **830**, L18 (2016), arXiv:1606.09558.

[155] A. Nishizawa, A. Sesana, E. Berti, and A. Klein, *Mon. Not. Roy. Astron. Soc.* **465**, 4375 (2017), arXiv:1606.09295.

[156] D. Gerosa, M. Kesden, E. Berti, R. O'Shaughnessy, and U. Sperhake, *Phys. Rev.* **D87**, 104028 (2013), arXiv:1302.4442.

[157] S. Stevenson, F. Ohme, and S. Fairhurst, *Astrophys. J.* **810**, 58 (2015), arXiv:1504.07802.

[158] E.D. Kovetz, I. Cholis, P.C. Breysse, and M. Kamionkowski, *Phys. Rev.* **D95**, 103010 (2017), arXiv:1611.01157.

[159] M. Fishbach and D.E. Holz, *Astrophys. J.* **851**, L25 (2017), arXiv:1709.08584.

[160] M. Zevin, C. Pankow, C.L. Rodriguez, L. Sampson, E. Chase, V. Kalogera, and F.A. Rasio, *Astrophys. J.* **846**, 82 (2017), arXiv:1704.07379.

[161] J.W. Barrett, S.M. Gaebel, C.J. Neijssel, A. Vigna-Gómez, S. Stevenson, C.P.L. Berry, W.M. Farr, and I. Mandel, *Mon. Not. Roy. Astron. Soc.* **477**, 4685 (2018), arXiv:1711.06287.

[162] D. Gerosa and E. Berti, *Phys. Rev.* **D95**, 124046 (2017), arXiv:1703.06223.

[163] C. Talbot and E. Thrane, *Astrophys. J.* **856**, 173 (2018), arXiv:1801.02699.

[164] D. Wysocki, J. Lange, and R. O. 'shaughnessy, (2018), arXiv:1805.06442.

[165] D. Gerosa, E. Berti, R. O'Shaughnessy, K. Belczynski, M. Kesden, D. Wysocki, and W. Gladysz, *Phys. Rev.* **D98**, 084036 (2018), arXiv:1808.02491.

[166] P. Amaro-Seoane, S. Aoudia, S. Babak, P. Binétruy, E. Berti, A. Bohé, C. Caprini, M. Colpi, N.J. Cornish, K. Danzmann, J.F. Dufaux, J. Gair, I. Hinder, O. Jennrich, P. Jetzer, A. Klein, R.N. Lang, A. Lobo, T. Littenberg, S.T. McWilliams, G. Nelemans, A. Petiteau, E.K. Porter, B.F. Schutz, A. Sesana, R. Stebbins, T. Sumner, M. Vallisneri, S. Vitale, M. Volonteri, H. Ward, and B. Wardell, *GW Notes, Vol. 6, p. 4-110* **6**, 4 (2013), arXiv:1201.3621.

[167] J. Samsing, *Phys. Rev. D* **97**, 103014 (2018), arXiv:1711.07452.

[168] J. Samsing, D.J. D'Orazio, A. Askar, and M. Giersz, (2018), arXiv:1802.08654.

[169] J. Samsing and D.J. D'Orazio, *Mon. Not. Roy. Astron. Soc.* **481**, 5445 (2018), arXiv:1804.06519.

[170] D.J. D'Orazio and J. Samsing, *Mon. Not. Roy. Astron. Soc.* **481**, 4775 (2018), arXiv:1805.06194.

[171] J. Samsing and D.J. D'Orazio, *Phys. Rev.* **D99**, 063006 (2019), arXiv:1807.08864.

[172] M. Zevin, J. Samsing, C. Rodriguez, C.J. Haster, and E. Ramirez-Ruiz, *Astrophys. J.* **871**, 91 (2019), arXiv:1810.00901.

[173] C.L. Rodriguez, P. Amaro-Seoane, S. Chatterjee, K. Kremer, F.A. Rasio, J. Samsing, C.S. Ye, and M. Zevin, *Phys. Rev.* **D98**, 123005 (2018), arXiv:1811.04926.

[174] B. Mikoczi, B. Kocsis, P. Forgacs, and M. Vasuth, *Phys. Rev. D* **86**, 104027 (2012), arXiv:1206.5786.

[175] V. Pierro and I.M. Pinto, *Nuovo Cimento B Serie* **111B**, 631 (1996).

[176] V. Pierro, I.M. Pinto, and A.D.A.M. Spallicci, *Mon. Not. Roy. Astron. Soc.* **334**, 855 (2002).

[177] B. Mikóczi, P. Forgács, and M. Vasúth, *Phys. Rev. D* **92**, 044038 (2015), arXiv:1502.00276.

[178] G. Schäfer, *Annals of Physics* **161**, 81 (1985).

[179] B.R. Iyer and C.M. Will, *Phys. Rev. D* **52**, 6882 (1995).

[180] C. Königsdörffer, G. Faye, and G. Schäfer, *Phys. Rev. D* **68**, 044004 (2003), gr-qc/0305048.

[181] S. Nissanke and L. Blanchet, *Class. Quant. Grav.* **22**, 1007 (2005), arXiv:gr-qc/0412018.

[182] T. Damour, A. Gopakumar, and B.R. Iyer, *Phys. Rev. D* **70**, 064028 (2004), gr-qc/0404128.

[183] C. Königsdörffer and A. Gopakumar, *Phys. Rev. D* **73**, 124012 (2006), gr-qc/0603056.

[184] N. Yunes, K.G. Arun, E. Berti, and C.M. Will, *Phys. Rev. D* **80**, 084001 (2009), arXiv:0906.0313.

[185] B. Moore, M. Favata, K.G. Arun, and C.K. Mishra, *Phys. Rev. D* **93**, 124061 (2016), arXiv:1605.00304.

[186] B. Moore, T. Robson, N. Loutrel, and N. Yunes, *Classical and Quantum Gravity* **35**, 235006 (2018), arXiv:1807.07163.

[187] B. Moore and N. Yunes, *arXiv e-prints* (2019), arXiv:1903.05203.

[188] S. Tiwari, A. Gopakumar, M. Haney, and P. Hemantakumar, (2019), arXiv:1905.07956.

[189] A. Nishizawa, E. Berti, A. Klein, and A. Sesana, *Phys. Rev. D* **94**, 064020 (2016), arXiv:1605.01341.

[190] EccentricPNwaveform code:
`https://github.com/sashwattanay/EccentricPNwaveformConvergence`.

[191] E. Berti, A. Buonanno, and C.M. Will, *Phys. Rev.* **D71**, 084025 (2005), arXiv:gr-qc/0411129.

[192] K. Yagi and T. Tanaka, *Phys. Rev. D* **81**, 064008 (2010), arXiv:0906.4269.

[193] E. Berti, A. Buonanno, and C.M. Will, *Phys. Rev. D* **71**, 084025 (2005), gr-qc/0411129.

[194] G.B. Arfken and H.J. Weber, *"Mathematical methods for physicists 6th ed.by George B. Arfken and Hans J. Weber. Published :Amsterdam; Boston : Elsevier, c2005. xii, 1182 p. : ill. ; 25 cm. Includes bibliographical references and index. ISBN :* (2005).

[195] T. Robson, N. Cornish, and C. Liu, *arXiv e-prints* (2018), arXiv:1803.01944.

[196] K. Martel and E. Poisson, *Phys. Rev. D* **60**, 124008 (1999), gr-qc/9907006.

[197] M. Vallisneri, *Phys. Rev.* **D77**, 042001 (2008), arXiv:gr-qc/0703086.

[198] K. Chatziioannou, A. Klein, N. Yunes, and N. Cornish, *Phys. Rev. D* **95**, 104004 (2017), arXiv:1703.03967.

[199] L. Lyons, *Statistics for Nuclear and Particle Physicists, by Louis Lyons, pp. 240. ISBN 0521379342. Cambridge, UK: Cambridge University Press, April 1989.* (1989) p. 240.

[200] L. Blanchet, *Living Reviews in Relativity* **17**, 2 (2014), arXiv:1310.1528.

[201] B. Moore and N. Yunes, (2019), arXiv:1903.05203.

VITA

Sashwat Tanay

University of Mississippi

204, Lewis Hall

Department of Physics and Astronomy

University, MS 38677-1848 USA

Education

- 2009-2013, B.Tech in Mechanical Engineering, Indian Institute of Technology Ropar, India

Awards, & Fellowships

- 2016-2020, Graduate School Honors Fellowship, Univ. of Mississippi ($12,000 in total)
- 2013-2015, Junior Research Fellowship, Tata Institute of Fundamental Research, Mumbai

Invited talks & lectures

- Univ. of Illinois Urbana-Champaign (lecture workshop) Jun 2022
- Montana State Univ. (Relativity, Astrophysics and Space Science Seminar) Apr 2022
- Max Planck Inst. for Gravitational Physics Potsdam (ACR Seminar) Jun 2021
- Simon Fraser Univ. (Cosmology Seminar) Sep 2020

Publications

- R. Samanta, S. Tanay, L. C. Stein *Closed-form solution of spining, eccentric binary black-holes at 1.5 post-Newtonian order (manuscript in preparation)*; YouTube link on the project and the associated MATHEMATICA package
- S. Tanay, L. C. Stein, *A more efficient way to compute the quasi-normal mode frequencies of Kerr black holes (manuscript in preparation)*; the associated PYTHON package
- S. Tanay, G. Cho, L. C. Stein *Action-angle variables of a binary black-hole with arbitrary eccentricity, spins, and masses at 1.5 post-Newtonian order* arXiv:2110.15351
- G. Cho, S. Tanay, A. Gopakumar, H. M. Lee *Generalized quasi-Keplerian solution for eccentric, non-spinning compact binaries at 4PN order and the associated IMR waveform* arXiv: 2110.09608
- S. Tanay, L. C. Stein, José T. Gálvez Ghersi *Integrability of eccentric, spinning black hole binaries up to second post-Newtonian order* arXiv:1905.08811
- S. Tanay, E. Berti, A. Klein, A. Nishizawa, *Convergence of Fourier-domain templates for inspiraling eccentric compact binaries* arXiv:1905.08811
- S. Tanay, M. Haney, A. Gopakumar, *Frequency and time domain inspiral templates for comparable mass compact binaries in eccentric orbits* arXiv:1602.03081